TARGET SELECTION FROM AIRBORNE MAGNETIC AND RADIOMETRIC DATA IN STEINHAUSEN AREA, NAMIBIA

A thesis submitted in partial fulfilment
of the requirements for the degree of
Masters of Sciences in

Economic Geology

Geology Department

Rhodes University

by

Corus Naudé

January 2012

ABSTRACT

The eastern branch of the late Proterozoic Damara Orogenic Belt of central Namibia hosts various copper, gold, manganese and uranium deposits, but in the vicinity of Steinhausen, approximately 145 km northeast of Windhoek, the Damara Belt becomes increasingly covered by recent Kalahari cover sediments resulting in little known geology and subsequent lack of discovered economic mineral deposits.

Airborne magnetic and radiometric data over the Steinhausen Study Area was enhanced through image processing and filtering to accentuate characteristics of subsurface geology that, by comparing these characteristics to known geology, aided in the interpretive mapping of lithology, structure and targets for follow-up exploration.

As a result, some important observations regarding the regional lithology can be drawn. An arenaceous stratigraphic unit that includes a coarse grained, glassy quartzite below the Kuiseb Formation equates to either the eastern Damaran equivalent of the Nosib Group subjected to high grade metamorphism or, alternatively, the upper part of the pre-Damaran sequence, immediately underlying the Damara. The Kuiseb Formation within the study area is uncharacteristically varied as compared to the same formation further west along the Damaran Orogen and can be subdivided into 5 separate units based on geophysical signature.

Structural features evident within the study area include the prominent Kudu- and Okahandja Lineaments and straddle an area of inferred uplifted stratigraphy of possibly pre-Damara age. The Ekuja Dome (Kibaran age and host to the Omitiomire copper deposit) is also clearly discernible on the airborne magnetic data and is cross-cut by an east-northeast structural zone.

Direct targets for follow-up exploration include the Rodenbeck intrusion, anomalous magnetic bodies and numerous radiometric anomalies present within the study area. Identified dome-like features are considered prospective for Omitiomire-style deposits and the Okatjuru Layered Complex is considered a possible source of copper, chromite, magnetite, ilmenite, nickel and the platinum group elements.

ACKNOWLEDGMENTS

I would like to thank Craton Mining for permission to use the data, and Karl Hartmann (Craton) for information on the Omitiomire copper deposit. Also, to Remote Exploration Services for providing me with the opportunity to undertake my studies on a part-time basis.

I would like to express my gratitude to Dr. Branko Corner for his invaluable guidance as well as for proofing of the thesis, and to my supervisors, the late Prof. John Moore for his insights and Prof. Yong Yao for his constructive input.

TABLE OF CONTENTS

TABLE OF CONTENTS ..... **I**

LIST OF TABLES ..... **III**

LIST OF FIGURES ..... **IV**

CHAPTER 1 ..... **1**

INTRODUCTION 1

CHAPTER 2 ..... **6**

GEOLOGICAL SETTING 6
2.1 The Damara Orogen *6*
2.2 Geology of the Steinhausen Study Area *8*

CHAPTER 3 ..... **15**

KNOWN MINERAL OCCURRENCES AND DEPOSITS WITHIN STEINHAUSEN PROJECT AREA 15
3.1 Omitiomire copper deposit *15*
3.2 Copper geochemical anomalies *16*
3.3 Manganese occurrences *16*
3.4 Nickel occurrences *17*

CHAPTER 4 ..... **19**

MINERAL DEPOSIT MODELS AND SOME EXAMPLES 19
4.1 Matchless stratiform massive sulphides *19*
4.1.1 Matchless Mine 20
4.1.2 Otjihase Mine 22
4.1.3 Ongeama Prospect 23
4.2 Kuiseb Formation hosted hydrothermal copper deposits *23*
4.2.1 Onganja Mine 24
4.3 Manganese deposits *25*
4.3.1 Otjosondu Manganese Field 25
4.4 Magmatic Nickel, Copper and Platinum Group Element (PGE) deposits *26*
4.4.1 Voisey's Bay Deposit 27
4.4.2 Alpine serpentinites within Damara Orogen 28
4.5 Hydrothermal gold deposits *28*
4.5.1 Navachab Gold Mine 29
4.5.2 Ondundu-Otjiwapa Gold Field 30
4.6 Uranium deposits *31*
4.6.1 Calcrete-hosted uranium deposits 32
4.6.1.1 Langer Heinrich Deposit 32
4.6.2 Classical vein deposits 33
4.6.2.1 Schwartzwalder Mine 34
4.6.2 Deposits associated with igneous rocks 34
4.7 Omitiomire-style copper *35*
4.8 Geophysical expressions of target models *37*

CHAPTER 5 ..... **44**

DATASETS AND PROCESSING 44
5.1 Geological Data *44*
5.2 Satellite Imagery *47*
5.2.1 Landsat ETM+ data 47

5.2.2 Shuttle Radar Topography Mission (SRTM) 54
5.3 Geophysical Data *56*
5.3.1 Airborne radiometric data 56
5.3.2 Airborne magnetic data 69
5.3.2.1 Total Magnetic Intensity (TMI) 70
5.3.2.2 First Vertical Derivative (FVD) 71
5.3.2.3 Reduction to Magnetic Pole (RTP) 72
5.3.2.4 Total Horizontal Derivative (THD) 75
5.3.2.5 Normalised Total Horizontal Derivative (TDX) 76
5.3.2.6 Analytic Signal (AS) 78
5.3.2.7 Potential Field Tilt Derivative (TDR) 80
5.3.2.8 Horizontal Derivative of the TDR (HD-TDR) 82
5.3.2.9 Theta Map 83

CHAPTER 6 85

INTERPRETATION AND DISCUSSION 85
6.1 Structural Mapping *88*
6.2 Stratigraphy and lithological mapping *90*
6.2.1 Features not related to specific stratigraphy 95
6.2.2 Kuiseb Formation 105
6.2.3 Hakos Group, Nosib Group and Eastern Basement 111
6.2.4 Pre-Damara Succession 113
6.2.5 Okatjuru Layered Complex 121
6.2.6 Ekuja-Otjihangwe Nappe Complex 123
6.3 Discussion *125*

CHAPTER 7 130

CONCLUSIONS 130

REFERENCES 132

APENDIX A 138

Metadata Files for Landsat Images: *138*

LIST OF TABLES

Table *Page*
TABLE 2.1: FACIES AND LITHOSTRATIGRAPHY OF THE DAMARA SEQUENCE AS PROPOSED BY PORADA (1985). 8
TABLE 4.1: NAVACHAB MINERAL RESOURCES AS AT 31 DECEMBER 2010. 29
TABLE 4.2: EXPECTED GEOPHYSICAL RESPONSE FOR POSSIBLE MINERAL OCCURRENCES IN STEINHAUSEN PROJECT AREA 37
TABLE 5.1: LANDSAT ETM+ IMAGE DETAILS 47
TABLE 5.2: DARK PIXEL EXCLUSION APPLIED TO LANDSAT ETM+ IMAGES 49
TABLE 5.3: RADIOMETRIC IMAGES STATISTICS 56
TABLE 6.1: SINGULAR MAGNETIC ANOMALIES 97

LIST OF FIGURES

Figure *Page*
FIGURE 1.1: STEINHAUSEN PROJECT AREA - LOCATION MAP. 3
FIGURE 1.2: STEINHAUSEN PROJECT AREA - FARM BOUNDARIES. 4
FIGURE 2.1: PRINCIPAL SUBDIVISION OF THE INTRACONTINENTAL BRANCH OF THE DAMARA OROGEN (AFTER PORADA, 1985; CORNER, 2008). 6
FIGURE 2.2: GEOLOGICAL SURVEY OF NAMIBIA GEOLOGY MAP. THE STUDY AREA ENCOMPASSES THE SHOWN LICENSES. 10
FIGURE 2.3: TECTONOSTRATIGRAPHIC SUBDIVISION OF THE UPPER BLACK NOSSOB RIVER AREA (AFTER KASCH, 1986). 11
FIGURE 5.1: EXTENT OF GEOLOGICAL MAPPING BY K.W. KASCH (1998, 2008). 45
FIGURE 5.2: DETAILED GEOLOGICAL MAPPING BY K.W. KASCH (1998, 2008). 46
FIGURE 5.3: FALSE COLOUR IMAGE OF LANDSAT (RED – BAND 4; GREEN – BAND 3; BLUE – BAND 2). 48
FIGURE 5.4: FALSE COLOUR IMAGE OF LANDSAT (RED – CLAY INDEX; GREEN – EXTENDED FE INDEX; BLUE – VEGETATION INDEX). 51
FIGURE 5.5: FALSE COLOUR IMAGE OF LANDSAT (RED – CLAY INDEX; GREEN – EXTENDED FE INDEX + CLAY INDEX; BLUE – EXTENDED FE INDEX). 52
FIGURE 5.6: FALSE COLOUR IMAGE OF LANDSAT DATA OVER EKUJA-DOME AREA. (RED – CLAY INDEX; GREEN – EXTENDED FE INDEX; BLUE – VEGETATION INDEX). 53
FIGURE 5.7: FALSE COLOUR IMAGE OF LANDSAT DATA OVER EKUJA-DOME AREA. (RED – CLAY INDEX; GREEN – EXTENDED FE INDEX + CLAY INDEX; BLUE – EXTENDED FE INDEX). 54
FIGURE 5.8: SHUTTLE RADAR TOPOGRAPHY MISSION - DIGITAL ELEVATION DATA OVER STUDY AREA. 55
FIGURE 5.9: HISTOGRAMS OF RADIOMETRIC IMAGES. 57
FIGURE 5.10: TOTAL COUNT RADIOMETRIC DATA. 58
FIGURE 5.11: TERNARY IMAGE OF RADIO-ELEMENT CONCENTRATION. 59
FIGURE 5.12: TERNARY IMAGE OF RADIO-ELEMENT CONCENTRATION WITH FIRST-ORDER TREND REMOVED. 60
FIGURE 5.13: HISTOGRAMS OF TREND REMOVED RADIOMETRIC IMAGES. 61
FIGURE 5.14: TERNARY IMAGE OF RADIO-ELEMENT CONCENTRATION STRETCHED TO TC RANGES. 62
FIGURE 5.15: POTASSIUM TO THORIUM RATIO. 64
FIGURE 5.16: URANIUM TO THORIUM RATIO. 65
FIGURE 5.17: SUM-NORMALISED RADIOELEMENT DATA, TERNARY IMAGE. 66
FIGURE 5.18: MAXIMUM-LIKELIHOOD CLASSIFICATION CLUSTER PROPERTIES. 67
FIGURE 5.19: MAXIMUM-LIKELIHOOD CLASSIFICATION OF NORMALISED RADIO-ELEMENT DATA. 68
FIGURE 5.20: TOTAL MAGNETIC INTENSITY IMAGE FROM THE GSN AIRBORNE MAGNETIC SURVEY. 70
FIGURE 5.21: FIRST VERTICAL DERIVATIVE (FVD) IMAGE FROM THE GSN AIRBORNE MAGNETIC SURVEY. 71
FIGURE 5.22: TOTAL MAGNETIC INTENSITY (TMI) IMAGE FROM THE GSN AIRBORNE MAGNETIC SURVEY OVER EKUJA DOME. 73
FIGURE 5.23: REDUCED TO MAGNETIC POLE (RTP) IMAGE FROM THE GSN AIRBORNE MAGNETIC SURVEY OVER EKUJA DOME. 74
FIGURE 5.24: TOTAL HORIZONTAL DERIVATIVE (THD) IMAGE FROM THE GSN AIRBORNE MAGNETIC SURVEY OVER EKUJA DOME. 75

FIGURE 5.25: NORMALISED TOTAL HORIZONTAL DERIVATIVE (TDX) IMAGE FROM THE GSN AIRBORNE MAGNETIC SURVEY OVER EKUJA DOME. 77
FIGURE 5.26: ANALYTIC SIGNAL (AS) IMAGE FROM THE GSN AIRBORNE MAGNETIC SURVEY OVER EKUJA DOME. 79
FIGURE 5.27: POTENTIAL FIELD TILT (TDR) IMAGE DERIVED FROM THE GSN AIRBORNE MAGNETIC SURVEY TMI OVER EKUJA DOME. 81
FIGURE 5.28: HORIZONTAL DERIVATIVE OF THE TDR (HD-TDR) IMAGE DERIVED FROM THE GSN AIRBORNE MAGNETIC SURVEY TMI OVER EKUJA DOME. 82
FIGURE 5.29: THETA MAP IMAGE DERIVED FROM THE AIRBORNE MAGNETIC SURVEY TMI OVER EKUJA DOME. 83
FIGURE 6.1: FVD FROM THE GSN AIRBORNE MAGNETIC SURVEY OF THE STEINHAUSEN PROJECT AREA. 86
FIGURE 6.2: TERNARY IMAGE FROM THE GSN AIRBORNE RADIOMETRIC SURVEY OF THE STEINHAUSEN PROJECT AREA. 87
FIGURE 6.3: STRUCTURAL INTERPRETATION OF STEINHAUSEN PROJECT AREA. 89
FIGURE 6.4: INTERPRETATION MAP OF STEINHAUSEN PROJECT AREA 91
FIGURE 6.5: LEGEND FOR INTERPRETATION MAP OF STEINHAUSEN PROJECT AREA. 94
FIGURE 6.6: FEATURES NOT RELATED TO SPECIFIC STRATIGRAPHY. 95
FIGURE 6.7: GEOPHYSICAL INTERPRETATION LEGEND FOR FIGURE 6.6 – FEATURES NOT RELATED TO SPECIFIC STRATIGRAPHY. 96
FIGURE 6.8: FORWARD MODEL OF STEINHAUSEN ANOMALY ALONG PROFILE B,B' (FIGURE 6.6). 99
FIGURE 6.9: ANOMALOUS URANIUM OVER STEINHAUSEN PROJECT AREA. 101
FIGURE 6.10: KUISEB FORMATION; HAKOS GROUP, NOSIB GROUP AND EASTERN BASEMENT; PRE-DAMARA SUCCESSION. 104
FIGURE 6.11: GEOPHYSICAL INTERPRETATION LEGEND FOR FIGURE 6.10 – KUISEB FORMATION. 105
FIGURE 6.12: COMPARISON OF MAGNETIC DATA OVER THE MATCHLESS MINE AND ANOMALIES WITHIN THE KUISEB FORMATION IN THE STEINHAUSEN PROJECT AREA... 110
FIGURE 6.13: GEOPHYSICAL INTERPRETATION LEGEND FOR FIGURE 4.10 – HAKOS GROUP, NOSIB GROUP AND EASTERN BASEMENT. 111
FIGURE 6.14: GEOPHYSICAL INTERPRETATION LEGEND FOR FIGURE 4.10 – PRE-DAMARA SUCCESSION (UPPER ARENACEOUS UNITS POSSIBLY CONSTITUTING THE NOSIB GROUP). 113
FIGURE 6.15: OKATJURU LAYERED COMPLEX; EKUJA-OTJIHANGWE NAPPE COMPLEX. 120
FIGURE 6.16: GEOPHYSICAL INTERPRETATION (A) AND LEGEND (B) – OKATJURU LAYERED COMPLEX (FROM FIGURE 6.15). 121
FIGURE 6.17: GEOPHYSICAL INTERPRETATION (A) AND LEGEND (B) – EKUJA-OTIHANGWE NAPPE COMPLEX (FROM FIGURE 6.15). 123
FIGURE 6.18: GEOPHYSICAL INTERPRETATION SUMMARY MAP 128

Chapter 1

INTRODUCTION

The northeast-trending branch of the Damara Orogenic Belt of central Namibia hosts various known mineral deposits, inter alia, the Matchless Belt stratiform massive sulphide deposits at the Otjihase- and Matchless Mines, the Omitiomire copper deposit, hydrothermal copper deposits at the Onganja mine and manganese deposits at the Otjosondu Manganese fields. In the vicinity of Steinhausen, located approximately 145 km northeast of Windhoek, the Damara Belt becomes increasingly covered by recent Kalahari cover sediments resulting in little known geology and subsequent lack of discovered economic mineral deposits. Regional geophysical data, limited exposures and past drilling information do, however, confirm the eastward continuation of the Damara Orogen, making the eastern areas highly prospective.

With this in mind, Cheetah Minerals Exploration (Pty) Ltd (Cheetah) acquired an Exclusive Reconnaissance License (ERL 74) over the Steinhausen Area that was investigated using published mapping, historic exploration results and the latest airborne geophysical data (Corner, 2006). Based on initial findings Exclusive Prospecting Licenses (EPL) were then acquired over the area.

Geological mapping of the area is severely hindered by the extensive Kalahari cover sediments. To overcome this fact, Craton Mining and Exploration (Pty) Ltd. (Craton) in Joint Venture with Cheetah, commissioned a detailed geophysical interpretation of the area in order to identify possible exploration targets within the 6 EPLs (collectively known as the Steinhausen License Block).

The object of this study is to compile a synergistic interpretation of the Steinhausen Area, an area of 10,237 km^2 encompassing the Steinhausen Licence Block (Figure 1.1), using existing airborne geophysical data as well as all other available geological information, in order to derive prospective target areas for follow-up exploration.

Geophysical datasets comprising medium resolution airborne magnetic and radiometric data were purchased from the Geological Survey of Namibia (GSN). Other products purchased from the GSN include preliminary digital 1:250,000 maps for the Windhoek and Otjiwarongo sheets as well as the 1980 1:1,000,000 digital Geological Map of Namibia. Additional geological data, that became available as the project progressed, included detailed field mapping by Dr. Karl Kasch in selected areas, as well as exploration borehole information.

The coordinate system used during interpretation and for all images produced in this thesis is WGS84 / UTM zone 33S. Figure 1.2 shows the study area in more detail including farm boundaries and names covered by the survey.

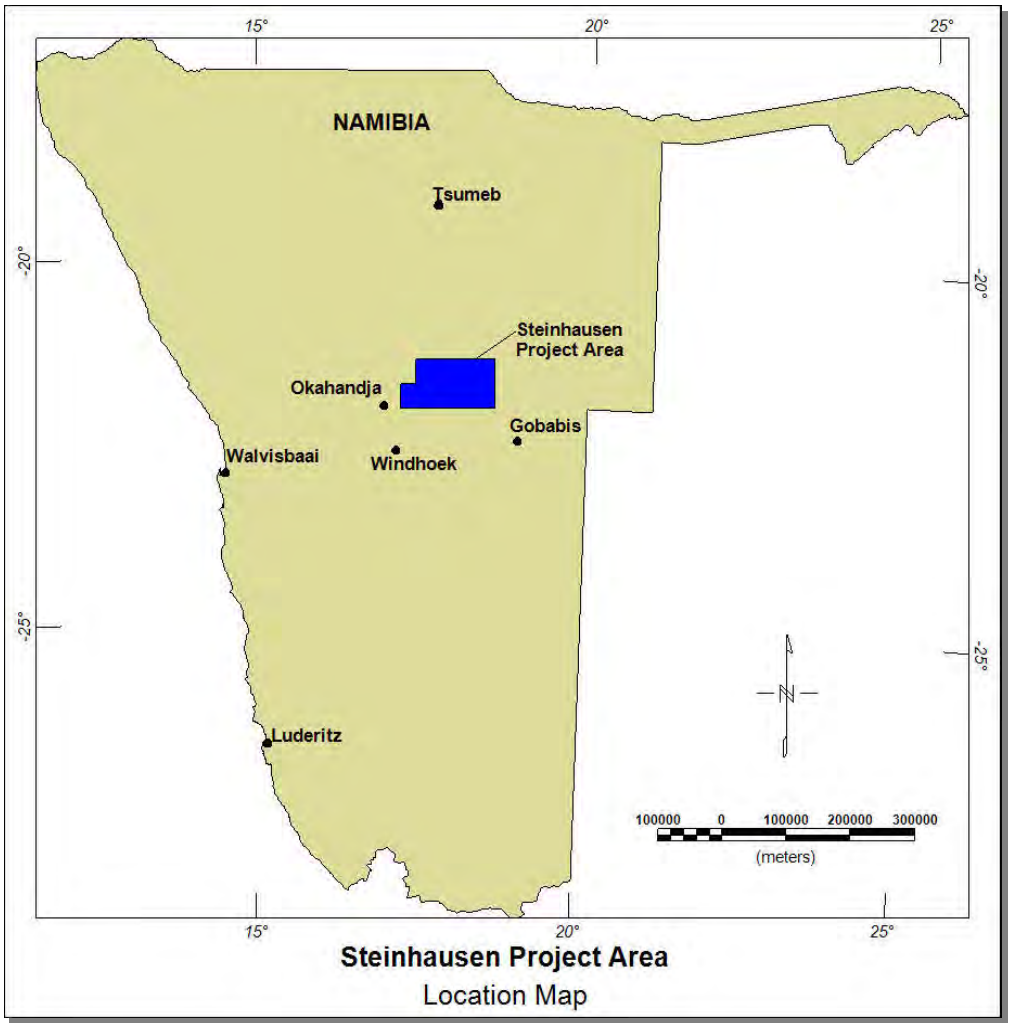

Figure 1.1: Steinhausen Project Area - location map.

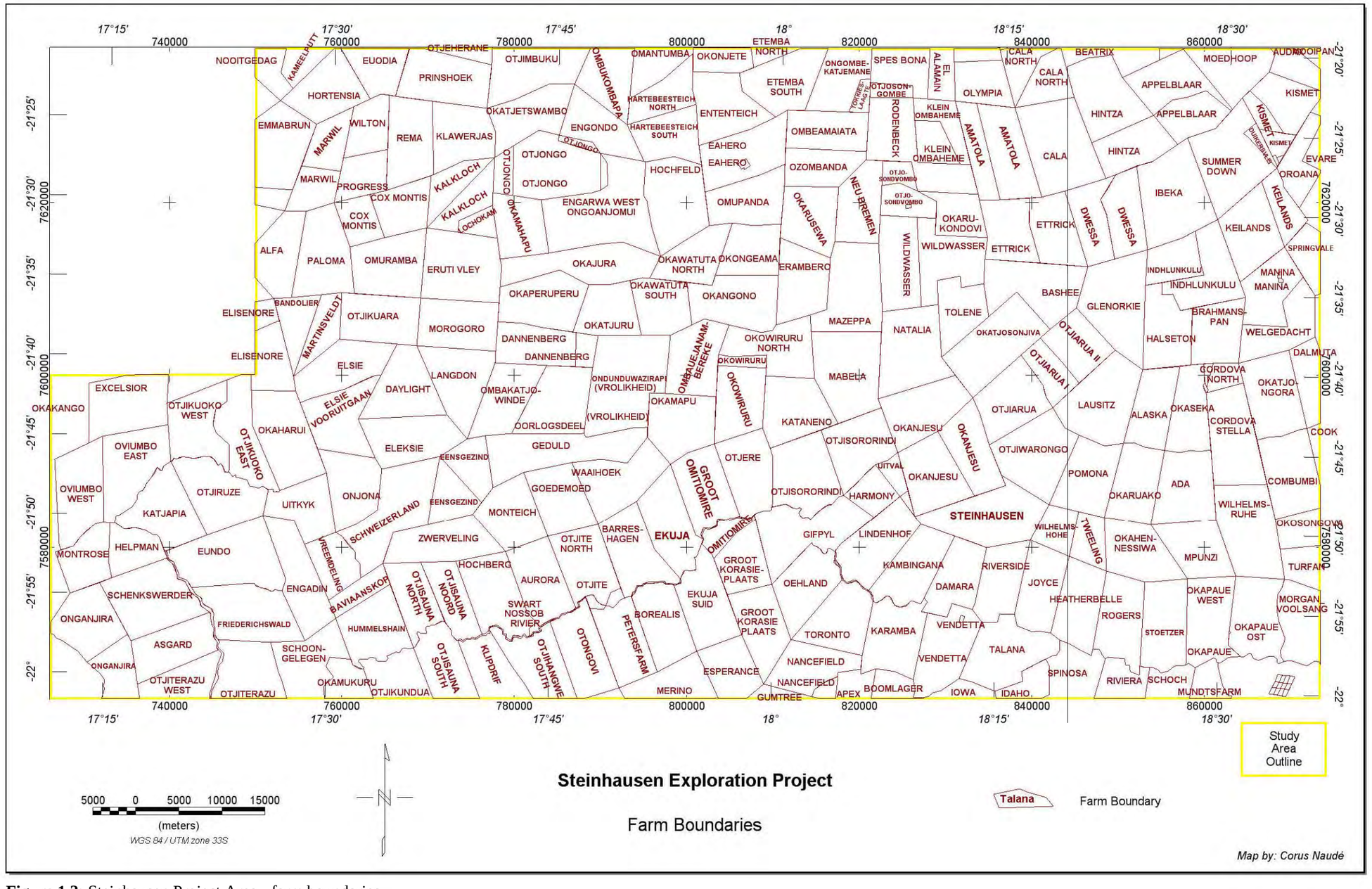

Figure 1.2: Steinhausen Project Area - farm boundaries.

Chapter 2

GEOLOGICAL SETTING

2.1 The Damara Orogen

The Damara Orogen consists of two divergent branches, one northward trending coastal branch that parallels the Atlantic coast in northern Namibia, and the other, an east-northeast trending intracontinental branch in north-central Namibia (Porada, 1985). Within the intracontinental branch, the Damara Orogen has been divided into several zones on the basis of stratigraphy, structure, grade of metamorphism, intrusives, age and aeromagnetic expression (Miller, 1983a; Corner, 2008). Figure 2.1 shows the main structural subdivisions of the intracontinental branch of the Damara Orogen in relation to the Steinhausen Study Area.

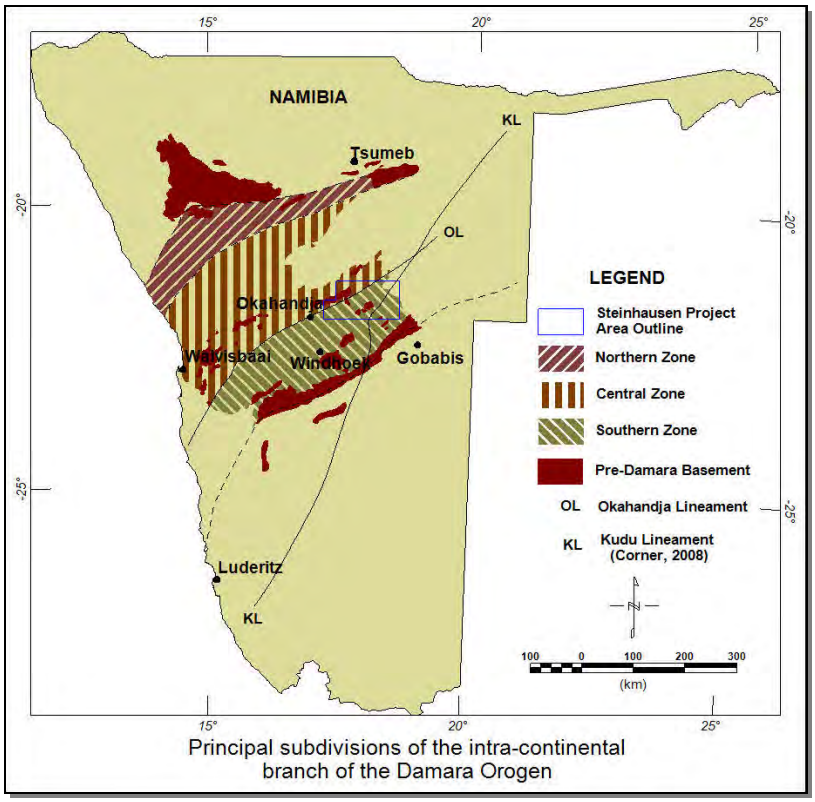

Figure 2.1: Principal subdivision of the intracontinental branch of the Damara Orogen (after Porada, 1985; Corner, 2008).

The depositional environments of Damaran rocks range from original rifting and spreading, to subsequent subduction and continental collision (Miller, 1983a). The basal succession (Nosib Group), consisting of quartzite, arkose, conglomerate, phyllite, calc-silicate and subordinate limestone and evaporitic rocks, were deposited in or proximal to intracontinental rifts (Miller, 1992b). Initial rifting was followed by carbonate deposition with very minor clastics (Otavi Group) on a stable platform, and variable depositional environments south thereof resulting in the formation of interbedded mica- and graphitic shists, quartzite, massflow deposits, iron-formation and within-plate basic lava (Kudis, Ugab and basal Khomas Subgroups, Miller, 1992b). These rocks were in turn overlain by the Kuiseb Formation (Miller, 1992b), which in the Southern Zone (SZ) or Khomas Trough is dominated by flysch-type metasedimentary rock, predominantly comprising a uniform succession of quartz-plagioclase-biotite schists with lesser graphitic and garnet-, kyanite-, staurolite-bearing varieties, as well as minor calc-silicate and amphibole-epidote metavolcanic layers (Moore, 2010).

Miller (1992b) summarised events related to the deformation that resulted from subduction and continental collision as follows:

- Deposition of Mulden Group (arenite and pelite) in the north, above Otavi Carbonates.

- Deposition of uppermost greywackes of the Kuiseb Formation as a fore-arc basin sequence in the SZ and deposition of the lower Nama Group in a foreland basin.

- Deposition of Upper Nama Group in the south.

- Syntectonic emplacement of serpentinites along the Southern Margin.

- Syn- to post-tectonic intrusion of granites in the Central Zone (CZ).

The Lithostratigraphy of the Damara Sequence as proposed by Porada (1985) is shown in Table 2.1 below.

Table 2.1: Facies and lithostratigraphy of the Damara Sequence as proposed by Porada (1985).

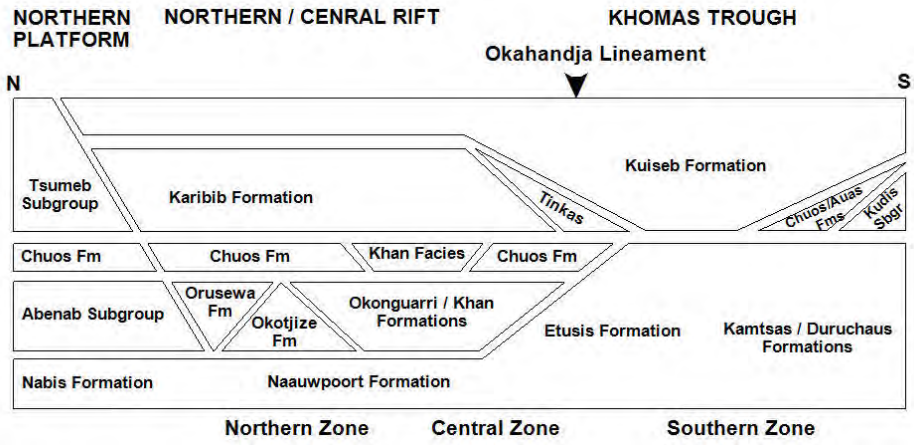

2.2 Geology of the Steinhausen Study Area

The Steinhausen Study Area is set within the CZ and the SZ of the Damara Orogenic Belt, in which structurally controlled windows of pre-Damaran basement occur. The area straddles two major northeast-trending crustal structures, the Okahandja (OL) and Kudu (KL) Lineaments, which are interpreted to have played a role in exposing pre-Damaran stratigraphy in the area (Corner, 2008).

Figure 2.2 shows a compilation of the GSN 1:1,000,000 geological map of Namibia (1980) and the 1:250,000 geological sheets of Windhoek and Okahandja. Due to the paucity of outcrop in the area, the geological description is of a very general nature.

More detailed localised geological mapping has been conducted in some parts of the study area, notably by Kasch (1986) in the upper Black Nossob River

area and in the western part of the study area, but is also limited in detail due to poor outcrop. Additional geological information has been derived from mapping and drillhole logs compiled by various exploration companies that historically held EPLs in the area.

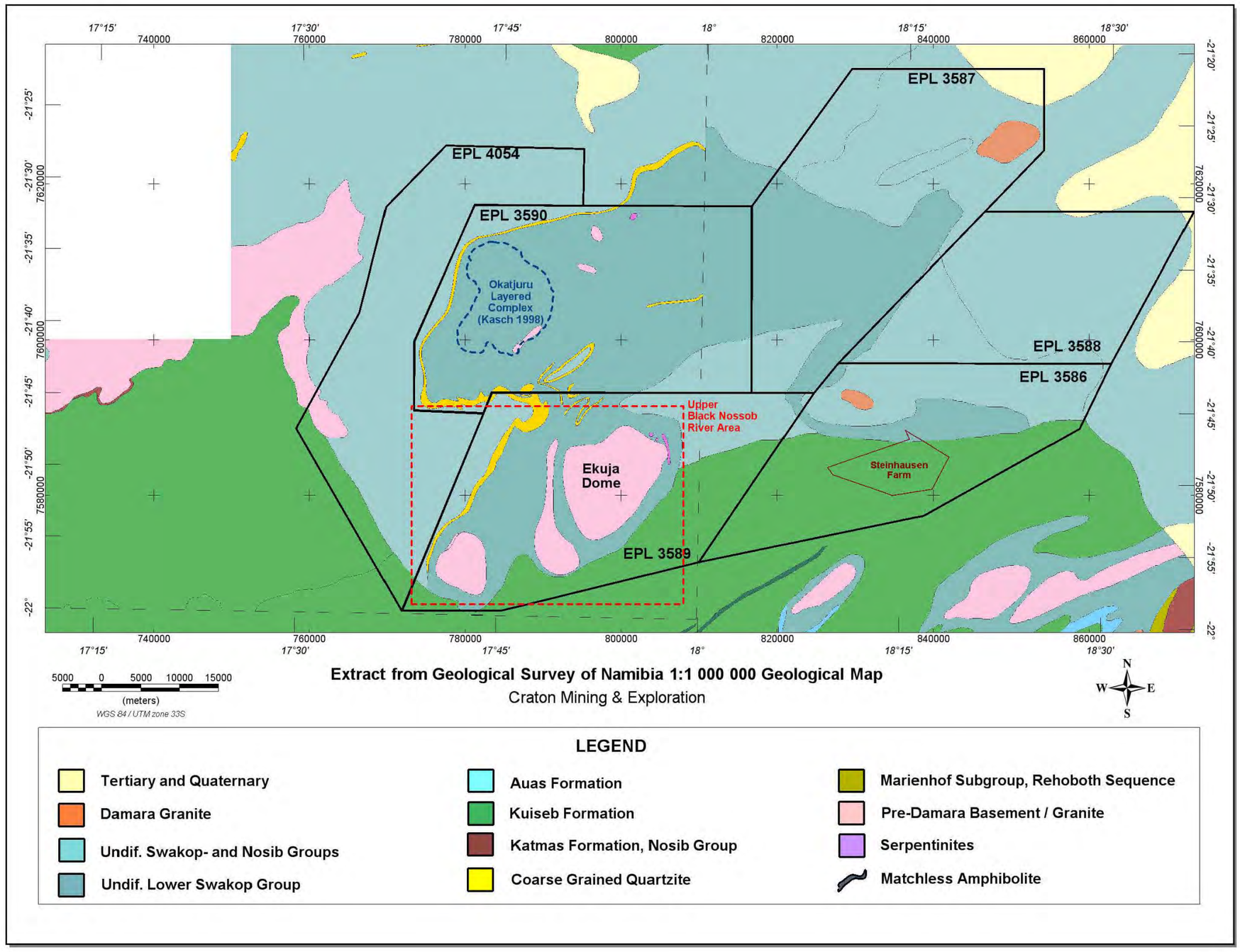

Figure 2.2: Geological Survey of Namibia geology map. The study area encompasses the shown licenses.

In the south-western portion (upper Black Nossob River area) of the study area, Kasch (1986) has distinguished three major tectonostratigraphic units (Figure 2.3) namely the Ekuja-Otjihangwe Nappe Complex (EONC), the Onjona-Vrolikheid Fold Complex (OVFC) and the Onyati Mountains Schist Belt (OMSB).

The EONC comprises a pre-Damara basement (amphibole, epidote and biotite schist) inlier (Steven *et al.*, 2000) underlying Damaran rocks, the majority of which were correlated with the Vaalgras Subgroup (biotite-muscovite schist, garnet- and kyanite-bearing schist, hornblende- and garnet-bearing schist, quartzite, and amphibolite with minor marble and calc-silicate rock), and minor occurrences of the Kudis Subgroup (thinly bedded platy quartzite and graphitic schist). Recent work (Corner, Kasch, pers. comm. 2009) has shown that these Damaran rocks are now accepted to be part of the Kuiseb Formation and not of the Vaalgras or Kudis Subgroups.

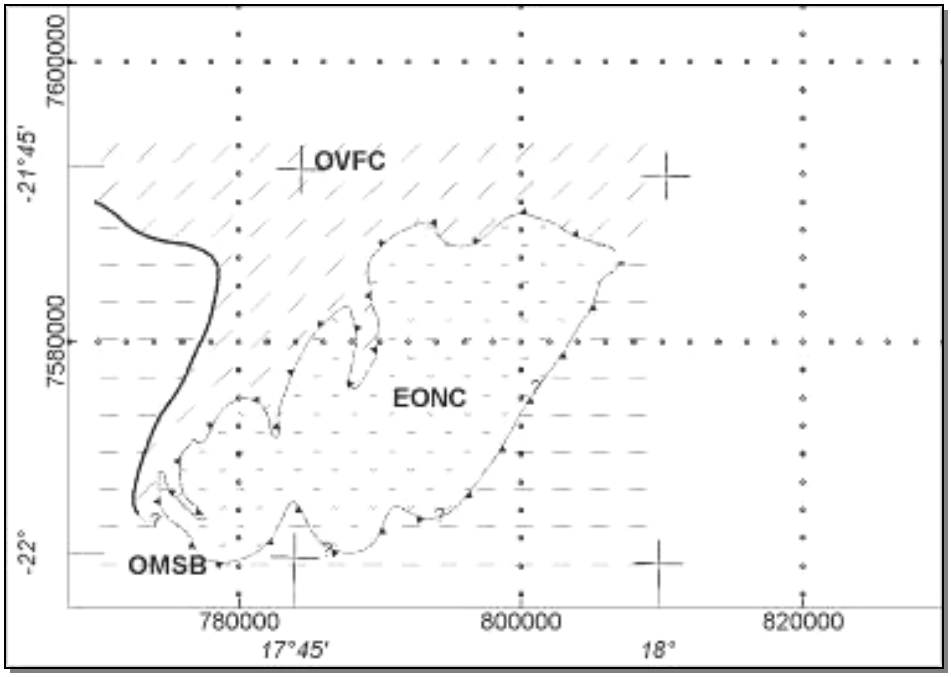

Figure 2.3: Tectonostratigraphic subdivision of the upper Black Nossob River Area (after Kasch, 1986).
EONC - Ekuja-Otjihangwe Nappe Complex, OVFC - Onjona-Vrolikheid Fold Complex, OMSB - Onyati Mountains Schist Belt.

The OVFC is separated from the EONC by the Hochberg thrust and consists of coarse-grained, white quartzite, white to pale blue marble, and minor grey quartz-muscovite schist. This same stratigraphy has been mapped further to the north-northwest by Kasch (1998) during field investigation by Mount Isa Mines Namibia (Pty) Ltd. in 1998. Although represented as Undifferentiated Lower Swakop Formation on GSN maps, Hoffmann (1989b) has questioned the inclusion of this stratigraphic unit into the Khomas Zone of the Damara sequence, and suggests that it is of pre-Damara age correlating with upper units of the Abbabis Metamorphic complex overlain by metasediments similar to the Duruchaus Formation of the Nosib Group which in turn is overlain by Kuiseb Formation schist.

The OMSB consists of the Kuiseb Formation of the upper Damara Sequence. Some syn-tectonic pegmatites have intruded the Kuiseb schists in the western extreme of the study area.

Towards the central-western side of the study area, Mount Isa Mines (MIM) identified a sequence of ultramafic rocks, amphibolites and anorthosites, based on Kasch's (1998) mapping. This sequence has been interpreted as a metamorphosed layered complex that has intruded basement gneiss and has been termed (by MIM) the Okatjuru Layered Complex (OLC).

Craton initiated further mapping which was completed during 2008 to the west and southwest of the OLC by Kasch (Corner, pers. comm., 2009). Here Kasch showed that the Kuiseb Formation in the southwest of the interpretation area includes an upper marble and a lower amphibolite unit. Also apparent is the occurrence of a glassy quartzite as part of the upper pre-Damara basement sequence.

Historical exploration to investigate the north-eastward extension of the Matchless Amphibolite Belt (MAB) was completed by Anglovaal in the south-eastern part of the study area. This resulted in a number of drillhole intersections of mostly schist and minor amphibolite of the Kuiseb

Formation (1997 EPL reports). Mapping by Gold Fields Prospecting Co (Pty) Ltd (Charles, 1987) has suggested the occurrence of Auas Formation rocks (feldspathic micaceous quartzites) collaring the Karamba Dome on the farms Karamba and Vendetta. This therefore places the Auas Formation within the Vaalgras Subgroup. This is in contrast to the stratigraphy as described by Hoffmann (1989a) where the Auas Formation is included as part of the Kudis Subgroup within the Hakos Terrane of the Southern Marginal Zone. For the purpose of this study Hoffmann's stratigraphy will be followed.

Chapter 3

KNOWN MINERAL OCCURRENCES AND DEPOSITS WITHIN STEINHAUSEN PROJECT AREA

3.1 Omitiomire copper deposit

The Omitiomire copper deposit, situated 120km northeast of Windhoek, was located by General Mining and Finance Corp (GMFC) from regional soil geochemistry in the mid 1970's (Corner, 2006). Intermittent exploration at Omitiomire since 1976 included soil geochemical, induced polarization (IP) and magnetic surveys with percussion and core drilling (Steven *et al.,* 2000).

Since 2007, Craton have completed more IP, magnetic and geochemical sampling and by November 2009 completed RC and diamond drilling totalling over 42,000 m. From this work, a resource of ore at Omitiomire was estimated, at a cut-off grade of 0.25% Cu, to be 117mT at 0.50% Cu of which approximately 80% are in the Inferred category and 20% in the Indicated category (K. Hartmann, pers. comm., 2011).

The Omitiomire deposit is hosted within the Ekuja basement dome (Kibaran-age) which comprises quartz-feldspar gneiss, amphibole and biotite-bearing schist and amphibolite. The copper mineralisation occurs within a zone of banded schist and mafic gneiss which underlies a unit of massive unmineralised quartz-feldspar (felsic) gneiss. The mineralisation occurs mainly as chalcocite and is preferentially concentrated in bands of epidote-bearing mafic rock, either in dark biotite schist, banded quartz-plagioclase-biotite-hornblende schist or in amphibolite (IBML, 2008).

The mineralised body strikes north-south, plunges to the north, and dips gently towards the east. It is cut by, or possibly associated with, later north-south trending faults (IBML 2009). Shrimp U-Pb ages for zircon cores are between 1115 Ma and 1063 Ma for the rocks of the mineralised sequence,

with zircon overgrowths and rims dated at approximately 600 Ma which is suspected to be the age of the main chalcocite-mineralising event (Steven *et al.*, 2000).

3.2 Copper geochemical anomalies

Various geochemical copper anomalies have been identified within the study area, more precisely on the farms Oorlogsdeel, Waaihoek, Ombakatjowinde and Vrolikheid (Schneider and Seeger, 1992). Historical exploration showed pyrrhotite, pyrite and chalcopyrite occurring as dissemination, veins and lenses mostly in association with amphibolite and calc-silicate rock together with biotite schist, quartzite, marble and gneiss.

Within the south-eastern portion of the study area further copper occurrences have been identified on the farms Karamba, Vendetta and Talana (Charles 1987). From Charles (1987), the anomalies on the farms Karamba and Vendetta are associated with metasediments surrounding the leucogneissic Karamba Dome, while on the farm Talana it is suggested that the copper is associated with amphibolite of the Matcheless Member (Kuiseb Formation).

3.3 Manganese occurrences

The farms Hochfeld and Eahero in the north-central part of the study area host a siliceous, ferruginous manganese horizon of at least 2m thick that could possibly be correlated with the Otjosondu Manganese Field which occurs to the west (Schneider, 1992).

3.4 Nickel occurrences

On the farm Oorlogsdeel a slightly anomalous nickel soil sample was reported (Roesener and Schreuder, 1992). No mention is made of possible underlying geology. The OLC as mapped by Kasch (1998) could be considered as a possible origin for this nickel anomaly.

Nickel concentrations of up to 991 ppm occur within the mafic schists that host the Omitiomire copper deposit (K. Hartmann, pers. comm., 2011).

Chapter 4

MINERAL DEPOSIT MODELS AND SOME EXAMPLES

Due to the geological setting of the Steinhausen Project Area, a few possible mineralisation styles can be envisaged.

4.1 Matchless stratiform massive sulphides

The Matchless Amphibolite Belt (also referred to as the Matchless Member) is a narrow linear unit of metabasites (mainly amphibolites) interlayered with quartz-mica schists of the Kuiseb Formation (Klemd *et al.,* 1989). Its geologically mapped strike extent is some 300 km, extending from east of Walvis Bay to the Steinhausen area. Various massive and semi-massive pyritic copper occurrences are associated with the Matchless Member, viz. Hope, Gorob, Niedersachsen, Matchless, Otjihase, Ongeama and Ongombo.

The Kuiseb formation consists of a thick succession of alternating quartz-rich and mica-rich schists (Miller *et al.,* 1983) while the amphibolites represent metamorphosed tholeiitic basaltic rocks that formed within an extensional tectonic setting (Breitkopf, 1988). The eastern part of the Matchless Member was emplaced as thin oceanic crust, and associated massive sulphide deposits were thus formed in a tectonic setting of initial ocean-floor spreading (Breitkopf, 1988), who also drew the comparison between the geology and geochemistry of the Matchless massive sulphide occurrences and Besshi-type deposits in the Sanbagawa Belt of south-western Japan.

A short discussion of mines situated along the eastern part of the Matchless Member follows:

4.1.1 Matchless Mine

The Matchless Mine, located 30 km southwest of Windhoek, was first exploited by Walwich Bay Copper Mining Company, which worked what is known today as the River Shoot Gossan from the 1850s until operation ceased in 1862 (Schneider and Seeger, 1992). Thereafter the mine passed through the hands of various small producers until 1961 when it was properly re-evaluated by the Tsumeb Corporation Ltd., and later put in production from 1970 to 1983 during which time production amounted to a total of 1.35 million ton grading 2.12% copper and 14.8% sulphur. The remaining reserves total 563 000 tons at an average grade of 2.21% copper (Schneider and Seeger, 1992). Mining activities were recently re-commenced by Weatherly International plc.

The lithology of the Matchless Mine can be described as follows (from Schneider and Seeger, 1992):

- Footwall Schist: quartz-biotite-sericite schist of the Kuiseb Formation.

- Footwall Amphibolite: intercalated large isolated lenticular bodies of dark green, medium to coarse-grained, compact, quartz-amphibole rock.

- Transition Schist: biotite-sericite rock containing frequent quartz lenses.

- Sericitic Quartzite: regularly foliated, silvery-white, pyritic quartz-sericite schist with sections of light-grey sericite quartzite. The principle host rock is characterized by heavy pyrite mineralisation and concentration of chalcopyrite mineralisation towards the hanging wall contact. A band consisting of chlorite-biotite-amphibole schist serves

as a marker horizon in mining because it coincides roughly with the lower limits of the ore-grade copper mineralisation.

- Intermediate Schist: quartzose biotite-sericite schist with stringers of chlorite schist and sericitic quartzite as well as bands of magnetite quartzite.

- Amphibolite Schist: dark olive-green, chlorite-biotite-amphibole schist, in places talcose and crumbly, characterised by the presence of large quartz boudins and well developed amphibole needles. The mineralisation within this unit is hosted by interbedded quartzite bands.

- Hanging wall Amphibolite: massive amphibolite with interbeds of mineralised magnetite quartzite.

- Hanging wall Schist: Identical to Footwall Schist.

The sulphide minerals at Matchless Mine are pyrite, chalcopyrite, pyrrhotite plus marcasite, sphalerite, bornite and galena (Schneider and Seeger, 1992). Klemd *et al.* (1989) favoured a two-stage process of copper concentration: an initial pre-metamorphic and pre-deformation concentration into a stratigraphic zone of sulphide-bearing rock and a subsequent metamorphic upgrading by the movement of copper in solution to produce structurally controlled ore shoots. This explains the occurrence of more stratabound pyrite as opposed to more structurally controlled chalcopyrite.

Klemd *et al.* (1989) described the deposit as consisting of three ore shoots of massive sulphide rock, plunging to the west at 30 º to 35º. The ore shoots are separated from one another by the sulphide-bearing Sericitic

Quartzite Unit. Each ore shoot is about 3 m thick and 120 m in strike length, and has been traced down-plunge to the NNW for 600 m by drilling.

4.1.2 Otjihase Mine

The Otjihase ore body was first developed by the Otjihase Mining Company in the early 1970s reaching production stage by 1975. Following a halt in production from 1979, the mine was redeveloped in 1982 and by the end of 1991 the ore reserves amounted to 10.177 million tons containing 2.62% copper, 20% sulphur and 10 g/t silver (Schneider and Seeger, 1992).

From Schneider and Seeger (1992) the geology of the Otjihase Mine is summarized below:

- In the vicinity of the mine, the Matchless Member consists of amphibolitic rocks and talc-chlorite schist forming discontinuous layers and lenses in the garnetiferous biotite-quartz and biotite-chlorite schists of the Kuiseb Formation. Magnetite quartzite present as both persistent beds (south-western part of deposit) and discontinuous lenses (lenticular pods or boudin-like structures) is considered to be an integral part of the ore deposition.

- Both secondary and primary ore zones are distinguished: the secondary body consists of reddish-brown gossan, ferruginous schist and magnetite quartzite. The mineralisation within the secondary ore includes limonitic boxworks with rare malachite and chrysocolla. The primary ore body consists of magnetite quartzite, variable schist and occasional amphibolite. Ore minerals include pyrite, chalcopyrite and sphalerite with minor pyrrhotite.

- A prominent ore shoot is present near the northern limits of the deposit. This ore shoot plunges about 14º north-westwards and follows a well-developed lineation observed in surface outcrops of magnetite quartzite. Small-scale isoclinal / recumbent folding in the ore zone suggests the possible presence of a large recumbent fold. The ore body is also cut by north-south trending faults with down throw to the west.

4.1.3 Ongeama Prospect

The Ongeama Prospect, situated 10 km northeast of the Otjihase Mine, has been investigated since 1971 and is estimated to contain ore reserves that amount to 468 700 t at 1.26% copper, 0.46% zinc and 5.36 g/t silver (Schneider and Seeger, 1992). Disseminated to massive pyrrhotite, pyrite, chalcopyrite and sphalerite mineralisation is confined to a lenticular magnetite quartzite, which is present as a narrow, elongate shoot which dips 14° to 16° northwest and plunges 7° to 8° west.

4.2 Kuiseb Formation hosted hydrothermal copper deposits

Various copper deposits exist within the thick schist succession of the Kuiseb Formation. The copper deposits are described as hydrothermal chalcopyrite-bearing quartz veins (Miller, 1983b; Miller, 1992a). Moore (2010) concludes that the Kuiseb Formation hosted hydrothermal copper deposits are generally unrelated to the syngenetic massive-sulphide copper deposits of the Matchless Belt, as the former were formed in a compressional setting with hydrothermal fluids having a metamorphic origin, opposed to the extensional rift setting with hydrothermal fluids derived from mafic volcanic components in the latter.

4.2.1 Onganja Mine

The Onganja Mine is situated approximately 65 km southeast of Okahandja (Miller, 1983b) and has been mined on a small scale since 1960 (Schneider and Seeger, 1992). By 1987 the estimated reserves were less than 300,000 t at 2% copper (Schneider and Seeger, 1992).

From Schneider and Seeger (1992), the quartz-copper veins at Onganja are confined to the crest of an antiform that plunges gently to the west and is considered to be the upper part of a hydrothermal system that was generated at the intersection of two major faults, one north-trending and the other trending north-westerly. Primary mineralisation (coarse pyrite, chalcopyrite, chalcocite and molybdenite) occurs in quartz and calcite veins that are brecciated, steeply dipping and trend north-south at right angles to the foliation of the host Kuiseb Formation schist (Schneider and Seeger, 1992).

The host lithology at the Onganja mine consists of basal quartz-plagioclase-biotite schist, followed by epidote-quartz rock, amphibolites schist, a second quartz-plagioclase-biotite schist and graphitic schist (Moore, 2010). Epidote-quartz rocks (dominant presence of epidote with magnetite) occur as a broad zone of discontinuous lenses and boudins within the quartz-plagioclase-biotite schists, with most of the mineralised veins concentrated in the immediate footwall if the epidote-quartz unit (Moore 2010).

Two other small deposits in close proximity of the Onganja deposit that have been mined are the Otjozonjati Mine and Thorn Tree Mine. Both these deposits consist of copper mineralisation within northward striking, brecciated quartz veins dipping at approximately 45° east (Schneider and Seeger, 1992).

4.3 Manganese deposits

During the initial rifting stage of the Damara Orogen, pauses in widespread glaciation were marked by the deposition of siliceous iron formation with up to 49% manganese (Miller, 1992a). The Otjosondu area (northwest of the study area) is the only known occurrence of economic manganese accumulation in the Damara Orogenic Belt even though iron formations are widespread throughout (Bühn *et al.,* 1992).

4.3.1 Otjosondu Manganese Field

The Otjosondu Manganese Field is located 150 km northeast of Okahandja, covers an area of approximately 240 km^2, and was mined intermittently since 1950 (Schneider, 1992).

The lithostratigraphy at Otjosondu is summarised by Bühn *et al.* (1992) as follows:

- Kuiseb Formation schists form the upper bracket of the sequence.
- Upper quartzites: glassy quartzites consisting of mostly coarse grained quartz with minor amounts of disseminated hematite in places. Feldspar and mica are very rare.
- Manganese-bearing unit: predominantly hematite quartzite and hematite-rich gneiss. Two major manganese horizons occur at bottom and top of the unit which is in sharp contact with upper and lower quartzites.
- Lower quartzites: similar to upper quartzite.
- Basal gneiss and schist.

The Damara deformation has caused the ore to be discontinuous and has thickened bodies in the noses of folds (Schneider, 1992). Bühn *et al.* (1992) have defined the following ore types:

- Braunite-hematite-jacobsite ore: massive ore with variable amounts of braunite, hematite and other Mn-Fe minerals. No banding was observed.

- Banded ore: banding of 1 to 3 mm thick layers of Mn clinopyroxene and Mn garnet with interlayered Ti-bearing terrigenous sediments.

- Feldspatic ores: lower Mn content, increased content of potassium feldspars.

Secondary enrichment within ore is confined to small, near-surface veins filled with pyrolusite and psilomelane (Schneider, 1992).

Secondary manganese deposition is present as scree deposits (rounded pebble to boulder size fragments of primary ore directly derived from primary ore horizon) and manganocrete (dark interstitial crusts, coatings and concretions) precipitated into and onto peripheral sands and weathered bedrock (Schneider, 1992).

4.4 Magmatic Nickel, Copper and Platinum Group Element (PGE) deposits

Magmatic Ni-Cu-PGE deposits are found in association with ultramafic and mafic bodies in diverse geological settings (Eckstrand and Hulbert, 2007). These deposits can be broadly divided into 2 sub-types; Ni-Cu sulphide-rich

ore associated with differentiated mafic / ultramafic sills, stocks and ultramafic volcanic flows, and (mostly) PGE ore associated with mafic / ultramafic layered intrusions (Eckstrand and Hulbert, 2007).

Within the Steinhausen Project Area the Okatjuru Layered Complex (OLC) consisting of ultramafic rocks, amphibolites and anorthosites (Kasch 1998) is analogous to certain magmatic Ni-Cu-PGE deposits (e.g. Voisey's Bay Deposit, located in north-eastern Canada).

4.4.1 Voisey's Bay Deposit

The Voisey's Bay Intrusion, consisting of a series of olivine gabbros, troctolites, ferrogabros and ferrodiorites within the anorthositic Nain Plutonic Suite (Eckstrand and Hulbert, 2007; Lightfoot, 2007), hosts Cu-Ni sulphide ore. The deposit consists of a series of sulphide lenses located within a sub-vertical dyke connecting an upper and lower magma chamber (Eckstrand and Hulbert, 2007; Naldrett, 2010). The dyke is believed to be a feeder for the magma chambers and three main Ni-Cu zones are located in widened parts of the feeder dyke (Eckstrand and Hulbert, 2007).

Naldrett (2010) illustrates three controls of mineralisation: the feeder dyke at Discovery hill where sulphide mineralisation is present at a widened section of the dyke, the Ovoid deposit interpreted as either a widening of the dyke or the base of the upper chamber, and lastly, the feeder dyke joining the Eastern Deeps intrusion where sulphides are concentrated at the mouth of the feeder to the intrusion. These three controls illustrate the relation of sulphide concentration to areas where denser material brought up by the magma flowing up the dyke could settle due to the decrease in rate of magma flow (Eckstrand and Hulbert, 2007; Naldrett, 2010).

The sulphide mineralisation consists of pyrrhotite, pentlandite, chalcopyrite with additional troilite and magnetite (Eckstrand and Hulbert, 2007). Zoning at the Ovoid deposit consists of a magnetite-rich centre followed by a pentlandite and chalcopyrite-rich zone with a third, pyrrhotite-rich zone, and is broadly consistent with a sulphide body cooling from the outside in (Naldrett, 2010).

4.4.2 Alpine serpentinites within Damara Orogen

Alpine serpentinites, tectonically emplaced ultramafic bodies (Roesener and Schreuder, 1992) proximal to the study area also suggest the possibility of similar Ni occurrences. Roesener and Schreuder (1992) discussed four serpentinite bodies located on the farms Okatuma Ost, Otjihaenena and Eorondemba:

The serpentinite bodies consist of dark green serpentinite core, ringed by an alteration zone of talc and containing lenses of talc and chlorite schist. The nickel and copper mineralisation at surface is associated with brecciated serpentinite and were ascribed to surface enrichments.

4.5 Hydrothermal gold deposits

There are several examples of orogenic gold deposits from Proterozoic terranes, including Ashanti-Obuasi in West Africa, Homestake in the U.S.A. and Pilgrim's Rest in South Africa (Robb, 2005). The formation of these deposits involve metamorphic fluids that have formed from crustal thickening, deformation, metamorphism and synorogenic magmatism, with gold deposition being generally late orogenic and hosted in high-angle thrust faults (Robb, 2005). With the Damara Orogen, the most notable gold

occurrences are the Navachab Gold Mine and the Ondundu-Otjiwapa Gold Field.

4.5.1 Navachab Gold Mine

The Navachab Gold Mine is located on the farm Navachab, approximately 10 km southwest of Karabib (Mindat.org, 2011).

The deposit was discovered in 1984, during a geochemical survey where small gossan fragments returned assay values of up to 11 g/t gold. Following an appraisal in 1986, a feasibility study in 1987 and subsequent construction, the first gold was produced in December 1989 (Burnett, 1992) from open pit mining (AngloGold Ashanti, 2010). The mineral resource at Navachab Gold Mine as at December 2010 is summarised in Table 4.1 (AngloGold Ashanti, 2010).

Table 4.1: Navachab mineral resources as at 31 December 2010.

Category	**Tonnes (millions)**	**Grade (g/t)**	**Contained Gold**	
			(Tonnes)	**(Moz)**
Measured	9.03	0.58	5.24	0.17
Indicated	42.83	1.11	47.50	1.53
Inferred	23.33	1.13	26.41	0.85
Total:	**75.20**	**1.05**	**79.15**	**2.54**

The lithology of the Navachab Mine area is summarised as follows (from Burnett, 1992):

- Footwall: quartzites and arkoses (Nosib Formation), mixtites (Chuos Formation), biotite shists interbedded with para-amphibolites and scattered marble lenses (Spes Bona Member). Footwall contains abundant pyrrhotite and pyrite.

- Main orebody: Okawayo Member comprising a calc-silicate marble unit overlain by amphibolite and followed by a thick marble unit and a top mottled dolomitic marble unit.

- Hanging wall: siliclastic and metamorphosed volcanoclastic rocks (Oberwasser Member).

The lower units are intruded by steeply dipping aplite and pegmatite dykes and the presence of a late-stage, bismuth-, fluorite- and boron-rich diorite approximately 800 m northeast of the main ore body is believed to be a possible heat source for the final concentration of gold (Burnett, 1992).

The styles of mineralisation are summarised by Burnett (1992) as follows:

- Massive echelon skarn bodies, elongated in an ENE-WSW direction and plunging at 30° north. These bodies are strata-bound within banded calc-silicate marble unit, and gold mineralisation occurs with replacement lenses of pyrrhotite and minor pyrite, chalcopyrite, calc-silicate minerals, garnet, biotite and quartz.

- Hanging wall banded grey marbles and mottled dolomite marbles hosts north-plunging crosscutting vein stockworks. Gold mineralisation occurs in quartz-calcite veins.

Locally abundant to massive sulphides (pyrrhotite with accessory pyrite, minor chalcopyrite and sphalerite) do not host gold mineralisation but are often in close proximity (Burnett, 1992).

4.5.2 Ondundu-Otjiwapa Gold Field

Situated 90 km northwest of Omaruru, the Ondundu-Otjiwapa Gold Field was discovered in 1917 and exploited from 1924 to 1963 resulting in a

total production of 448.504 kg gold from both alluvial and hard-rock mining (Burnett, 1992).

The gold mineralisation is hosted in quartz-feldspar veins occurring parallel to bedding planes within metaturbidites (impure phyllite and quartz-mica-feldspar schist) of the Kuiseb Formation (Burnett, 1992). The deposit is confined to an area of approximately 10 km^2 of intense folding (Burnett, 1992). Small mineralised quartz veins contain calcite, siderite, pyrite and marcasite and are believed to be of hydrothermal origin with an average grade of 5.8 g/t gold (Burnett, 1992).

4.6 Uranium deposits

Nash and Granger (1981) list the following types of uranium deposits:

- quartz-pebble conglomerate deposits,
- unconformity-type deposits,
- deposits in ultrametamorphic rocks,
- classical vein deposits,
- deposits associated with igneous rocks,
- deposits in sandstone, and
- other deposits including calcrete-hosted deposits.

Considering the geological setting of the Steinhausen Area, the most likely deposit types that may be encountered in the survey area includes: calcrete-hosted deposits, classical vein deposits and deposits associated with igneous rock.

4.6.1 Calcrete-hosted uranium deposits

(a) The calcrete-hosted uranium deposits are classified as surficial uranium ores formed by accumulation of (mostly) carnotite within calcretised fluvial drainage channels (Robb, 2005), which represent the remains of rivers from previous high rainfall intervals that drained uranium-fertile source regions. The main process involved in the precipitation and concentration of uranium mineralisation is related to high rate of groundwater evaporation associated with arid climates (Robb, 2005). The Langer Heinrich Deposit serves as an example of a calcrete-hosted uranium deposit.

4.6.1.1 Langer Heinrich Deposit

A summary of the Langer Heinrich Deposit is discussed below (from Roesener and Schreuder, 1992b):

Situated approximately 90 km east of Swakopmund to the south of the Langer Heinrich Mountain, the mineralisation was first discovered in the late 1950s.

The Langer Heinrich valley is a 13 km-long, east-west trending palaeo-channel which transects the Bloedkoppie Granite (containing on average 10 to 15 g/t U_3O_8) in the east, and interbedded fine-grained metapelite, metagreywacke and calc-silicate beds of the Tinkas Member (Khomas Subgroup) in the central and western parts. The northern bank of the

palaeo-channel is formed by pink quartzites of the Etusis Formation (Nosib Group).

Calcrete terraces within the Langer Heinrich valley indicate original sediment thickness of the palaeo-channel as 60 m at a width of between 200 m and 1000 m. Palaeo-channel sediments are mostly covered by 1 to 2 m of scree. Channel fill sediments usually consist of basal conglomerate or breccia followed by alterations of siltstone, conglomerate, breccia and calcareous arkose, but mineralisation (carnotite) is not confined to a specific sediment type. Carnotite is irregularly distributed and occurs as small patches and lenses, around pebbles and in cracks and may be finely disseminated.

4.6.2 Classical vein deposits

The classical vein deposits are structurally controlled deposits within a variety of host rock types, including metasediments and granites which can be divided into two end-members (from Nash and Granger, 1981):

- Veins with simple mineralogy: veins which are characterised by carbonate, specular hematite and pitchblende and are interpreted as being formed by metamorphic-hydrothermal fluids. The Schwartzwalder mine in Colorado serves as an example of a classical vein deposit with simple mineralogy, and will be discussed below.

- Veins with complex mineralogy: uranium veins which show complex mineralogy and chemistry that include Ag, Co, Ni, Bi, Cu, Au, Se and As, mostly in the form of sulphides, selenides and sulfarsenides. The Shinkolobwe deposit in the Shinkolobwe-Copperbelt area of the Democratic Republic of the Congo (D.R.C.) and Zambia serves as an example of a classical vein deposit with complex mineralogy. Some

features of the Shinkolobwe deposit are similar to those of unconformity-type uranium deposits.

4.6.2.1 Schwartzwalder Mine

From Nash and Granger (1981), the Schwartzwalder Mine occurs in early Proterozoic metasediments about 25 km west of Denver, Colorado. Favoured hosts are garnet-biotite gneiss, quartz-biotite schist, calc-silicate gneiss and quartzite.

Structures hosting the uranium deposits are subsidiary to major Precambrian faults, and show shallow dipping horsetail veins which steepen in dip where they join major faults. Ore shoots have a strike length of approximately 200 m and extend to a depth of 900 m.

Characteristic minerals are pitchblende, coffinite, adularia, ankerite and pyrite. Precambrian metasediments are favoured as the source of uranium.

4.6.2 Deposits associated with igneous rocks

The deposits associated with igneous rocks are divided into three sub-classes (Nash and Granger, 1981):

- Deposits in alkalic rocks: high uranium, thorium, niobium, zirconium and REE associated with alkalic complexes, e.g. nepheline syenites and carbonatites. Examples of these include the Palabora carbonatite complex in South Africa.

- Deposits in contact zones: located in contact metamorphic aureoles of granite plutons. Genesis is debated between possible hydrothermal and supergene mechanisms. Examples include Midnight Mine in the U.S.A. and the Mary Kathleen mine in Australia.

- Volcanogenic deposits: volcanogenic deposits are varied in form and structural setting and are believed to be of probable hydrothermal origin in volcanic rocks. Uranium deposits are associated with rhyolitic plugs and domes (Spor Mountain, U.S.A.), faults cutting hypabyssal intrusives and outflow tuffs (Marysvale, U.S.A.), volcaniclastic sediment fillings of palaeo-channels and calderas (McDermit, U.S.A.). Other deposits are associated with ignimbrites, agglomerates, ash-flow tuffs, as well as metamorphosed subaerial and subaqueous volcanogenic rocks.

4.7 Omitiomire-style copper

The copper deposit at Omitiomire was outlined in Chapter 3. The possibility of similar occurrences within the study area is plausible.

A summarised description of the deposit geology follows (from K. Hartmann, pers. comm., 2011).

Two main geological units exist at the Omitiomire deposit:

- Unmineralised leuco-gneisses, interpreted as being metamorphosed dacite and rhyolite, with quartz, plagioclase, variable amounts of biotite and trace amounts of garnet and sphene.

- Mineralised mafic schist and gneiss, interpreted as being metamorphosed basaltic andesite, consisting mainly of quartz, plagioclase, biotite and amphibole, which are usually inter-banded with more felsic layers.

The copper mineralisation is dominated by chalcocite disseminated within the mafic rocks and is commonly associated with magnetite. Higher grade zones contain coarse blebs of chalcocite which post-date and over print foliation in biotite-amphibole schist implying remobilisation or emplacement of copper during the late Damaran Orogeny. Near surface mineralisation has been partially oxidised to malachite, chrysocolla and native copper. Some elevated nickel concentrations (up to 991 ppm) have been recorded within the mafic schists but generally have an inverse relation to copper concentration.

The mineralized body is sheet-like, striking north-south and with moderate dip to the east. The upper contact is a sharp thrust structure between hanging-wall white gneiss and mineralised schist and amphibolite. The lower mineralisation boundary is more diffuse and repetition through folding and thrusting is also present.

4.8 Geophysical expressions of target models

The typical geophysical expression that is expected for each of the envisaged mineral occurrences is summarised in Table 4.2 below.

Table 4.2: Expected geophysical response for possible mineral occurrences in Steinhausen Project Area

Type of occurrence	Geophysical expression
Matchless stratiform massive sulphides	**Regional:** Linear magnetic unit associated with magnetite quartzite within magnetically quiet units of Kuiseb Formation. Conductive electromagnetic (EM) target from massive sulphides. **Local:** Anomalous magnetic features associated with magnetic quartzite and pyrrhotite. Structure controlling ore shoots may have magnetic expression. Conductive EM anomalies from massive sulphides. Induced polarisation (IP) depicting high chargeability values over disseminated sulphides. Controlled source audio magnetotelluric (CSAMT) for mapping conductivity features are increasingly used for similar Beshi-type deposits (Bishop and Lewis, 1992).

Type of occurrence	Geophysical expression
Kuiseb Formation hosted hydrothermal copper deposits	**Regional:** Uncharacteristically noisy magnetic Kuiseb Formation due to presence of magnetite rich epidote-quartz rock (Moore, 2010). Regional crosscutting structural features may have magnetic expression. **Local:** Magnetic anomalies arising from boudins and lenses of epidote-quartz rocks closely associated with mineralised zones (Moore, 2010). Resistive features may be associated with quartz veining. Chargeable IP anomalies associated with disseminated sulphides.

Type of occurrence	Geophysical expression
Manganese deposits	**Regional:** Strong magnetic expression (possibly remanent) due to concentration of Fe and Mn minerals. High percentage of Fe and Mn may give rise to conductive EM targets. High density bodies detectable with gravimetric surveys. **Local:** Manganese bearing unit (predominantly hematite quartzite and hematite-rich gneiss (Bühn *et al.,* 1992)) may be detected by magnetic surveys as hematite exhibits weak induced magnetisation and sometimes strong remanence (Gunn and Dentith, 1997). Fe-Mn ore mineral jacobsite, also strongly magnetic. High density gravity anomaly arising from concentration of Fe-Mn minerals. Massive braunite-hematite-jacobsite ore (Bühn *et al.,* 1992) expected to show as conductive EM target.

Type of occurrence	Geophysical expression
Magmatic Ni-Cu-PGE deposits	**Regional:** Magnetite, being a common primary mineral in mafic / ultramafic rock (Lightfoot, 2007) mostly results in higher magnetic susceptibility than surrounding metasediments, aiding in the identification of magnetically anomalous plug-like features and larger intrusive structures. Elevated abundance of olivine and pyroxene in mafic / ultramafic rock also result in higher density than surrounding country rock (Lightfoot, 2007) thus resulting in a positive gravity anomaly. Ultramafic bodies hosting nickel sulphides give rise to a strong EM response (Ford *et al.,* 2007). Mafic intrusive and ultramafic volcanics tend to show low radioelement concentration (Nicolet and Erdi-Krausz, 2003). **Local:** The presence of pyrrhotite and magnetite in many nickel-sulphide deposits implies possibility for direct detection of ore zones from magnetic data (Gunn and Dentith, 1997). Massive sulphides will show strong density contrast resulting in good gravity anomalies (Ford *et al.*, 2007). Conductive EM response from massive sulphides. High chargeability IP response from disseminated sulphides.

Type of occurrence	Geophysical expression
Hydrothermal gold deposits	**Regional:** Though gold deposits exhibit a wide spectrum of magnetic properties, magnetic data could be employed to identify lithologies and structures prone to hosting such deposits (Ford *et al.*, 2007; Gunn and Dentith, 1997). **Local:** Presence of pyrrhotite in footwall and replacement lenses in skarn at Navachab (Burnett, 1992) implies strong and possibly remanent (Gunn and Dentith, 1997) local magnetic anomalies. Destruction of magnetite resulting from alteration may lead to local magnetic lows (Airo, 2002; Ford *et al.*, 2007; Gunn and Dentith, 1997). Local relative changes in radioelement concentrations due to alteration processes (potassic alteration) leading to anomalous K/Th ratios (Airo, 2002; Ford *et al.*, 2007). Conductive EM anomalies may be associated with faults and alteration (Ford et al., 2007). At Navachab, massive sulphides proximal to gold mineralisation (Burnett, 1992) will give rise to strong conductive EM anomalies. Disseminated sulphides often associated with gold deposits will result in chargeable IP anomalies while massive quartz veining will result in resistivity highs (Ford *et al.*, 2007).

Type of occurrence	Geophysical expression
Uranium deposits	**Regional:** Elevated uranium counts in radiometric data. Palaeo-channel fill may result in shallow EM conductors. Anomalous magnetic features associated with igneous plugs, domes and metamorphic aureoles (deposits associated with intrusive rocks) and structure (classical vein deposits). **Local:** Elevated uranium counts in radiometric data. Anomalous Radon Value from RadonX™ surveys; a radon emanometry survey methodology (Corner *et al.*, 2009). Shallow EM conductors delineating palaeo-channels.
Omitiomire-style copper	**Regional:** Domal features from magnetic data. Mafic mineralised units and associated magnetite (Hartmann, pers. comm.) could give rise to concentric to broken magnetic fabric, internal to domal features. **Local:** Magnetic anomalies due to association of magnetite with mineralisation (Hartmann, pers. comm.). Disseminated chalcocite mineralisation (IBML, 2008; IBML, 2009; Hartmann, pers. comm.) could result in high chargeability IP response.

Chapter 5

DATASETS AND PROCESSING

Map generation, CAD work and processing of airborne geophysical data were completed utilising GEOSOFT Oasis Montaj software. Automated classification of radiometric data was compiled by GRASS GIS, an Open Source Software.

5.1 Geological Data

Apart from the geological maps from the GSN as discussed in Chapter 2, other geological data were mostly collected by K.W. Kasch as part of field work undertaken for Mount Isa Mines Namibia (Pty) Ltd in 1998 (Kasch 1998), and further mapping being done by him for Craton in the south-western sector of the Steinhausen Area during 2008 (Corner, pers. comm., 2009). Due to the more detailed collection of information on actual outcrop, his geological description was used as the basis for geological correlation to other datasets. Figure 5.1 shows the extent of Kasch's geological mapping.

As seen in Figure 5.1, Kasch's geological mapping is restricted to the south-west, mostly due to the extensive Kalahari sand cover present further northeast. Important features from Kasch's mapping include the presence of a lower amphibolite unit and an upper marble unit within the Kuiseb Formation schists. These units may play a role in future Kuiseb Formation mapping as important marker horizons. Figure 5.2 shows these units in more detail.

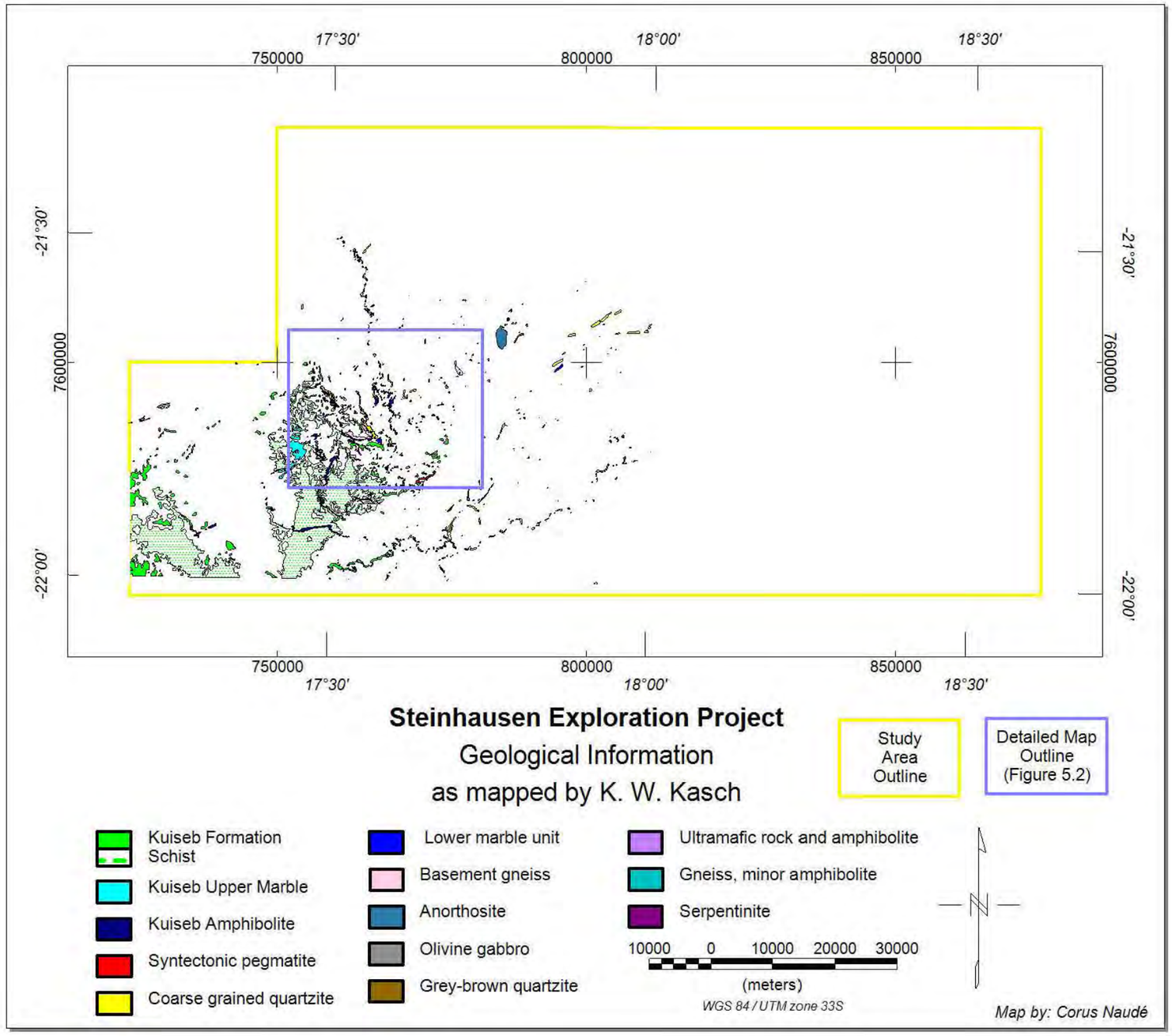

Figure 5.1: Extent of geological mapping by K.W. Kasch (1998, 2008).

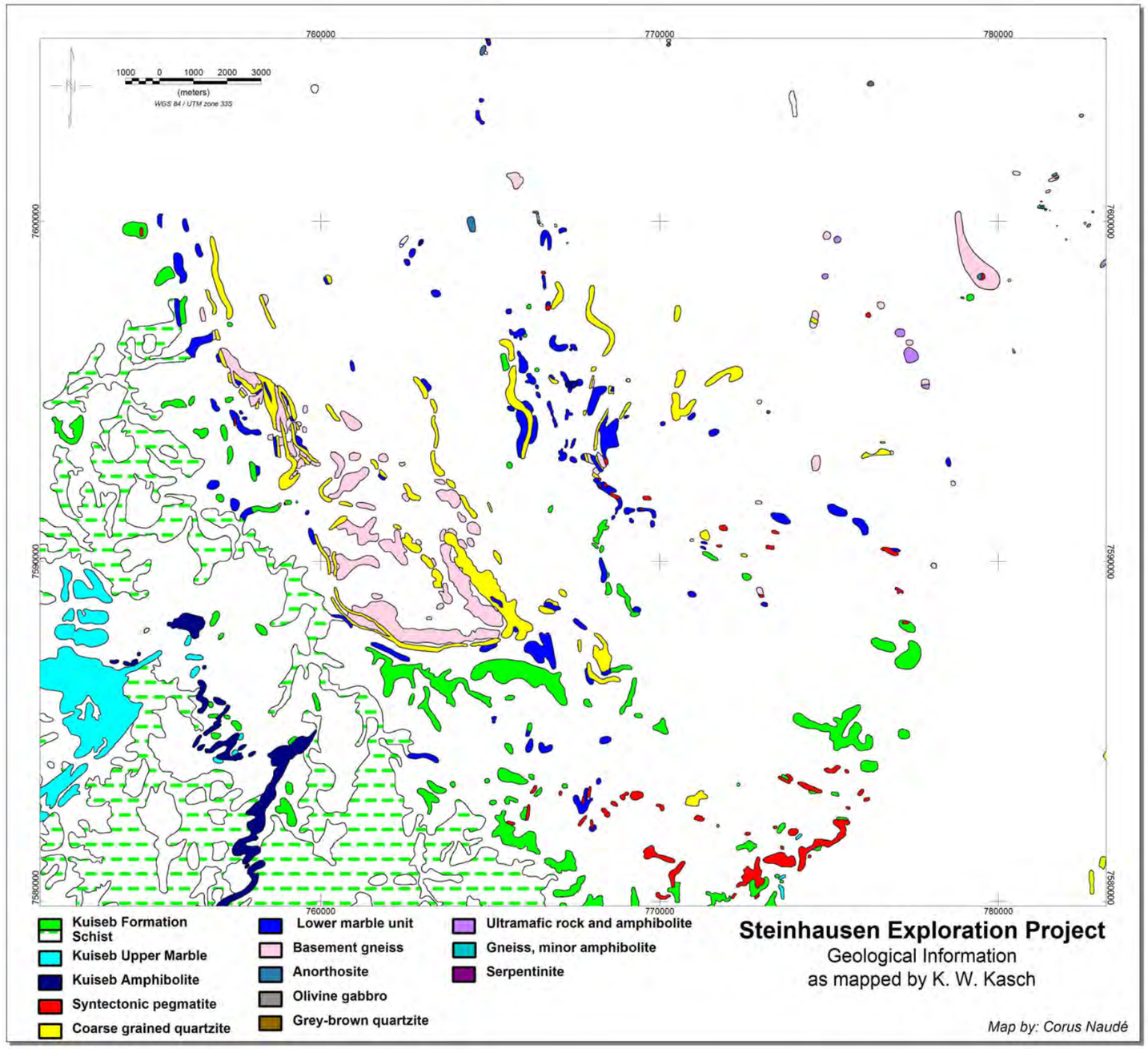

Figure 5.2: Detailed geological mapping by K.W. Kasch (1998, 2008).

5.2 Satellite Imagery

The Satellite imagery over the survey area was downloaded from the Global Land Cover Facility (http://glcfapp.glcf.umd.edu:8080/esdi/index.jsp) on the 29th of August 2009. The available data included Landsat ETM+ and Shuttle Radar Topography data.

5.2.1 Landsat ETM+ data

The survey area is covered by the following two scenes: Path 177 Row 075, Path 178 Row 075.

The data obtained consist of geo-referenced tiff images of separate Landsat ETM+ bands as specified in Table 5.1 below:

Table 5.1: Landsat ETM+ Image Details

Path 177 Row 075			**Path 178 Row 075**	
Acquisition Date	24 April 2000		Acquisition Date	17 May 2000
Resolution Bands 1, 2, 3, 4, 5, 7	28.5 m		Resolution Bands 1, 2, 3, 4, 5, 7	28.5 m
Resolution Band 6	57.0 m		Resolution Band 6	57.0 m
Resolution Band 8	14.25 m		Resolution Band 8	14.25 m
Cloud Cover	0		Cloud Cover	0

The metadata files for the Landsat images used, shown in Appendix A, detail the image processing and attributes as downloaded from the Global Land Cover Facility.

Figure 5.3 shows the false colour image (red – band 4, green – band 3 and blue – band 2) for the two scenes covering the survey area.

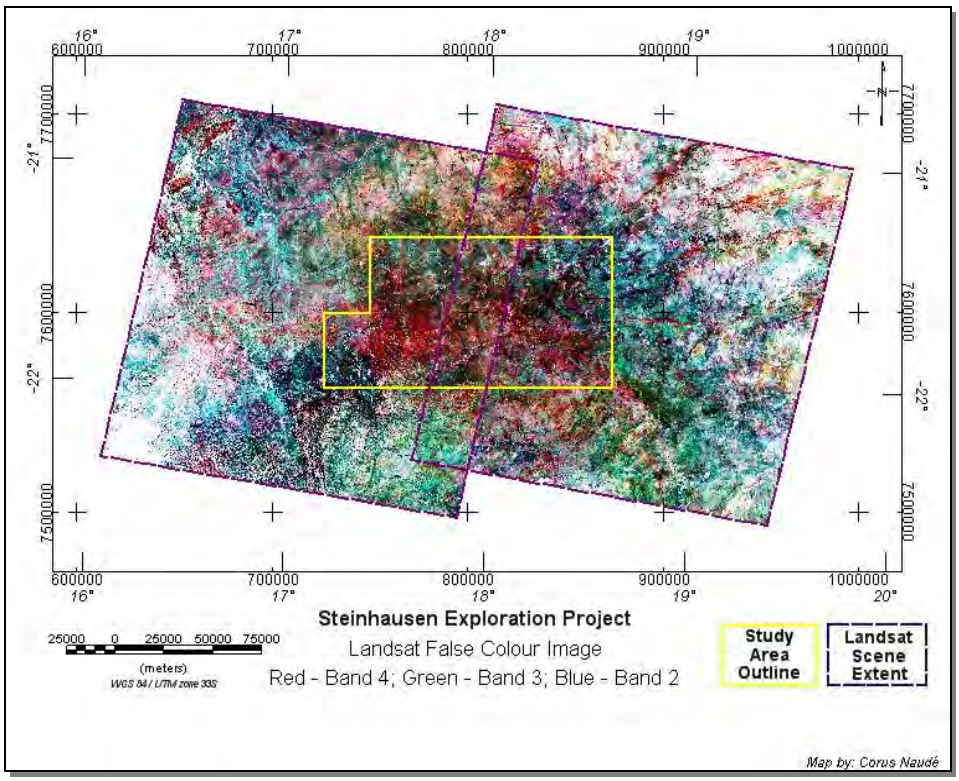

Figure 5.3: False colour image of LANDSAT (red – band 4; green – band 3; blue – band 2).

The capacity of available Landsat imagery in the visible near-infrared (VNIR) and the short-wave infrared (SWIR) allows for limited application in mineral exploration and relies on the ability to identify spectral gradients typical of Fe-bearing minerals as well as gradients in the spectral response for clays, micas, carbonates and sulphates (Crósta and De Souza Filho, 2009). By applying image ratioing or subtraction, differences between images are accentuated and similarities suppressed (Bedell and Crósta, 2009). As the spectra for Fe-bearing minerals show strong absorption of energy for band 1 (and band 2) as oppose to band 3 of Landsat ETM+ data, by ratioing band 3 to band 1 (or band 2) the presence of Fe-bearing minerals will be accentuated. Clay-bearing minerals show strong absorption for band 7 as oppose to band 5 and by ratioing band 5 to band 7, concentrations of these minerals will be accentuated (Crósta and De Souza Filho, 2009).

Before ratioing could be applied a crude atmospheric correction had to be applied by means of a technique called dark pixel exclusion. This consists of selecting pixels on the images that correspond to clear water or shaded areas, noting the selected pixels' Digital Number (brightness) for each band and subtracting appropriate values from bands 1, 2 and 3. Table 5.2 shows the process for the two scenes covering the survey area.

Table 5.2: Dark Pixel Exclusion applied to Landsat ETM+ Images

Path 177 Row 075							
X (WGS84 UTM 34 N)	Y (WGS84 UTM 34 N)	DN Value (Band 1)	DN Value (Band 2)	DN Value (Band 3)	DN Value (Band 4)	DN Value (Band 5)	DN Value (Band 7)
176555	-2446196	53	40	31	32	17	13
183854	-2447249	55	49	38	19	11	9
196199	-2435736	56	46	32	23	12	13
195587	-2436031	52	43	36	19	13	12
190149	-2444481	53	45	38	25	9	11
Correction		**32**	**21**	**12**	**0**	**0**	**0**

Path 178 Row 075							
X (WGS84 UTM 34 N)	Y (WGS84 UTM 34 N)	DN Value (Band 1)	DN Value (Band 2)	DN Value (Band 3)	DN Value (Band 4)	DN Value (Band 5)	DN Value (Band 7)
726052	-2340956	86	97	120	37	10	10
722530	-2342962	87	99	121	37	11	11
725785	-2341312	88	96	115	35	11	11
721872	-2435498	56	48	42	67	78	78
702927	-2434918	58	47	35	16	11	11
703784	-2435076	60	52	41	16	12	12
658960	-2456994	53	45	35	17	11	11
659733	-2457410	53	40	37	15	11	11
Correction		**38**	**25**	**20**	**0**	**0**	**0**

Products derived from image ratioing suggested by Crósta and De Souza Filho (2009) include the so-called Abrahams' Ratio used for alteration

mapping whereby the ratio for clay (bands 5/7) is displayed as red, the ratio for iron (bands 3/1) in green and the ratio for vegetation (bands 4/3) in blue. This results in an image where alteration will be depicted as yellow as both red and green should be accentuated. Another image for alteration mapping depicts the clay ratio in red, the iron ratio in blue and the sum of the clay ratio and iron ratio in green thus accentuating areas of possible alteration in white.

Image subtraction is another way of accentuating differences between images and can therefore also be used to highlight changes in spectral features. Other image arithmetic applied includes complex ratios e.g. the vegetation index (Bedell and Crósta, 2009). The vegetation index (IND_{veg}) is the arithmetic result of band 4 (TM_{B4}) and band 3 (TM_{B3}) as follows (Bedell and Crósta, 2009):

$$IND_{veg} = \frac{(TM_{B4} - TM_{B3})}{(TM_{B4} + TM_{B3})} \quad \text{(a)}$$

In a similar fashion an iron index could be created by using band 3 (TM_{B3}) and band 1 (TM_{B1}). In order to better differentiate between iron minerals and vegetation it was decided to also take into account the difference between bands 5 (TM_{B5}) and 4 (TM_{B4}) from within the iron-spectrum. This was done by creating an extended Fe-index (IND'_{Fe}) as depicted in equation (b).

$$IND'_{Fe} = \frac{((TM_{B3} - TM_{B1}) + (TM_{B5} - TM_{B4}))}{(TM_{B1} + TM_{B3} + TM_{B4} + TM_{B5})} \quad \text{(b)}$$

The calculation of a clay index (IND_{OH}) was based on the absorption of band 7 as per equation (c):

$$IND_{OH} = \frac{(TM_{B5} - TM_{B7})}{(TM_{B5} + TM_{B7})} \quad \text{(c)}$$

From the calculated images, alteration colour images could be created as suggested by Crósta and De Souza Filho (2009). Figure 5.4 shows the clay index in red, extended Fe index in green and vegetation index in blue similarly to the Abrahams' Ratio (Crósta and De Souza Filho, 2009). Figure 5.5 depicts clay index in red, the sum of the clay index and extended Fe index in green and extended Fe index in blue.

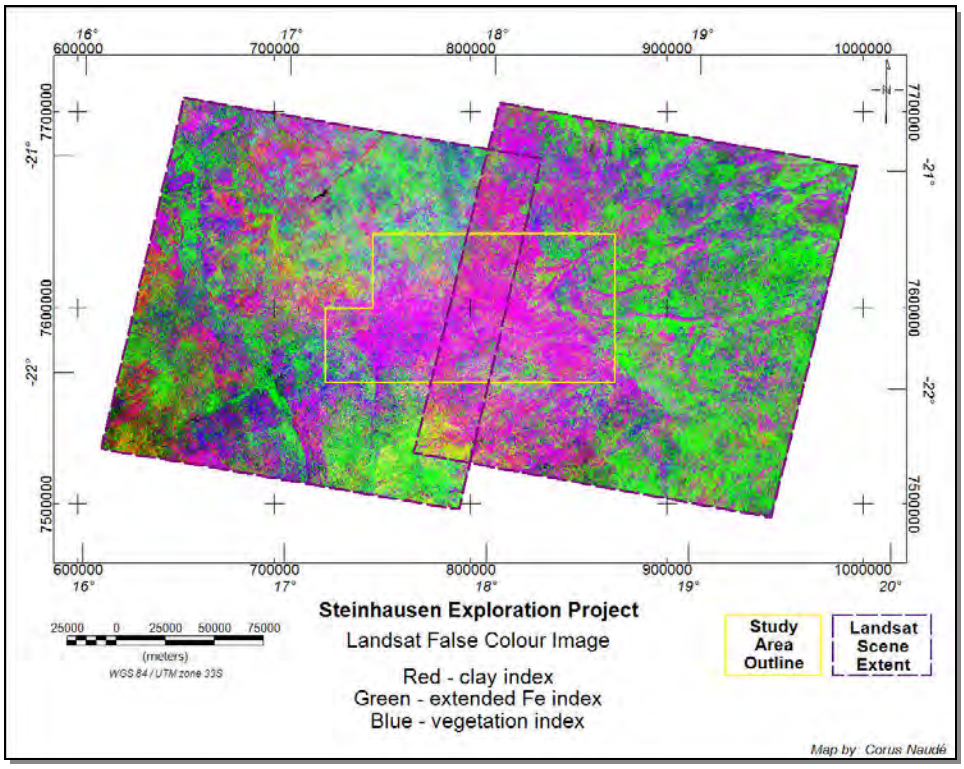

Figure 5.4: False colour image of LANDSAT (red – clay index; green – extended Fe index; blue – vegetation index).

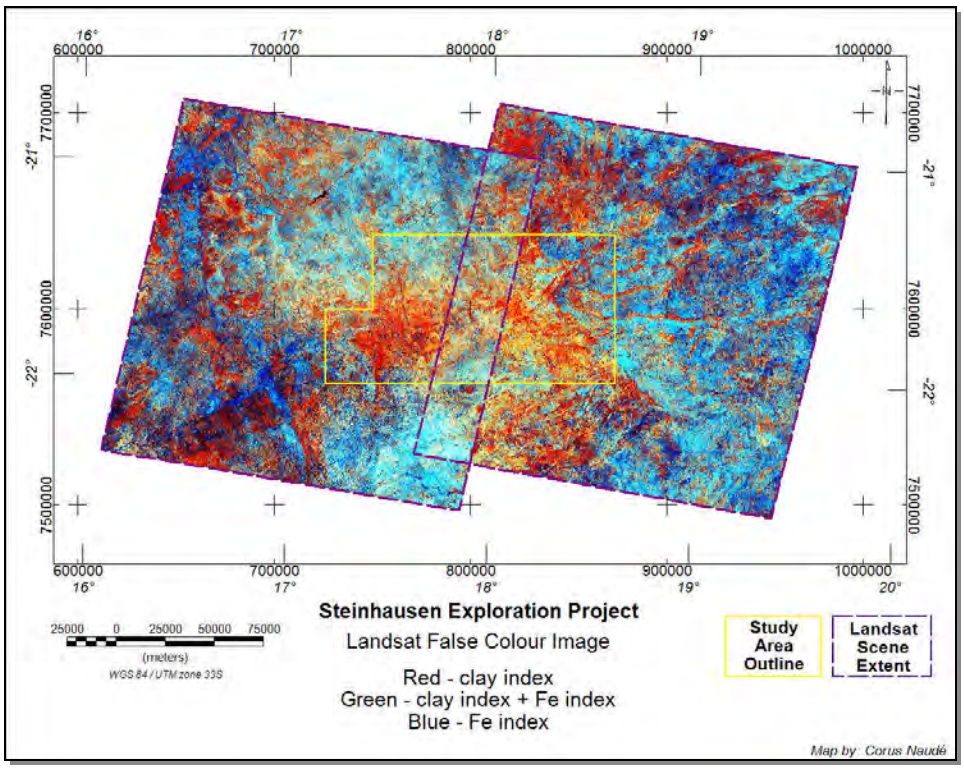

Figure 5.5: False colour image of LANDSAT (red – clay index; green – extended Fe index + clay index; blue – extended Fe index).

Figures 5.6 and 5.7 show the same ratios as in Figures 5.4 and 5.5 respectively but zoomed in over the Ekuja Dome area, thus highlighting the detail obtained from the Landsat data.

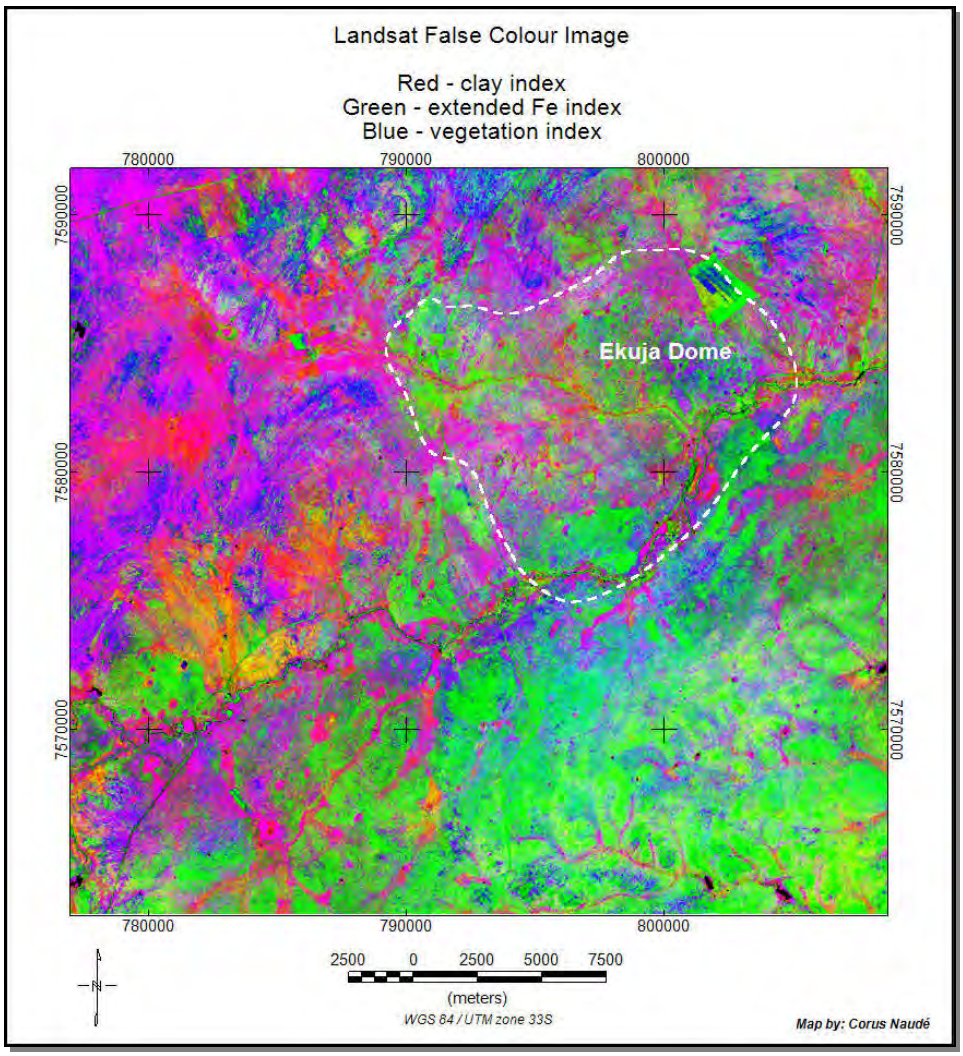

Figure 5.6: False colour image of LANDSAT data over Ekuja-dome area. (red – clay index; green – extended Fe index; blue – vegetation index).

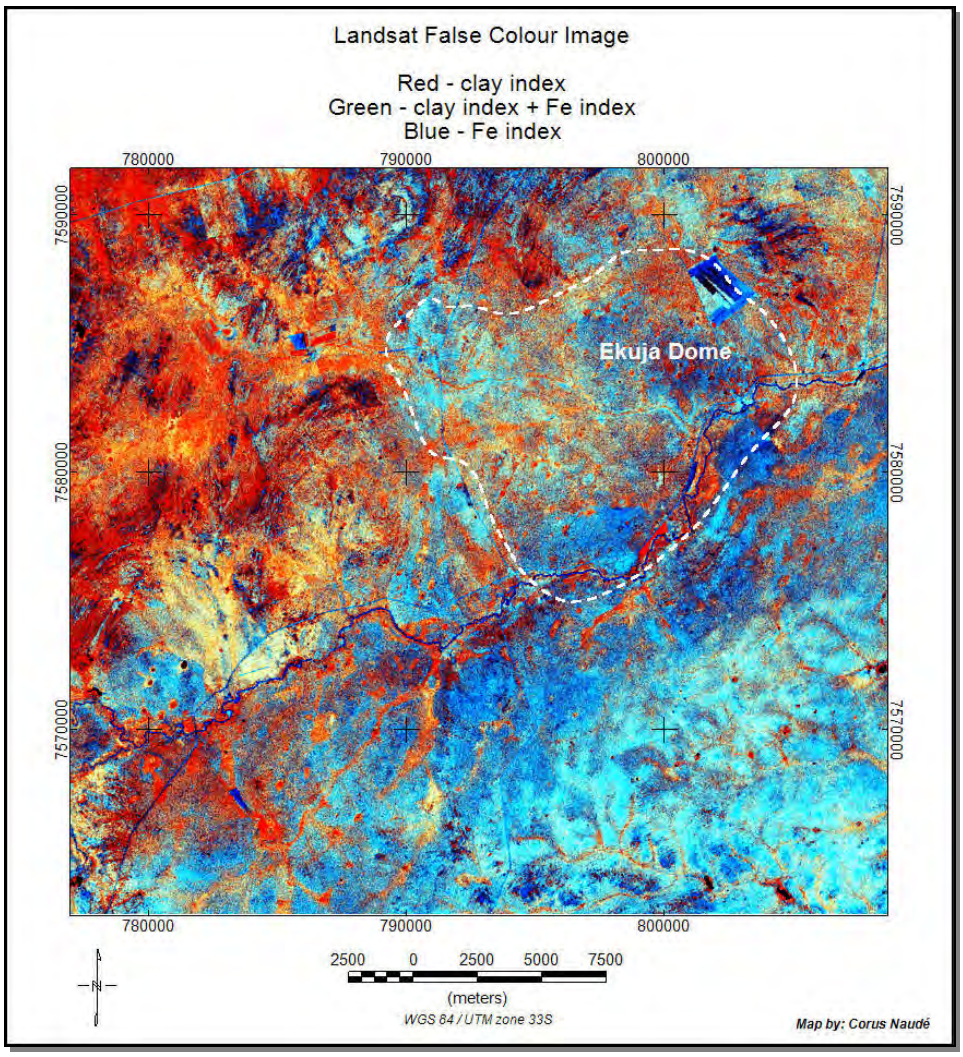

Figure 5.7: False colour image of LANDSAT data over Ekuja-dome area. (red – clay index; green – extended Fe index + clay index; blue – extended Fe index).

5.2.2 Shuttle Radar Topography Mission (SRTM)

During an 11 day mission in February 2000, the Space Shuttle Endeavour utilised an onboard radar system to obtain the most complete, highest resolution digital elevation model of the Earth. The project was a joint endeavour of NASA, the National Geospatial-Intelligence Agency, and the German and Italian Space Agencies (Farr *et al.*, 2007). The elevation data from this mission were made available to the public as 90 m cell size images. Figure 5.8 shows the digital elevation data of the Steinhausen Area.

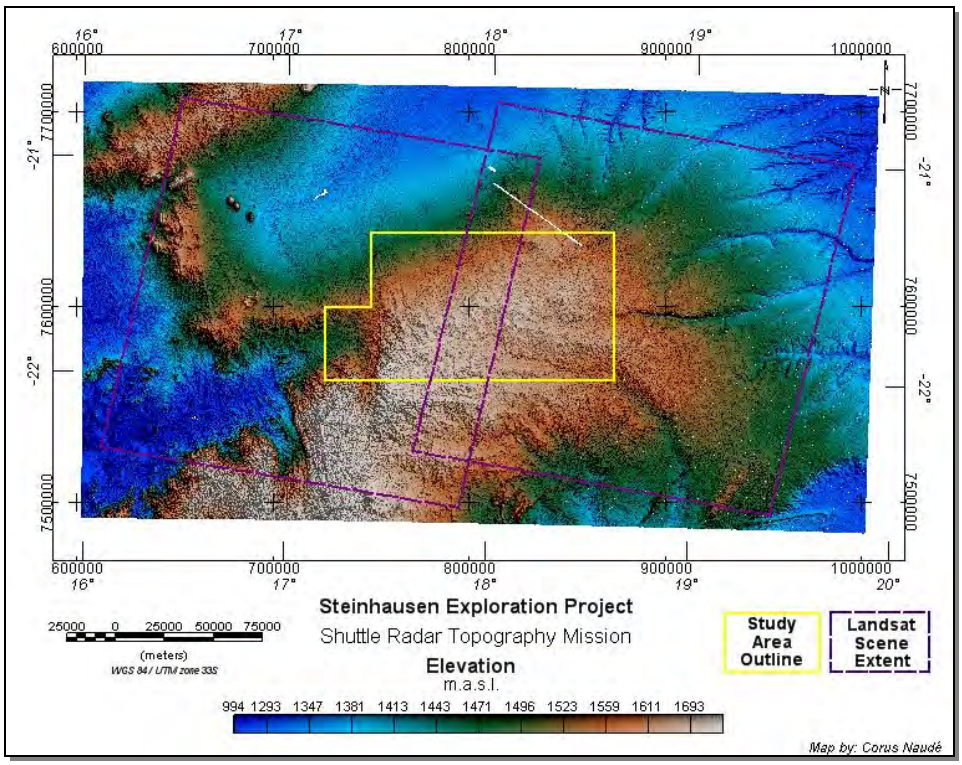

Figure 5.8: Shuttle radar topography mission - digital elevation data over study area.

5.3 Geophysical Data

The medium resolution airborne magnetic and radiometric data (200 m line pacing) obtained from the GSN over the Steinhausen Area consist of gridded images (GEOSOFT format, 50 m cell sized) of the Total Magnetic Intensity, First Vertical Derivative, Total Count Radiometrics, Potassium, Thorium and Uranium.

5.3.1 Airborne radiometric data

The statistical distribution of the data values of Total Count (TC), Potassium (K), Thorium (Th) and Uranium (U) as represented on the Geosoft Images are summarised in Table 5.3. This shows the minimum and maximum values represented on each grid as well as the following percentiles: 20, 40, 60, and 80. The negative values in counts are attributed to the mathematical function involved with stitching separate grids together whereby static shifts are applied to each grid in order to obtain a common mean (Corner, pers. comm.). For qualitative interpretation, the absolute radio-element concentration is not critical though as lithological discrimination is based on relative differences in concentration between the various radio-elements.

Table 5.3: Radiometric images statistics

	Min	**20%**	**40%**	**60%**	**80%**	**Max**
Total Count	-73.5	-48.2	-34.6	-20.9	-5.5	138.1
Potassium	0.086	0.668	0.831	1.046	1.318	4.222
Thorium	-12.589	-7.148	-5.234	-3.156	-0.313	42.131
Uranium	-4.094	-2.213	-1.584	-0.955	-0.135	7.158

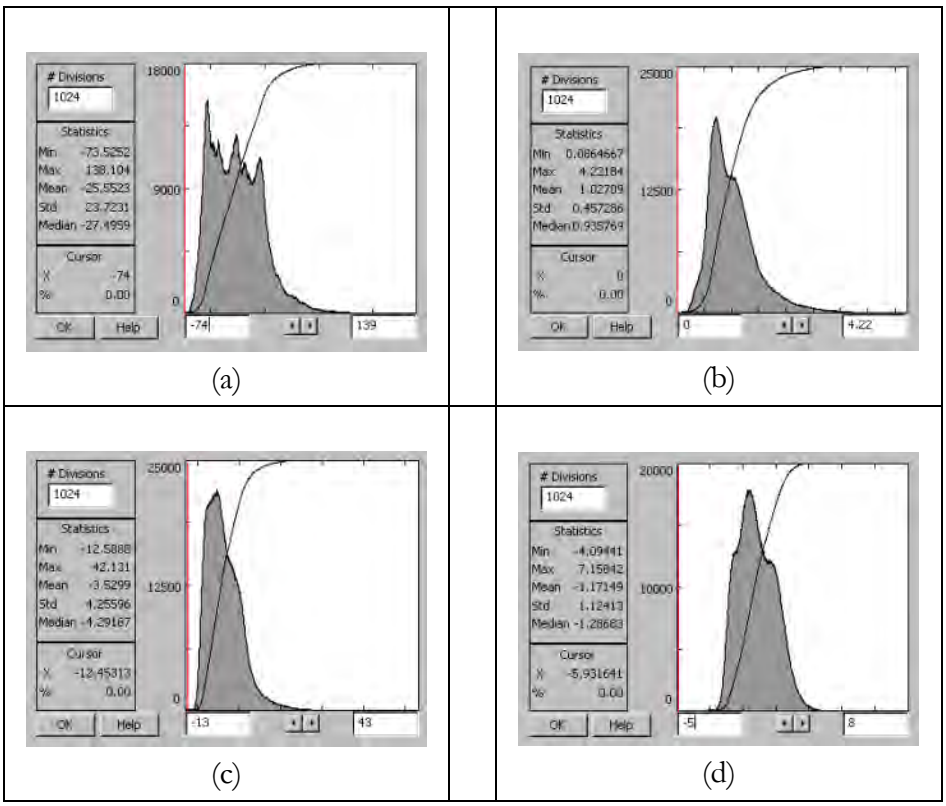

Figure 5.9: Histograms of radiometric images.
(a) Total Count; (b) Potassium; (c) Thorium; (d) Uranium.

Histograms of the images are displayed in Figure 5.9 which suggest the presence of distinct radiometric populations (domains).

Data processing of the radiometric data was focused on image enhancement to better distinguish between adjacent lithological units. This at times leads to transformation of the data in such a way that the data values achieved do not reflect "true" ground concentrations of radio-element data but rather an enhanced relative concentration of radio-elements.

Figure 5.10 shows the Total Count Radiometric Data (TC) over the Steinhausen Project Area. As can be seen from Figure 5.10, the radiometric data do not cover the Steinhausen Project Area completely, with no available data over a 12 km wide strip on the eastern side of the area. This strip was

not purchased due to the blanketing effect if the Kalahari cover in the east. A clear east-west trend is also visible where the eastern side of the area generally shows lower counts than that of the western side. This is due to the presence of thickening Kalahari cover sediments towards the east. Only 50 cm of non-residual unconsolidated cover will mask all radiation from depth.

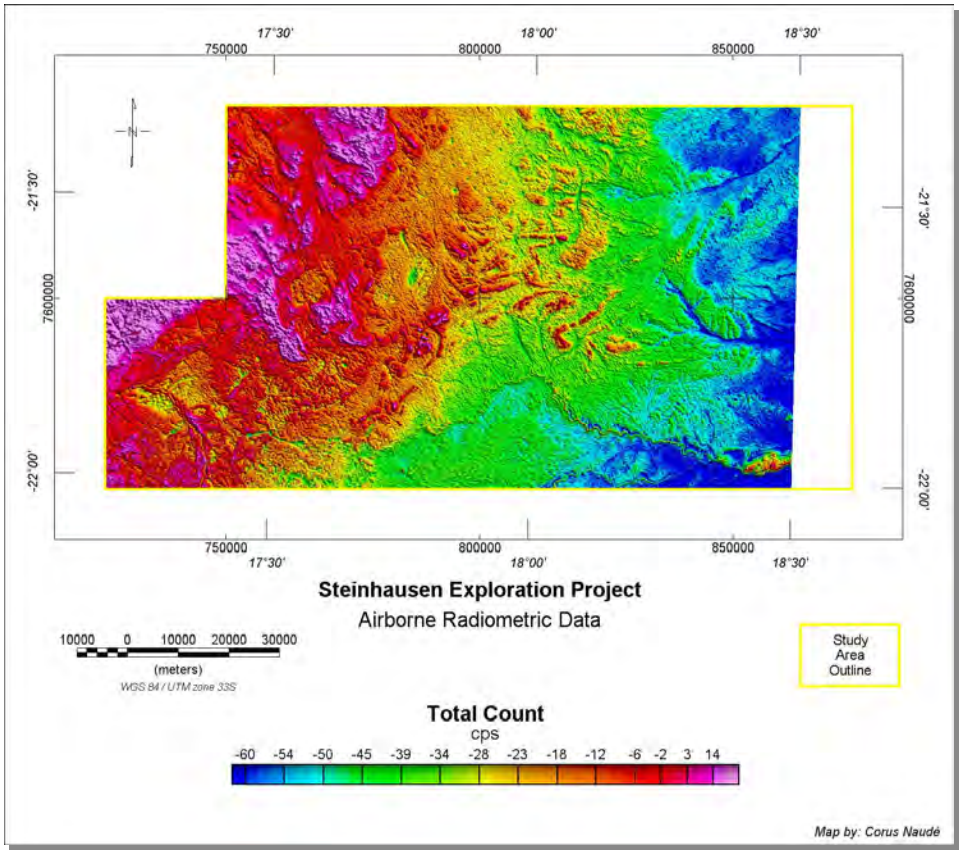

Figure 5.10: Total count radiometric data.

A standard way of displaying the Potassium (K), Thorium (Th) and Uranium (U) data is as a ternary image whereby a colour composite image is generated by proportioning red, green and blue colours to the radio-element concentration values of K, Th and U respectively (Nicolet and Erdi-Krausz, 2003). In keeping with this standard, the ternary image displayed in Figure 5.11 utilised red for displaying K, green for Th and blue for U.

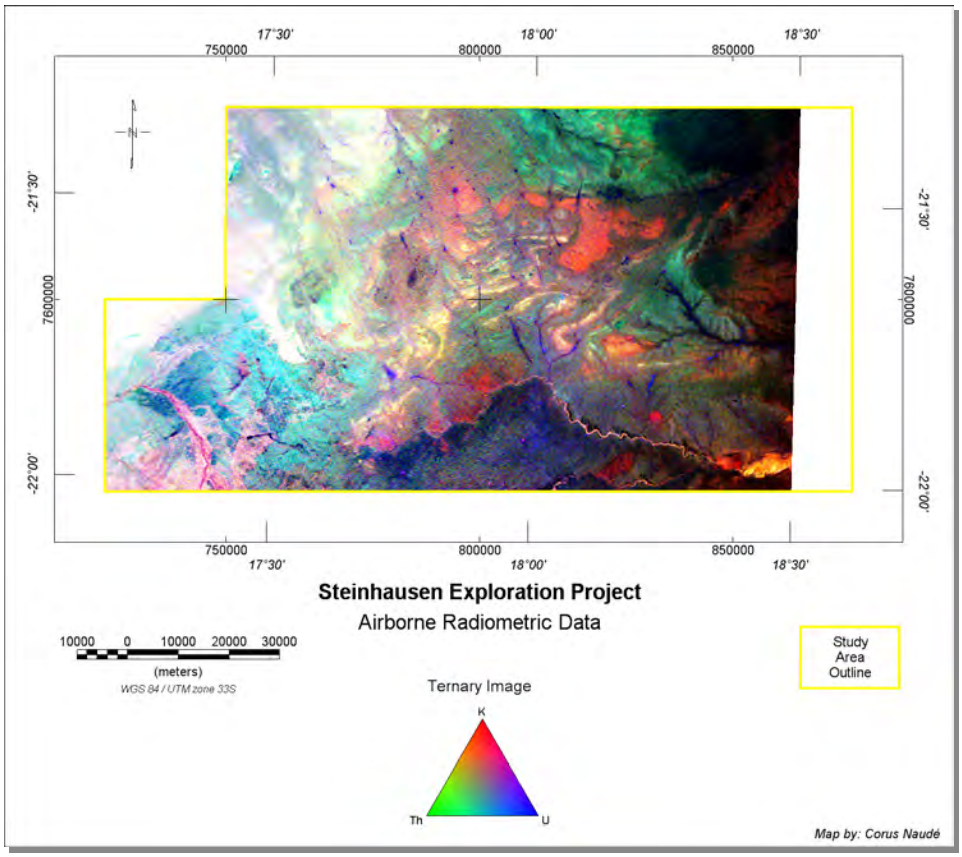

Figure 5.11: Ternary image of radio-element concentration.

The ternary image also confirms the observation made from the TC image in that the radio-element concentrations are far more subdued in the east as compared to the west. This results in a ternary image showing excessively bright colours in the west as opposed to dark colours in the east. In order to enhance the colour ratios across the image, a grid-filtering technique was applied whereby a linear trend is removed from the gridded data. This in effect increments data values in the east and decrements data values in the west to obtain a more even spread of data values across the whole image. Trend removing was done for each grid (TC, K, Th and U) separately. The resultant ternary image of trend-removed data is shown in Figure 5.12 allowing a clearer distinction between lithological elements in the eastern and western extremes of the image.

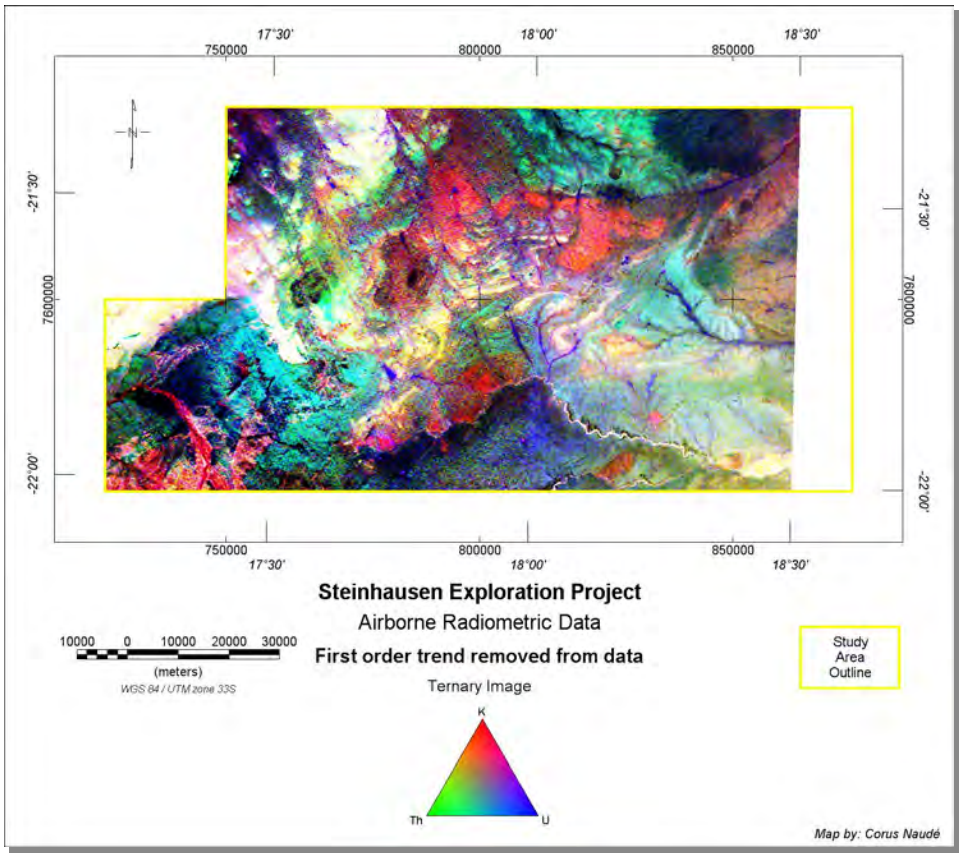

Figure 5.12: Ternary image of radio-element concentration with first-order trend removed.

A drawback of trend-removal filtering of the data as explained above is that large, separate populations within the original data are destroyed. This is best explained by comparing the histograms of trend removed images as shown in Figure 5.13 with those of the original images (Figure 5.9). In effect, trend removal is therefore a useful tool in enhancing relative element concentrations within smaller populations (which is most useful for local lithological mapping) by destroying the dominating effect that the large populations have on an image's colour scaling.

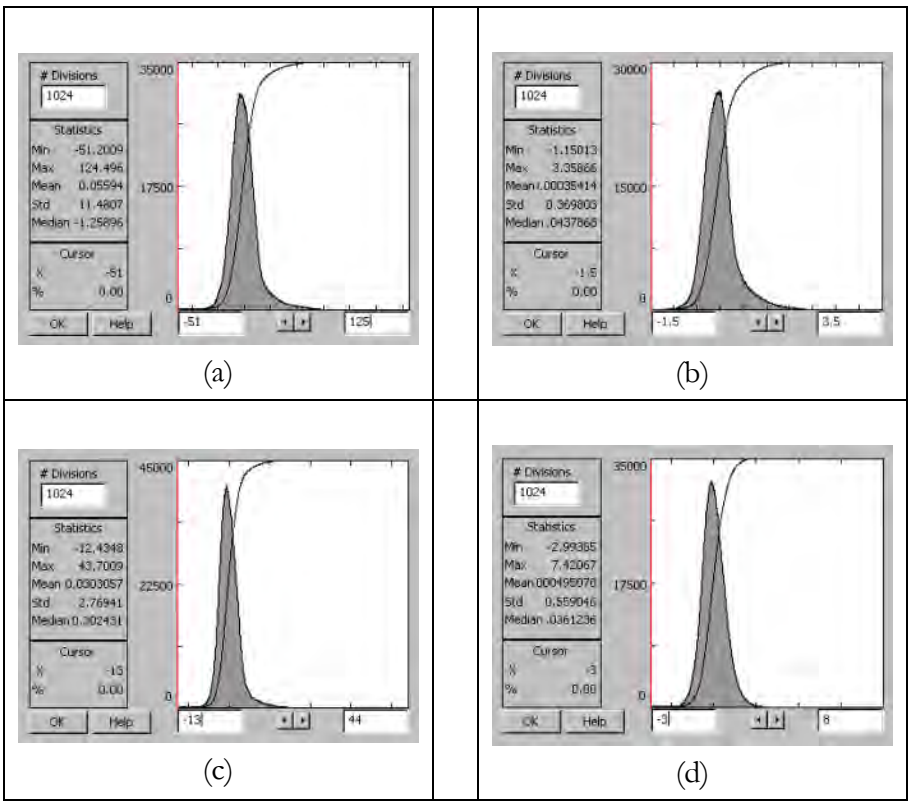

Figure 5.13: Histograms of trend removed radiometric images.
(a) Total Count; (b) Potassium; (c) Thorium; (d) Uranium.

An alternative approach to overcoming effects of large populations is to create separate grids (images) of the radio-elements from selected ranges taken from the TC image. Ideally the ranges should be selected to represent population distribution, but due to population overlap it was decided to select ranges based on TC percentiles. Thus windowed data for each of K, Th and U were created where TC was lower than 20%, between 20% and 40%, between 40% and 60%, between 60% and 80% as well as for above 80%. The resultant data are displayed as ternary images as usual combined into one image as shown in Figure 5.14.

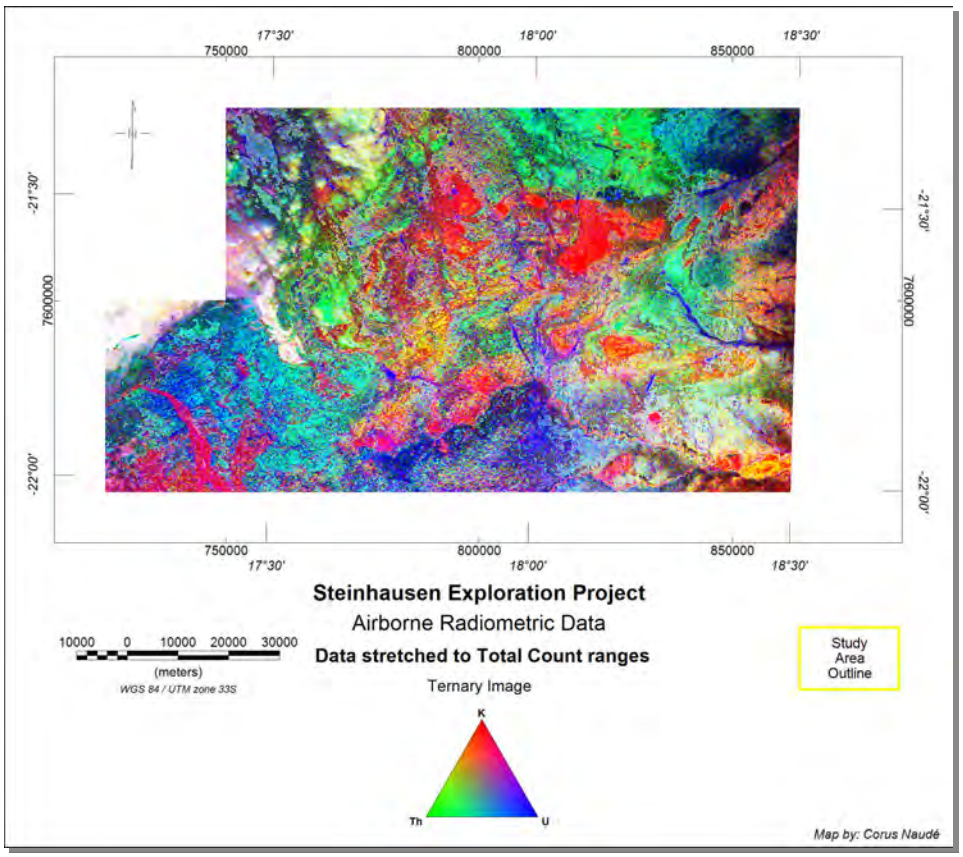

Figure 5.14: Ternary image of radio-element concentration stretched to TC ranges.

Computing the arithmetic ratio of radio-element grids is a way to suppress the effect of environmental factors (for example soil moisture, vegetation and topography) on the radiometric response resulting in a better correlation of the radiometric response to the actual geological units (Nicolet and Erdi-Krausz, 2003). It has also been shown that potassic alteration often results in elevated K radiation especially in mafic rocks which could result in elevated K / Th ratio and in a similar way, elevated U / Th could be indicative of alteration whereby Th was leached out of metasedimentary rocks (Airo, 2002). Taking into account the statistical data distribution as shown in Table 5.3, the following equations were formulated and applied to the radio-element grids, before computing the ratios. This was done in order to assure that all data in each grid are positive (thus avoiding dividing by zero) and applying a linear

stretching to the data, effectively scaling data from above 0 to below 100 for each of K, Th and U.

$$K_p = K\left(\frac{100}{4.3}\right) \tag{d}$$

$$Th_p = (Th + 13) \times \left(\frac{100}{55.5}\right) \tag{e}$$

$$U_p = (U + 4.1) \times \left(\frac{100}{11.3}\right) \tag{f}$$

$$R_{KTh} = \frac{K_p}{Th_p} \tag{g}$$

$$R_{UTh} = \frac{U_p}{Th_p} \tag{h}$$

Equations (d), (e) and (f) apply a linear stretch to each of the radioelement images (K, Th and U) from 0 to 100. Constants used in equations (d), (e) and (f) were calculated from the image statistics as shown in Table 5.3. Thereafter a potassium-thorium ratio was calculated from equation (g) (shown in Figure 5.15) and a uranium–thorium ratio from equation (h) (shown in Figure 5.16).

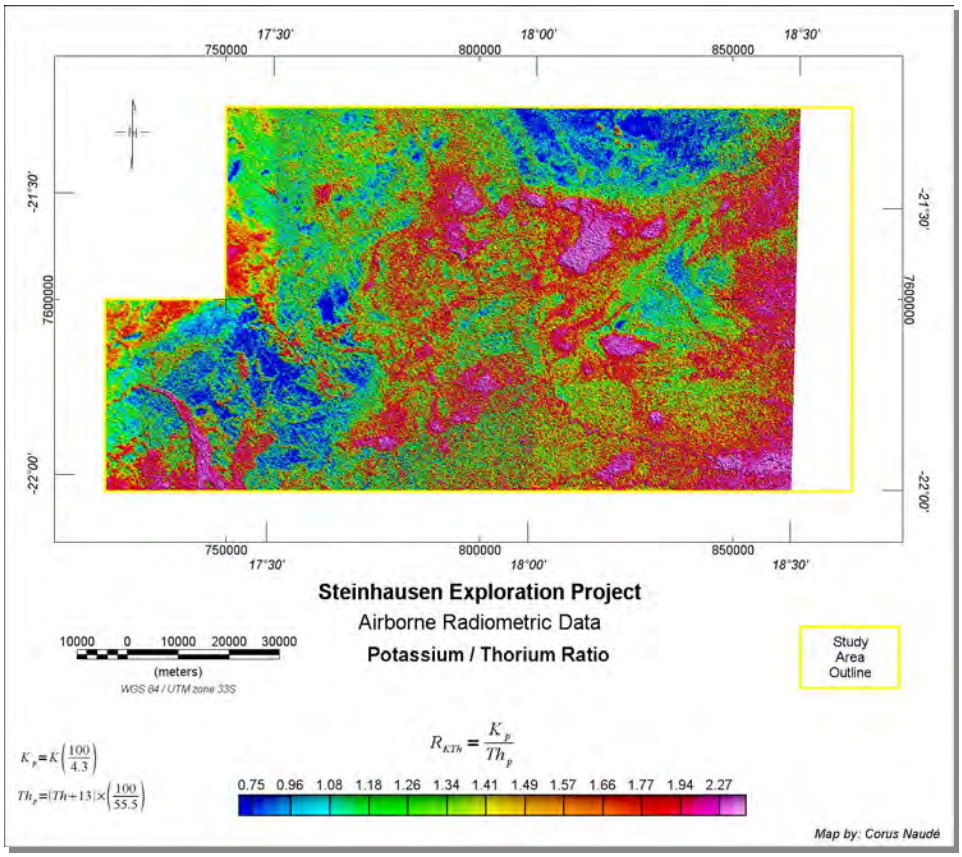

Figure 5.15: Potassium to thorium ratio.

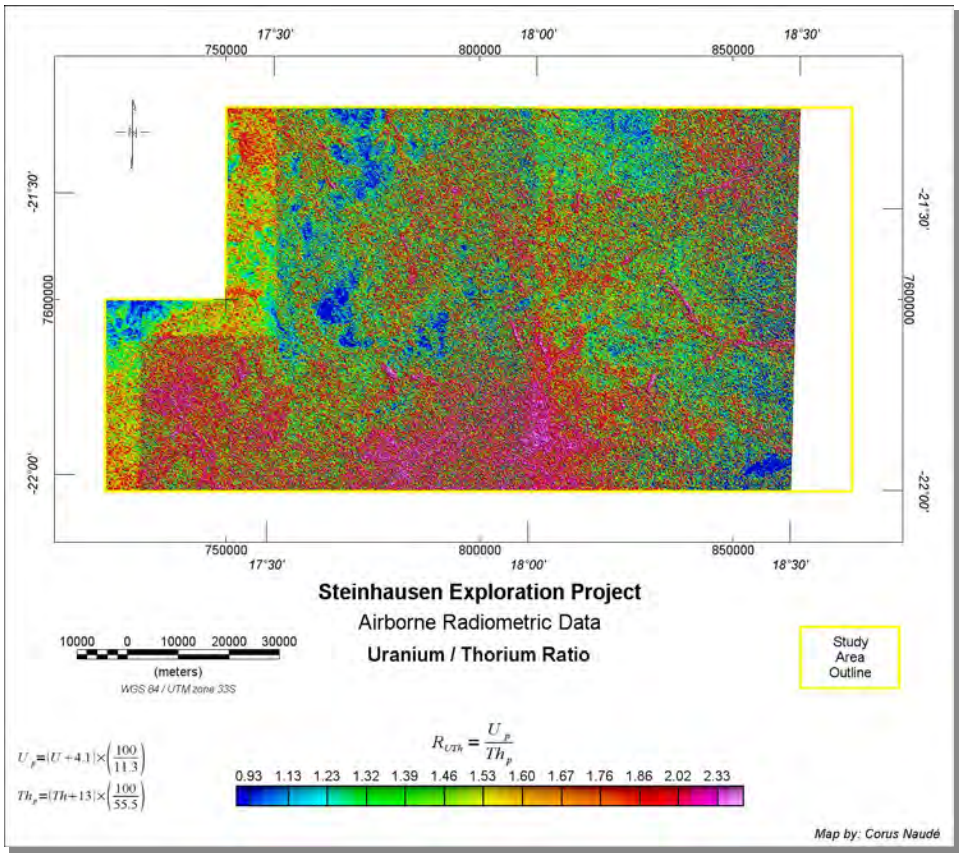

Figure 5.16: Uranium to thorium ratio.

Converting K, Th and U data to relative radio-element abundance was done by sum-normalization. This has the advantage of suppressing vegetation and soil moisture effects as well as producing a ternary image where colour variations can be quantitatively related to the ternary legend (Nicolet and Erdi-Krausz, 2003). Calculation of relative radio-element abundance for each element was done by means of equations (i), (j) and (k) (Nicolet and Erdi-Krausz, 2003) and the resultant ternary image displayed in Figure 5.17.

$$K_n = \frac{K_p}{K_p + Th_p + U_p} \quad \text{(i)}$$

$$Th_n = \frac{Th_p}{K_p + Th_p + U_p} \tag{j}$$

$$U_n = \frac{U_p}{K_p + Th_p + U_p} \tag{k}$$

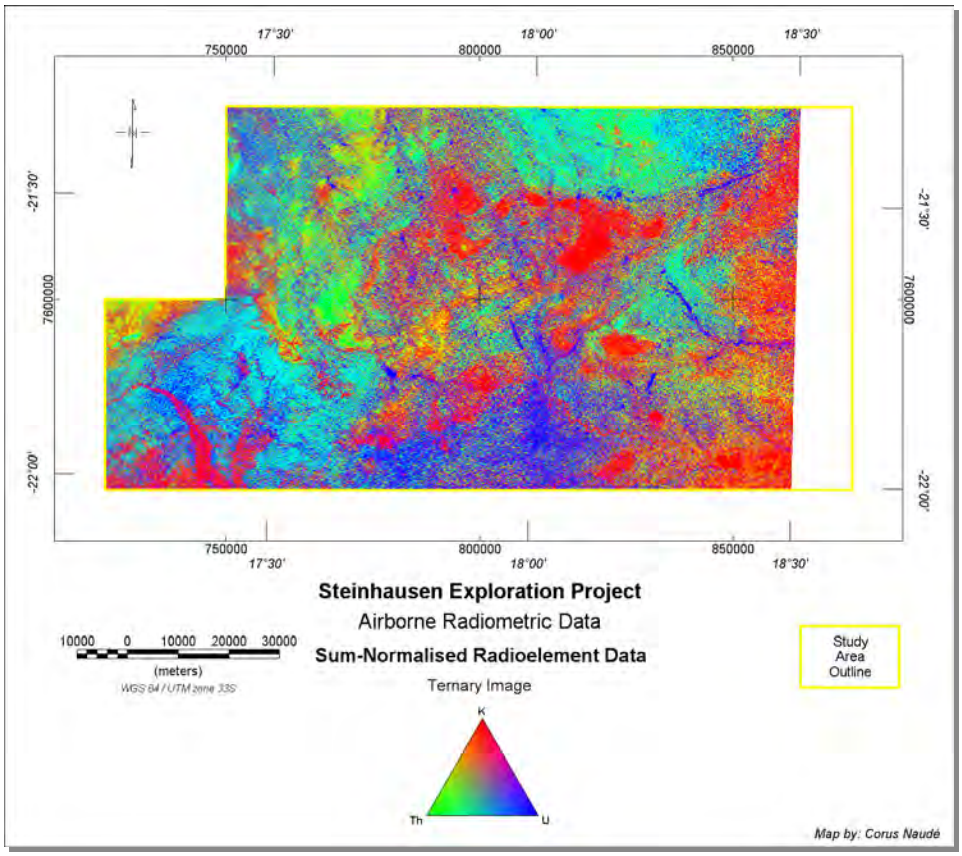

Figure 5.17: Sum-normalised radioelement data, ternary image.

Using automated classification to process radiometric images is a useful method for analysing large radiometric datasets whereby individual pixels are grouped into classes of similar radiometric response (Nicolet and Erdi-Krausz, 2003). GRASS GIS software has a clustering and classification algorithm utilising the maximum-likelihood classification scheme. Clustering

is done in either a supervised or unsupervised manner where, in the former, the user defines various areas of known geology that are then used to determine statistical clusters that will be used for the classification for the complete image or, in the latter, the clusters are automatically determined based on statistical means and variances. After clusters have been identified, maximum-likelihood classification is done to assign each pixel to the cluster to which it is most likely to belong.

In order to avoid the classification being dominated by the regional trend that is present in the radiometric data as described above, the following input images were used for the unsupervised classification computed for the Steinhausen Area: Normalised K (from equation (i)), Normalised Th (from equation (j)), Normalised U (from equation (k)) and K/Th ratio (from equation (g)). For simplicity the data were clustered into 6 classes only. Cluster properties are shown in Figure 5.18.

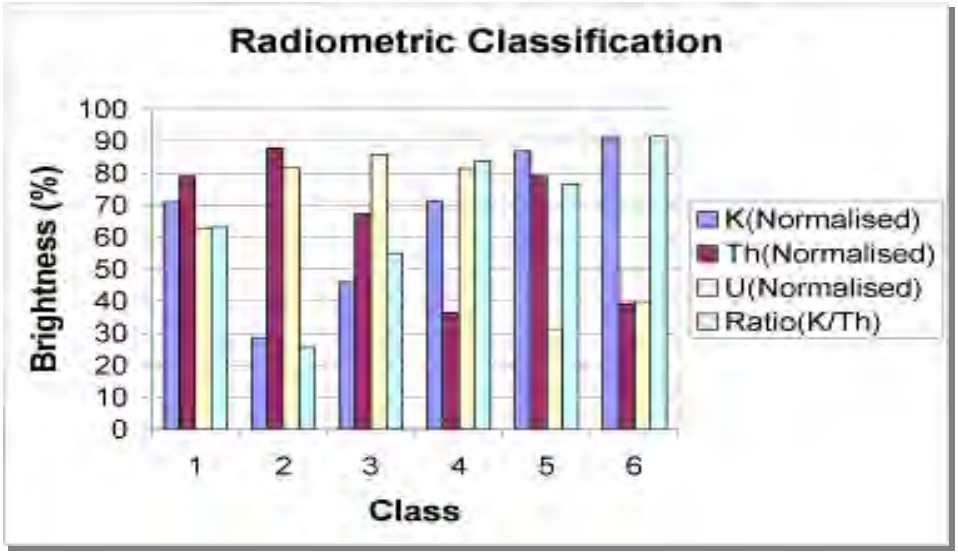

Figure 5.18: Maximum-likelihood classification cluster properties.
Class 1: Equal brightness for K, Th, U and K/Th
Class 2: High Th and U
Class 3: High U, moderate Th
Class 4: High K/Th ratio, high U
Class 5: High K and Th, Low U, K/Th high
Class 6: High K, Low Th and U.

Classification of radiometric data in this manner simplifies the radiometric description of lithologies as well as creates clear boundaries between classes that could aid in contact mapping. Figure 5.19 shows the resultant classified image.

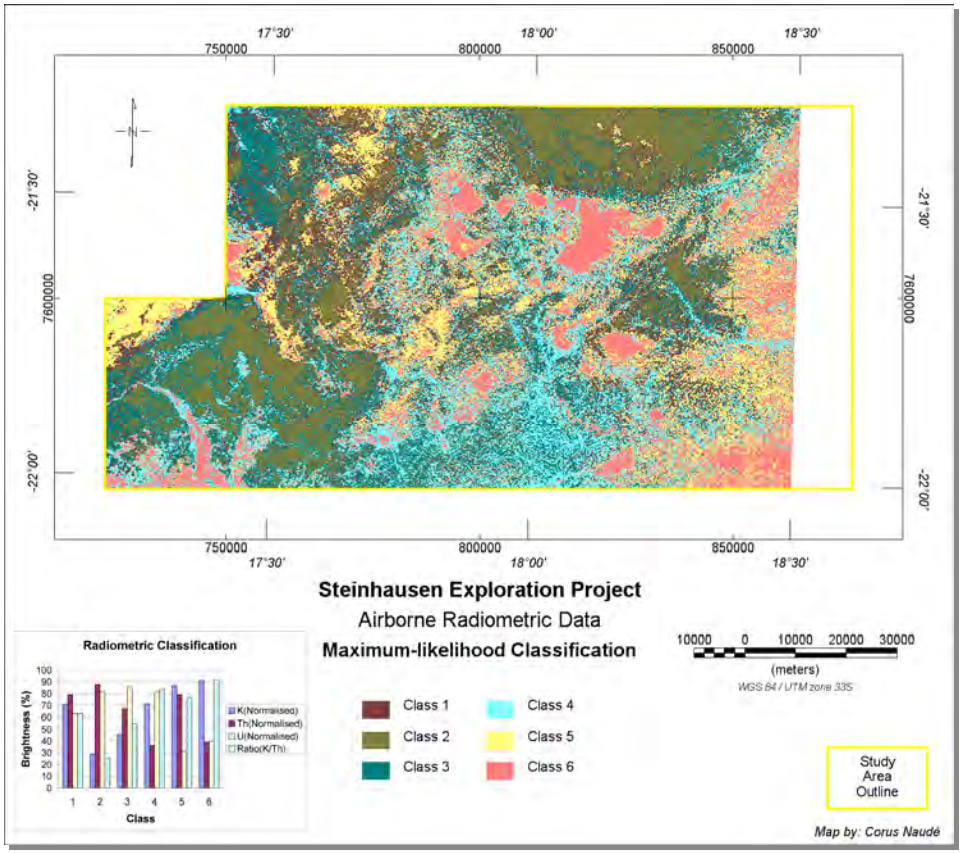

Figure 5.19: Maximum-likelihood classification of normalised radio-element data.

5.3.2 Airborne magnetic data

The airborne magnetic data consist of a Total Magnetic Intensity (TMI) grid image (Figure 5.20) and a First Vertical Derivative (FVD) grid image (Figure 5.21), both in Geosoft format. In order to conduct a qualitative interpretation of the magnetic data as represented by the images in Figures 5.20 and 5.21, it is necessary to apply numerous filters with the aim of extracting important information that aid in the identification of geological structure, contacts and properties of magnetic units. Considerations that need to be taken into account when designing filters for interpreting the magnetic data include (from GETEC, 2010):

- the dependency of the induced magnetic field on longitude and latitude due to the different orientation of the Earth's magnetic field relative to the survey position on the Earth's surface,

- the superposition of magnetic anomalies due to proximal bodies or vertical changes in magnetic properties, and

- the dipolar nature of any magnetic field.

It is therefore clear that the shape of a magnetic anomaly not only depends on the shape, depth and susceptibility of the perturbing body, but also on the direction of its magnetisation and the direction of the regional field. Proximity of the magnetic body to the magnetic sensor will also have an effect on its observed magnetic signature with deeper bodies showing as long wavelength features as opposed to narrow, high frequency signature of shallow magnetic bodies. By applying various filters, different properties of the magnetic field could be highlighted or suppressed as required in order to properly locate and interpret magnetic features. The different filters applied as part of the interpretation process for this study are discussed below.

5.3.2.1 Total Magnetic Intensity (TMI)

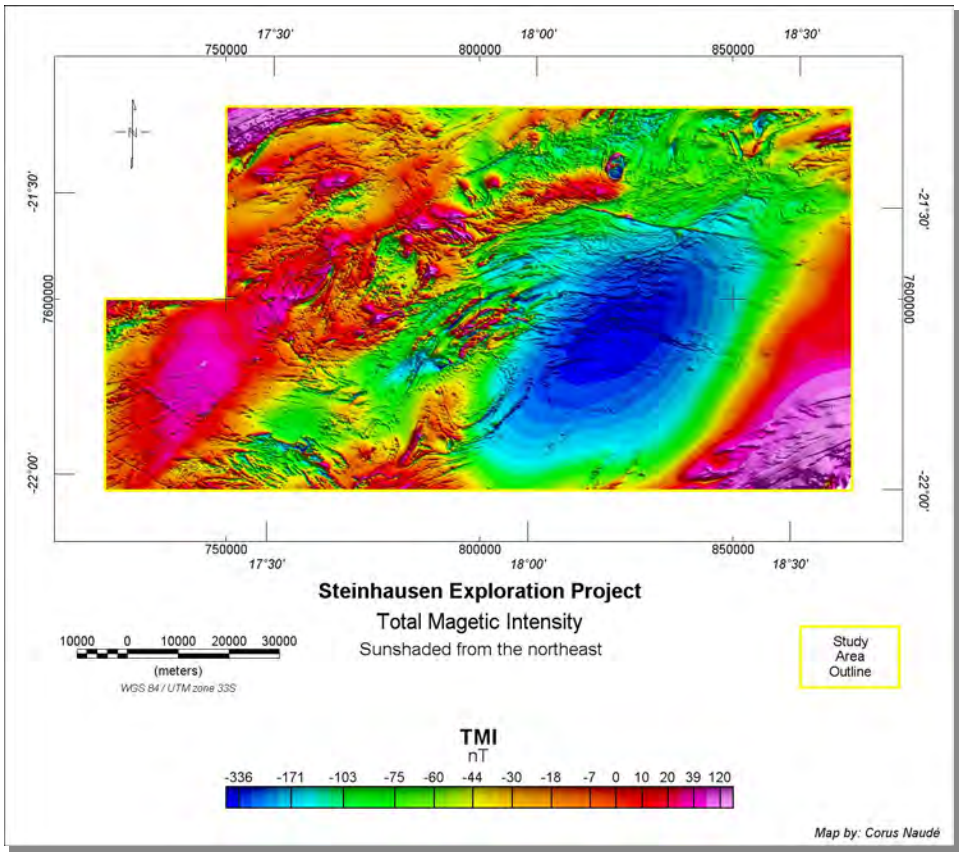

Figure 5.20: Total Magnetic Intensity image from the GSN airborne magnetic survey.

The TMI at any given point is specified by both a direction and a magnitude and as such it is a vector field that can be expressed as a function of its x, y and z components:

$$TMI = f(x, y, z) \tag{1}$$

5.3.2.2 First Vertical Derivative (FVD)

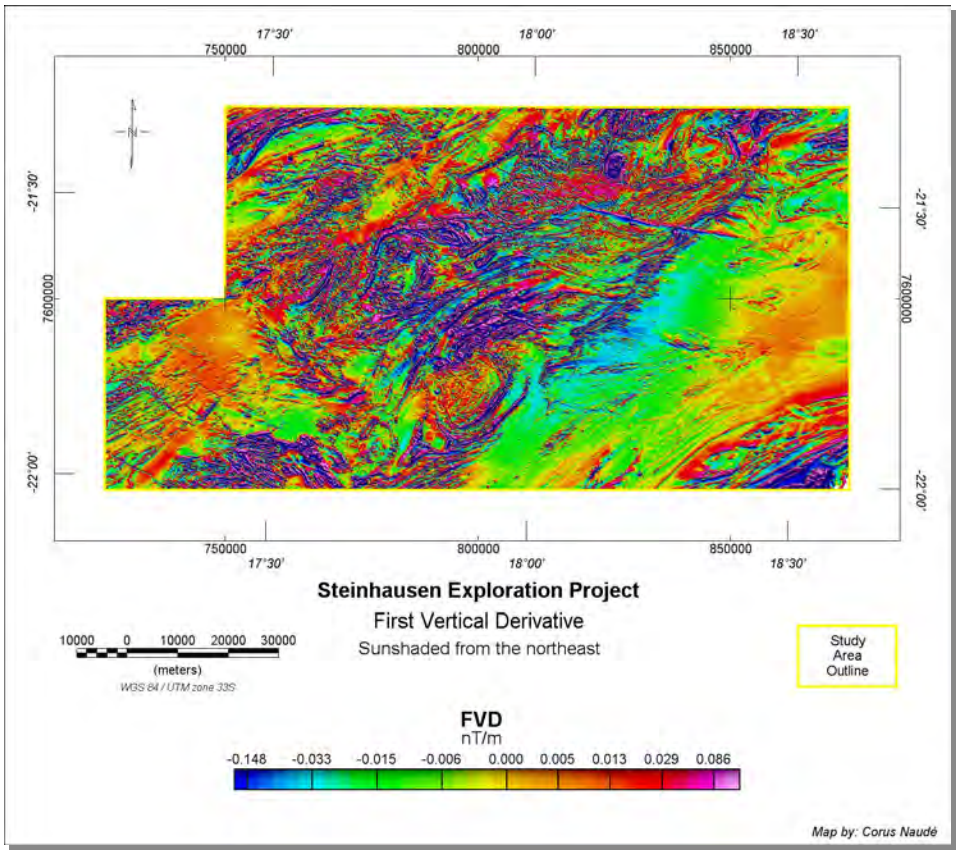

Figure 5.21: First Vertical Derivative (FVD) image from the GSN airborne magnetic survey.

The FVD is the derivative of the TMI in the z direction,

$$FVD = \frac{\partial f}{\partial z} \qquad \text{(m)}$$

and enhances anomalies over shallow magnetic bodies. The FVD reaches its maximum values above magnetic units with zero cross-over the edge of near-vertical symmetrical bodies.

5.3.2.3 Reduction to Magnetic Pole (RTP)

Due to the dipolar nature of the geomagnetic field, magnetic anomalies located within the study area will be asymmetrical even for bodies for which the magnetic source distribution is symmetrical. At the Earth's magnetic poles, the Earth's magnetic flux is vertical and therefore a symmetrical body will show a symmetrical induced magnetic field. The RTP takes an observed total magnetic field grid and transforms it into a magnetic grid that would result had the area been surveyed at the magnetic pole (MacLeod *et al.*, 1993). The RTP thus removes asymmetries to simplify the interpretation. The filter is computed in the frequency domain by the operator (Cooper and Cowan, 2005)

$$A'(u,v) = \frac{A(u,v)}{(\sin\theta + i\cos\theta\sin(\varphi + \alpha))^2} \qquad \text{(n)}$$

where $A(u,v)$ is the amplitude at frequencies (u,v), θ and φ are the geomagnetic inclination and declination respectively, and a is $\tan^{-1}(v/u)$ (Cooper and Cowan, 2005). If the inclination and declination of the present-day field is used, i.e. the induced field, anomalies of remanently magnetised bodies will not necessarily appear symmetrical.

To illustrate the effect of calculating the RTP from TMI data, Figure 5.22 shows the TMI image of a portion of the survey area in the vicinity of the Ekuja Dome, opposed to Figure 5.23 which shows the RTP image of the same area.

The residual filters described in the remainder of this section are aimed at accurately mapping magnetic bodies as well as contacts and structure visible from the magnetic data. Accurate positioning is however complicated by the asymmetrical nature of the TMI. In order to correctly position magnetic anomalies, contacts and structure, these residual filters should be created from the RTP.

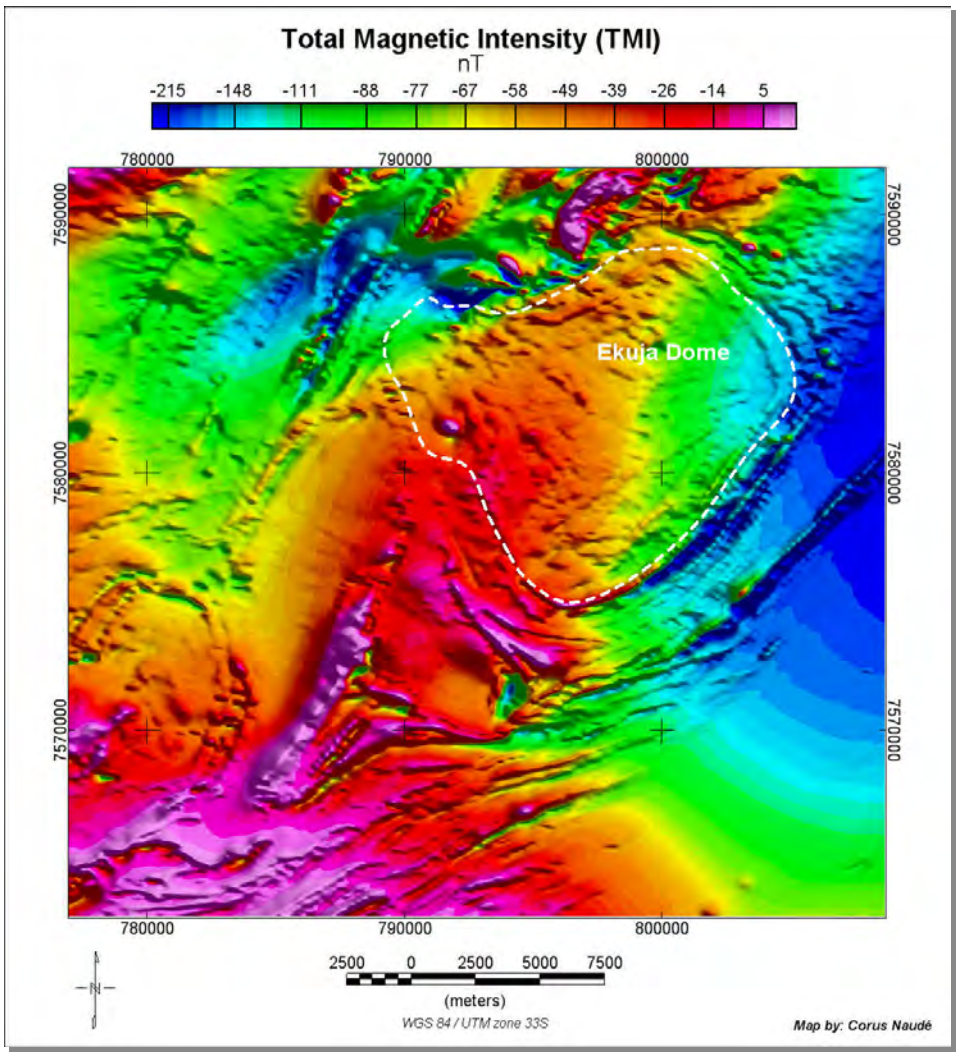

Figure 5.22: Total Magnetic Intensity (TMI) image from the GSN airborne magnetic survey over Ekuja Dome.

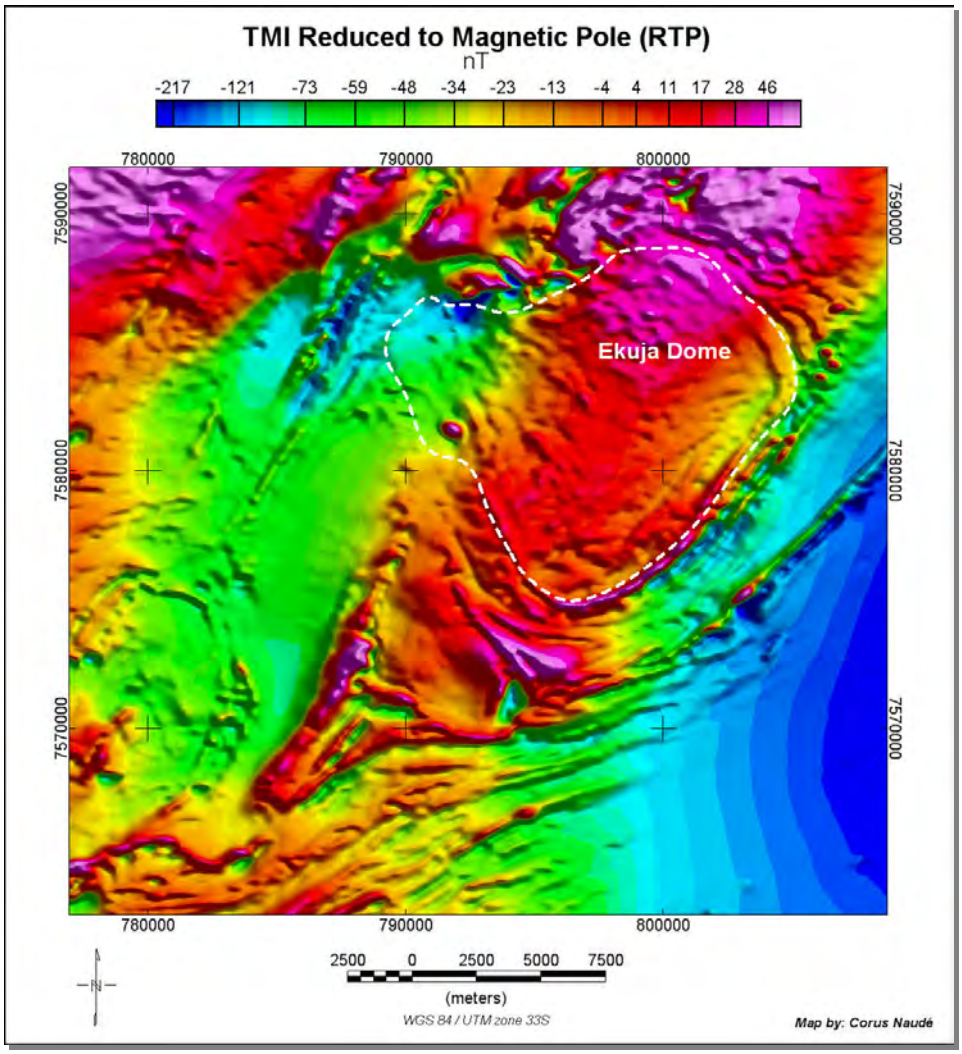

Figure 5.23: Reduced to Magnetic Pole (RTP) image from the GSN airborne magnetic survey over Ekuja Dome.

5.3.2.4 Total Horizontal Derivative (THD)

The THD is defined as (Cooper and Cowan, 2008)

$$THD = \sqrt{\left(\frac{\partial f}{\partial x}\right)^2 + \left(\frac{\partial f}{\partial y}\right)^2} \tag{n}$$

and reaches its maximum over contacts of symmetrical bodies. It is thus very useful for contact mapping. Figure 5.24 shows the THD image of a portion of the survey area in the vicinity of the Ekuja Dome.

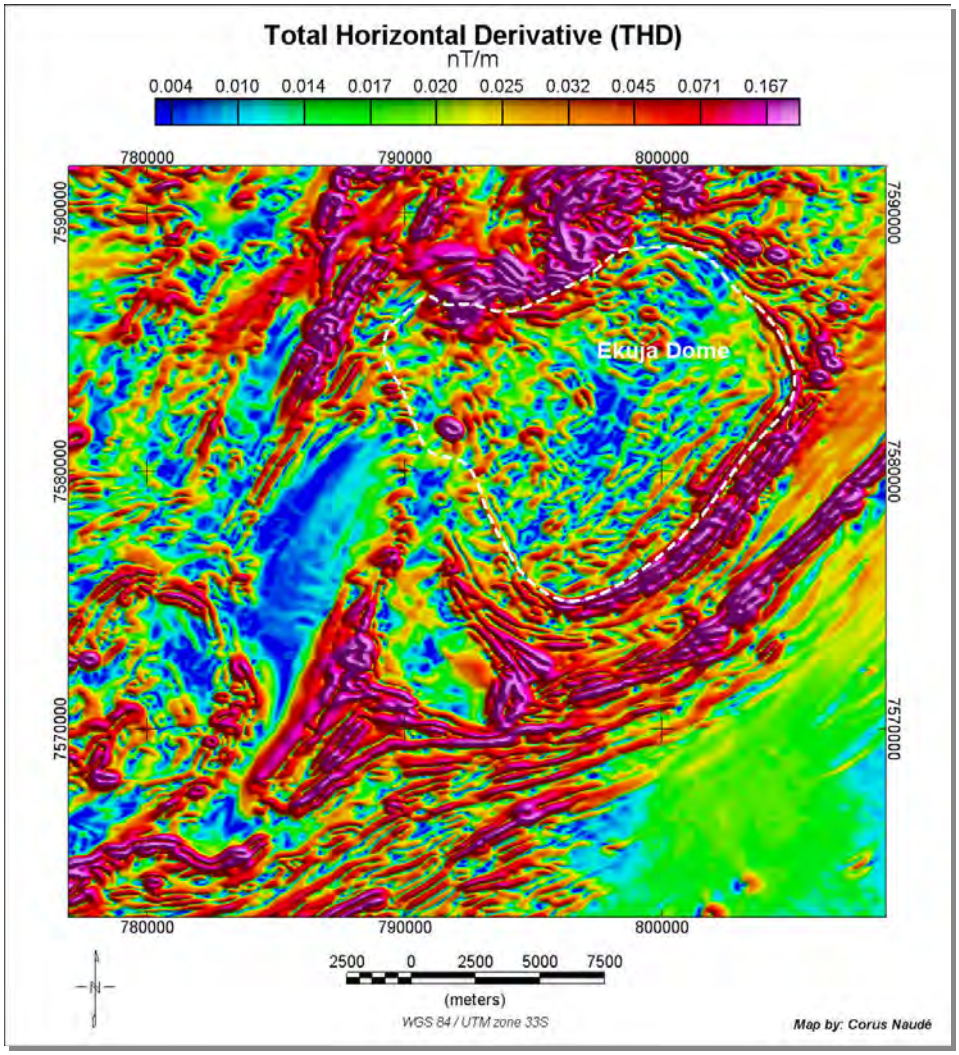

Figure 5.24: Total Horizontal Derivative (THD) image from the GSN airborne magnetic survey over Ekuja Dome.

5.3.2.5 Normalised Total Horizontal Derivative (TDX)

Cooper and Cowan (2006), proposed the normalization of the THD by the FVD in order to enhance more subtle features. The TDX is defined as (Cooper and Cowan, 2006)

$$TDX = \tan^{-1}\left(\frac{\sqrt{\left(\frac{\partial f}{\partial x}\right)^2 + \left(\frac{\partial f}{\partial y}\right)^2}}{\left|\frac{\partial f}{\partial z}\right|}\right) \quad \text{(o)}$$

and, similar to the THD, has maxima at the edges of magnetic bodies but with added detail in areas of low magnetic signal as is evident by comparing Figure 5.25 of the TDX over Ekuja Dome to that of the THD as shown in Figure 5.24.

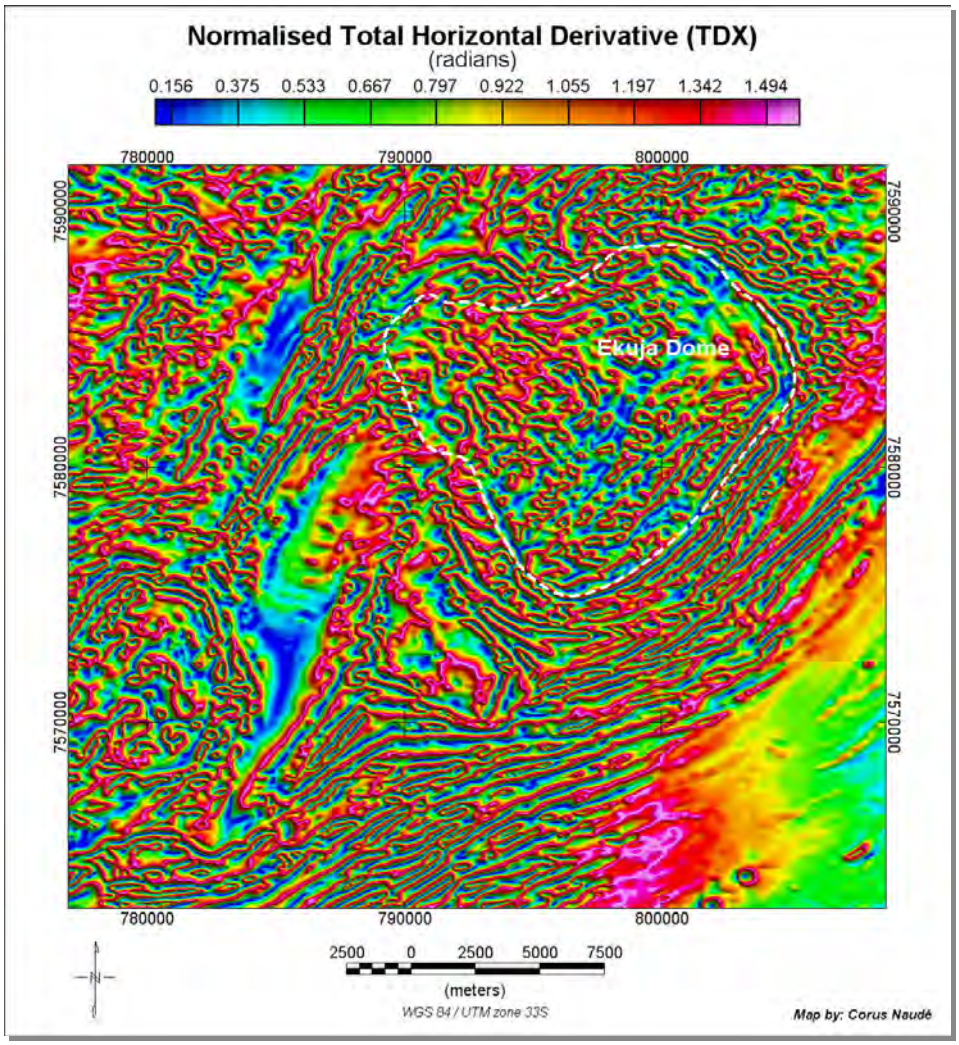

Figure 5.25: Normalised Total Horizontal Derivative (TDX) image from the GSN airborne magnetic survey over Ekuja Dome.

5.3.2.6 Analytic Signal (AS)

The Analytic Signal is commonly used in the interpretation of magnetic data as it is believed to be independent of the direction of magnetisation thus producing maxima directly over discrete bodies and their edges and the width of the maximum being indicative of the depth of the body (MacLeod *et al.,* 1993). This is not always the case though and is based on various simplifications as pointed out by Li (2006). Li (2006) concludes that "the AS is independent of nothing but depends on everything that the gravity or magnetic field itself may depend: the burial depth, extent, dipping angle of a source body, body's magnetisation direction, and earth's magnetic-field direction", but nevertheless points out that in the absence of accurate remanent magnetisation information or at low latitudes the AS could enhance qualitative interpretations. The AS is defined as (MacLeod *et al.,* 1993)

$$AS = \sqrt{\left(\frac{\partial f}{\partial x}\right)^2 + \left(\frac{\partial f}{\partial y}\right)^2 + \left(\frac{\partial f}{\partial z}\right)^2} \qquad (p)$$

and is shown if Figure 5.26 for the Ekuja Dome area. Although the AS is a derivative product, which enhances magnetic fabric, apart from its above attributes, it has a mapping shortcoming in that 2 dimensional features often tend to break up into bull's eye anomalies, and strike continuity is lost.

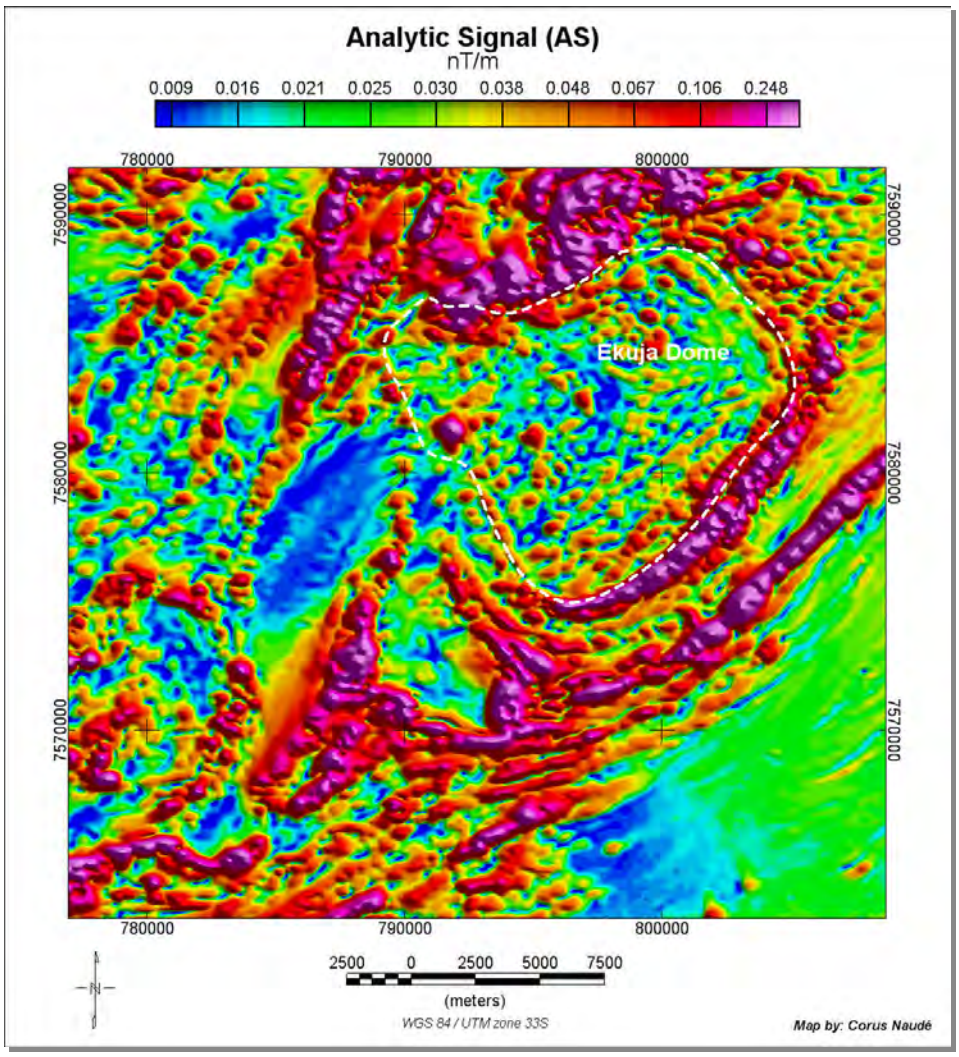

Figure 5.26: Analytic Signal (AS) image from the GSN airborne magnetic survey over Ekuja Dome.

5.3.2.7 Potential Field Tilt Derivative (TDR)

The Potential Field Tilt (TDR), illustrated in Figure 5.27, is sometimes named the tilt derivative and is defined as follows (Verduzco *et al.*, 2004):

$$TDR = \tan^{-1}\left(\frac{\left(\frac{\partial f}{\partial z}\right)}{\sqrt{\left(\frac{\partial f}{\partial x}\right)^2 + \left(\frac{\partial f}{\partial y}\right)^2}}\right) \qquad (q)$$

From equation (q) the amplitudes of the TDR are restricted to $-\pi/2$ and $\pi/2$. This acts as an automatic gain control that equalises amplitude output of TMI anomalies (Verduzco *et al.*, 2006). Subtle anomalies in magnetically quiet areas are thus enhanced relative to higher amplitude anomalies. The TDR has the property of peaking over magnetic bodies with its zero-crossover close to the edge of the body. It is an excellent filter for fabric mapping, i.e. arising from shallow geological features, and shows better spatial resolution than the first vertical derivative.

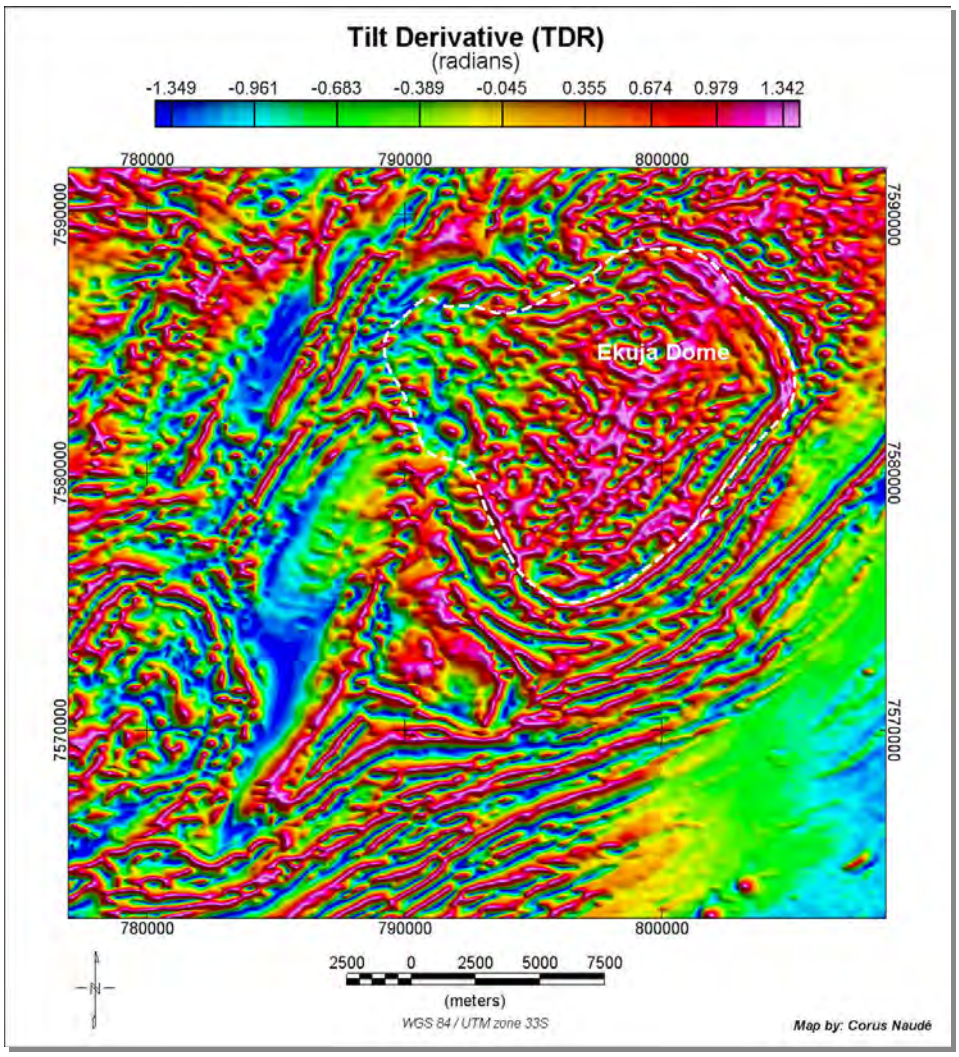

Figure 5.27: Potential Field Tilt (TDR) image derived from the GSN airborne magnetic survey TMI over Ekuja Dome.

5.3.2.8 Horizontal Derivative of the TDR (HD-TDR)

The HD-TDR effectively calculates the combined derivative of the TDR in the x and y directions as per equation (r) (Verduzco *et al.*, 2006).

$$HD-TDR = \sqrt{\left(\frac{\partial TDR}{\partial x}\right)^2 + \left(\frac{\partial TDR}{\partial y}\right)^2} \qquad (r)$$

This results in an image that shows maxima over the contacts of magnetic units. The HD-TDR is thus also very useful for contact mapping, as an adjunct to the THD.

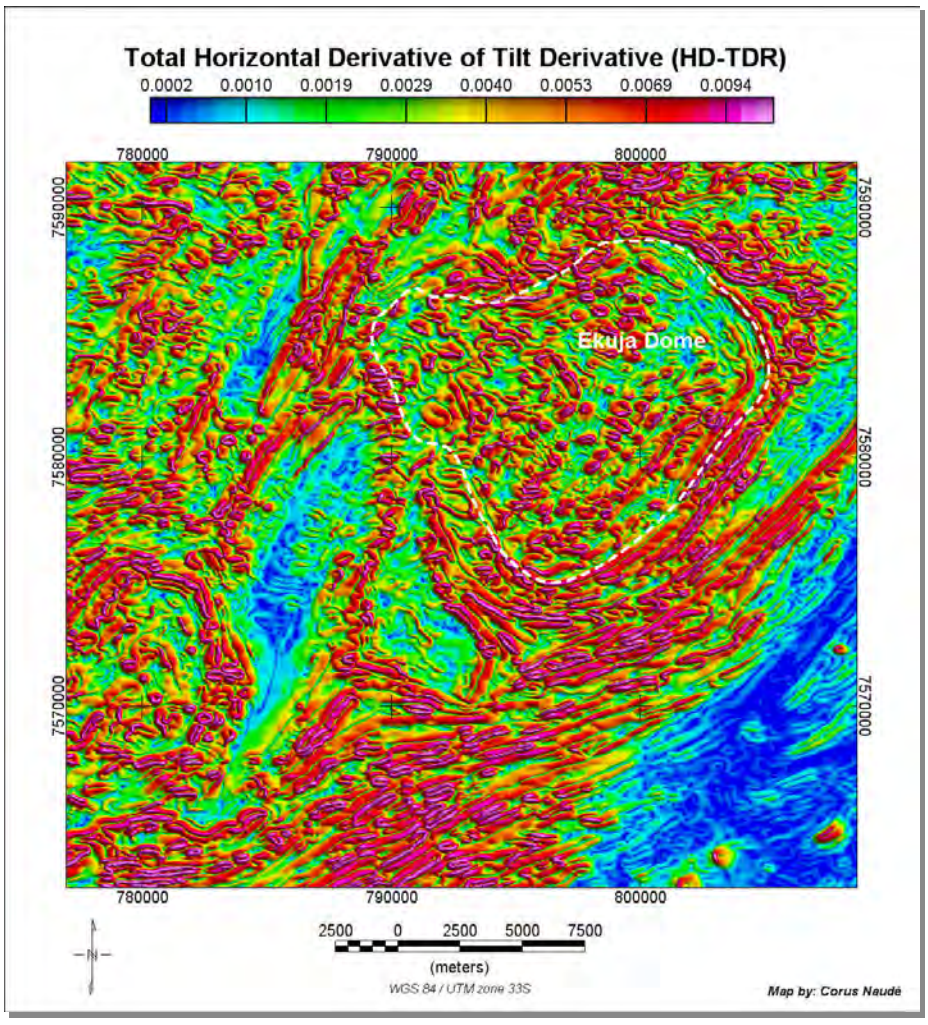

Figure 5.28: Horizontal Derivative of the TDR (HD-TDR) image derived from the GSN airborne magnetic survey TMI over Ekuja Dome.

5.3.2.9 Theta Map

The theta map (or theta derivative) as defined in equation (s) (Cooper and Cowan, 2006) peaks over a simple vertical contact and coincides with the zero-crossings of the FVD, TDR and TDX derivates (Fairhead and Williams, 2006). This filter is therefore also applied for contact and fabric mapping.

$$Theta = \cos^{-1}\left(\frac{\sqrt{\left(\frac{\partial f}{\partial x}\right)^2 + \left(\frac{\partial f}{\partial y}\right)^2}}{\sqrt{\left(\frac{\partial f}{\partial x}\right)^2 + \left(\frac{\partial f}{\partial y}\right)^2 + \left(\frac{\partial f}{\partial z}\right)^2}}\right) \quad \text{(s)}$$

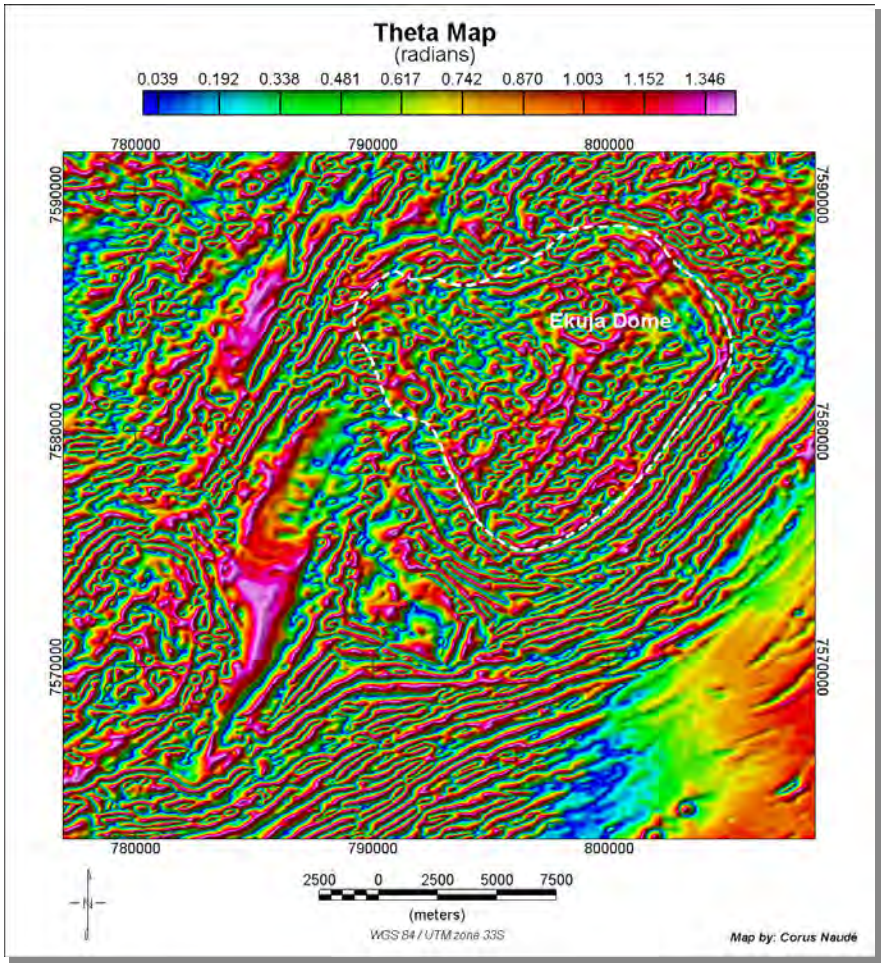

Figure 5.29: Theta Map image derived from the airborne magnetic survey TMI over Ekuja Dome.

Chapter 6

INTERPRETATION AND DISCUSSION

The geophysical interpretation consists of structural, stratigraphic and lithological mapping. The geological control for stratigraphic mapping of the area is very limited due to Kalahari cover. Mapping by Kasch (1986) has indicated some outcrops along the banks of the Black Nossob River in the vicinity of the Ekuja dome and EONC. The exploration map compiled for MIM Exploration by Kasch (1998), the mapping of the Okatjuru Layered Complex and surrounds by Kasch (Corner, pers. comm., 2009) during 2008, and borehole data from various EPL reports were used to classify geophysical responses for different geological units. However, there are no geological controls available (apart from very general GSN 1:1000000 map) over the entire northern, central and north-eastern parts of the study area. Over these areas the correlation of geophysical responses to lithological units is thus subject to ground truthing.

Figure 6.1 and Figure 6.2 show the FVD and ternary radiometric image respectively for easy referral during the following discussion.

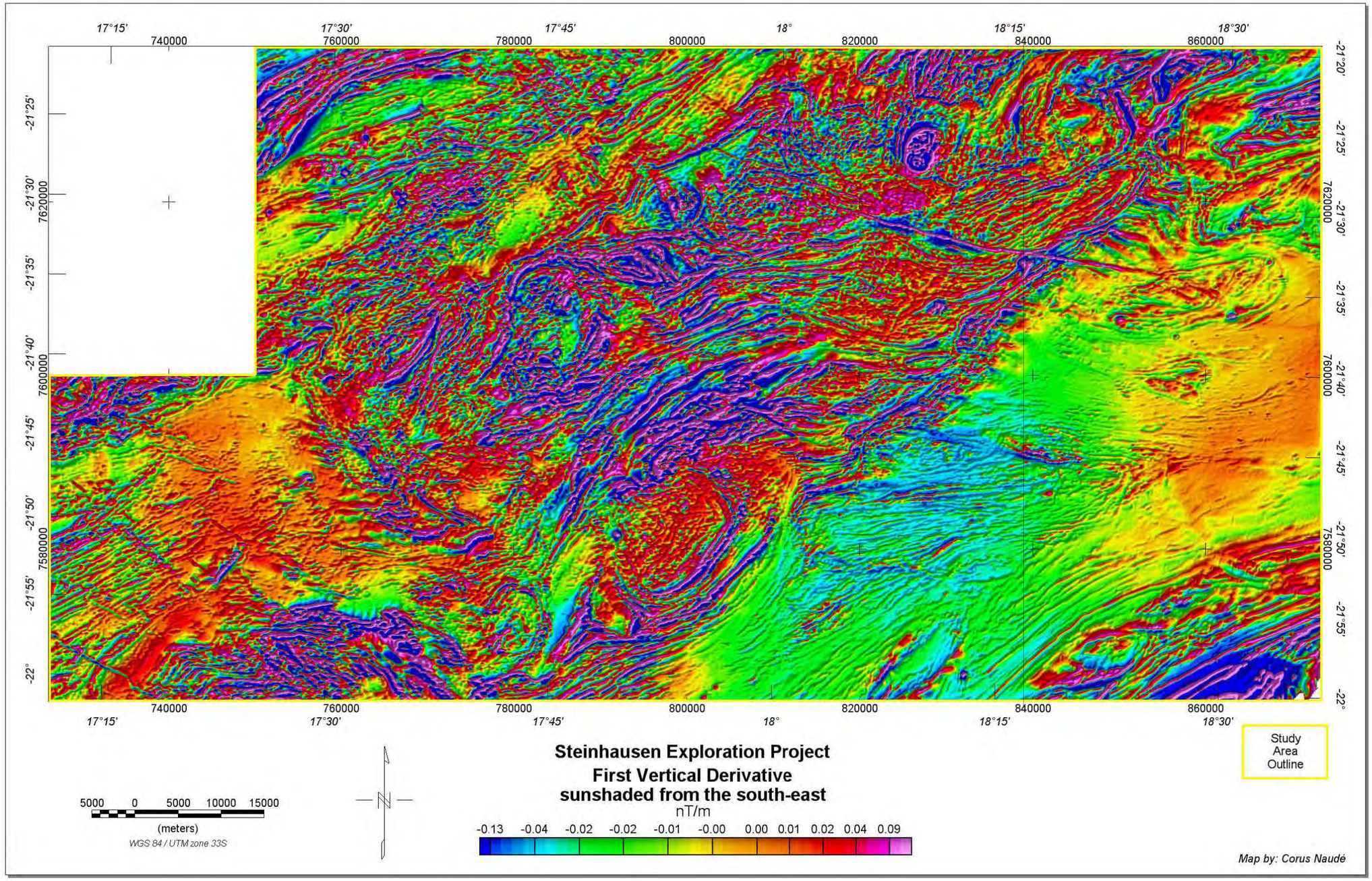

Figure 6.1: FVD from the GSN airborne magnetic survey of the Steinhausen Project Area.

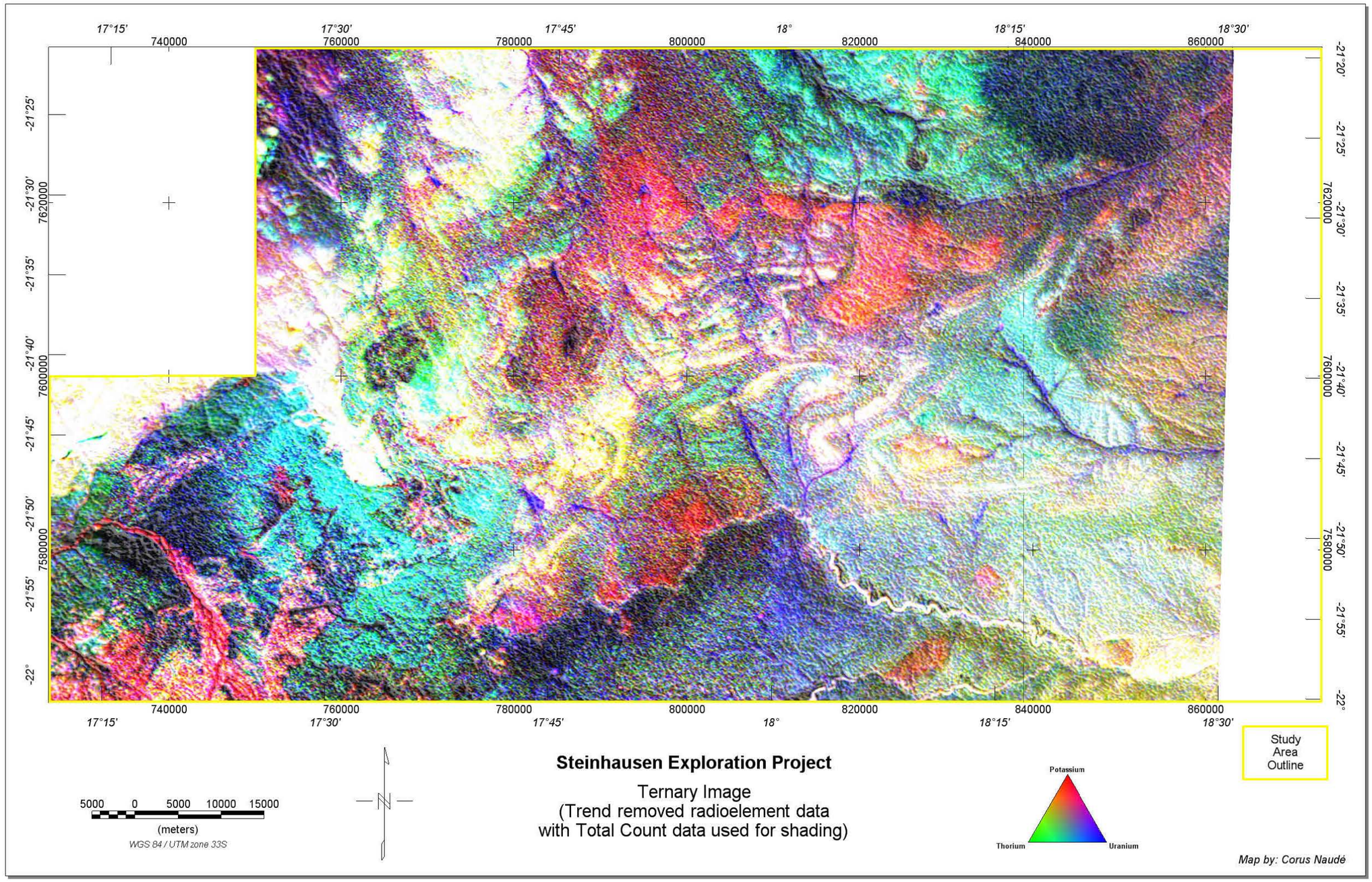

Figure 6.2: Ternary Image from the GSN airborne radiometric survey of the Steinhausen Project Area.

6.1 Structural Mapping

Structural features were divided into three groups: lineaments, regional faults and faults / fractures. The term lineament refers to a large-scale fault zone having a much broader swath of faulting up to 30 km in width, either continuous or disrupted (Richards, 2000). Distinguishing between lineaments and regional faults is subjective and based on strength of appearance, continuity over large distances or whether features occur as observable terrain boundaries on gridded images. Similarly, the differentiation between regional faults and faults of smaller scale is also subjective. Differentiation between fault types, e.g. thrust, normal, listric, strike slip, bedding parallel, and their chronology is often difficult if not impossible to ascertain from geophysical data alone unless a clear sense of movement is seen. Low angle faults, often associated with mineral occurrences, are mostly equivocal from the magnetic data as lithological contacts will have similar expressions. Mapped structural features are presented in Figure 6.3.

An array of east-west trending structures were identified across the EONC and believed to possibly have some control on mineralisation within the EONC (Corner, pers. comm., 2009). Faults (regional as well as minor) delineated within this east-west trending zone were mapped as a separate layer called E-W Structural Zone (Figure 6.3).

Two lineaments, the Okahandja Lineament (OL) in the northwest and the Kudu Lineament (KL) (Corner, 2000, 2008) in the centre of the area are clearly discernable in the magnetic data striking northeast. Observed from Figures 6.1 and 6.3, it is apparent that these two lineaments form important geological boundaries, with the area between them displaying a clearly different magnetic fabric. This study corroborates the interpretation by Corner (2008) that uplift has taken place between the two lineaments, resulting in the exposure of deeper, magnetically more active units.

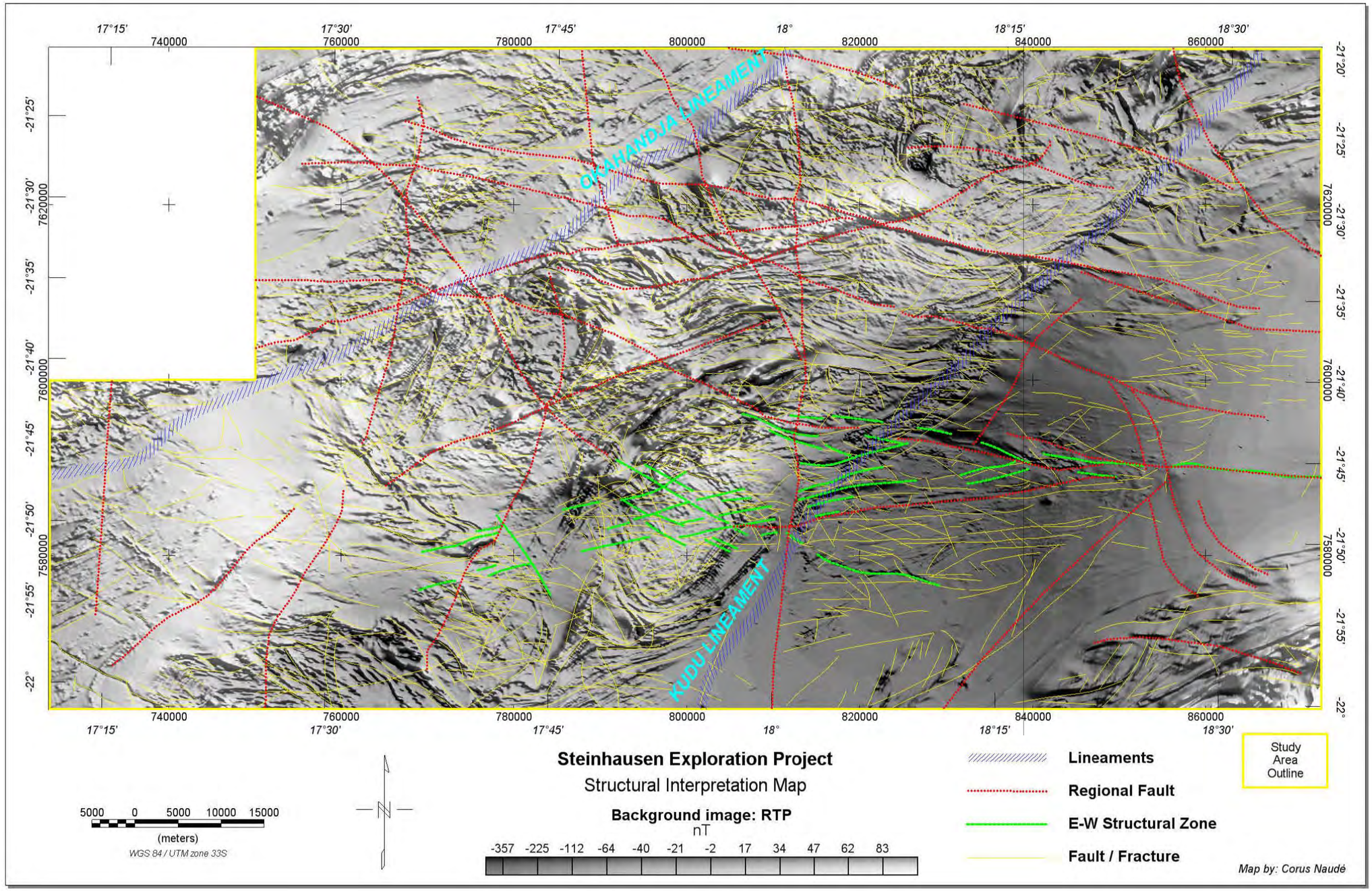

Figure 6.3: Structural interpretation of Steinhausen Project Area.

6.2 Stratigraphy and lithological mapping

A number of interpretive layers have been compiled which highlight lithologies and features that are evident from the geophysical data. These are shown in Figure 6.4 and are discussed below. A large format 1:100,000 scale version of Figure 6.4 accompanies this thesis as a fold out map.

The geological backdrop to this map is derived from a combination of sources including, early GSN mapping, the mapping campaigns of Kasch (1998, 2008), earlier interpretation of the geophysical data by Corner (2006, pers. comm., 2009), and the current detailed interpretation of the author as discussed below for the various stratigraphic units.

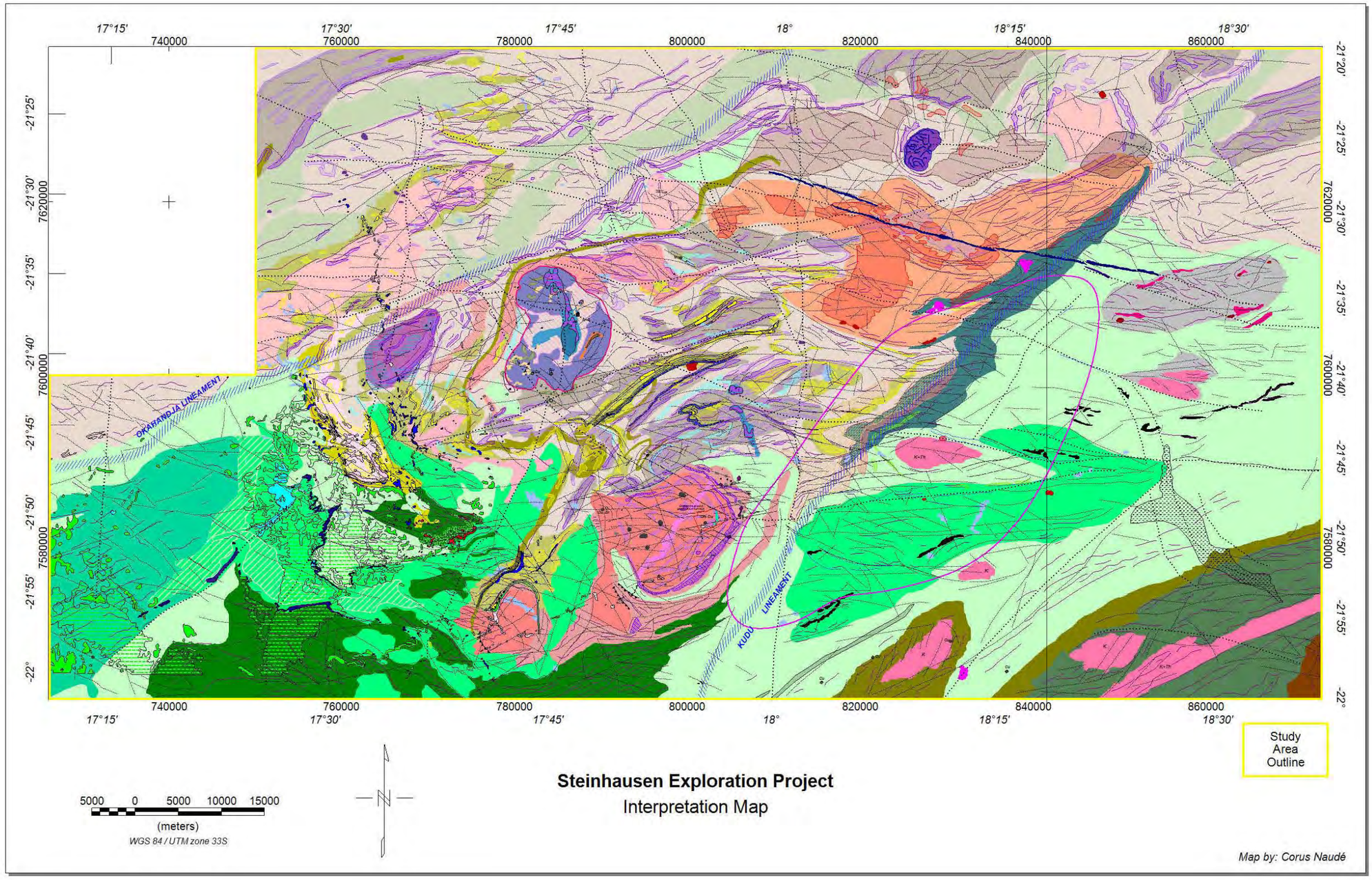

Figure 6.4: Interpretation map of Steinhausen Project Area.
(For legend refer to Figure 6.5 below)

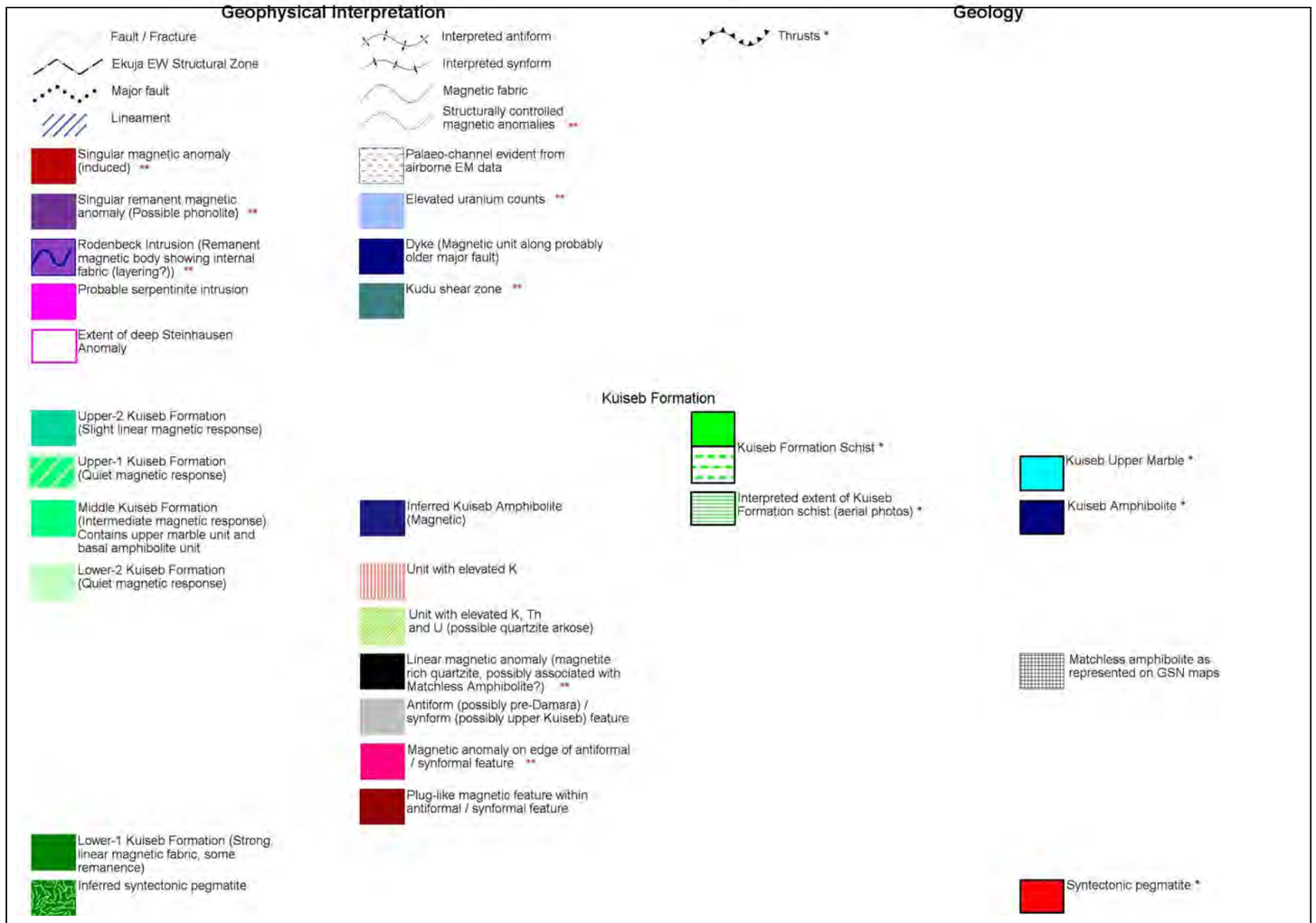

Figure 6.5 (Part 1 of 3)

Hakos Group

Kudis Subgroup. (Linear magnetic features within quiet magnetic fabric)

Undifferentiated lower Damara (Strong, linear magnetic fabric, some remanence)

Eastern Basement

K + Th + U Plug

K + Th — Granite (elevated K and Th)

K — Granite (elevated K)

Possible granite (uniform magnetic fabric)

Nosib Group

Nosib Group (Quartzite, conglomerate, schist, carbonate (from GSN 1:1 000 000 map))

Pre-Damara Succession

Undifferentiated pre-Damara

Upper pre-Damara (Broken magnetic fabric with higher Th and U but low K)

Quiet magnetic unit mostly with higher Th and U counts

Lower pre-Damara (Broken to linear magnetic fabric but with elevated K values (low Th and U))

Unit with high frequency, mostly linear magnetic fabric across strike

Unit with less intense, high frequency, mostly linear magnetic fabric across strike

High K counts within quiet magnetic unit

Area of demagnetization **

Magnetic anomaly within zone of demagnetization **

High K counts within lower pre-Damara

Arenaceous stratigraphy grouped (Units 1-6, possible Nosib) **

1. Unit of elevated K, Th, and U (Closely associated with mapped coarse grained quartzite) **

3. Inferred Glassy Quartzite **

5. Onjona Basement Collar (Thrust zone including Onjona Basement Gneiss and Arenaceous Units)

Unit of elevated Th and U

Zone of strong magnetic units within pre-Damara sequence

Strong magnetic unit (induced) within pre-Damara

Strong magnetic unit (remanent) within pre-Damara

Inferred lower marble unit

Low radiometric Total Count unit within Daylight Dome (inferred anorthosite)

Daylight Dome (Domal feature within linear magnetic fabric of pre-Damara stratigraphy)

Probable Basement Dome (North)

Onjona East Basement (Elevated 'spotty' K appearance)

Onjona Basement Gneiss (Quiet magnetic signature and high radiometric count. Possible association with Abbabis or Hohewater Metamorphic Complex)

Basement unit of pre-Damara succession (Broken magnetic signature and high radiometric count. Possible association with Abbabis or Hohewater Metamorphic Complex)

Basement unit of pre-Damara succession (Broken magnetic signature and intermediate radiometric count. Possible association with Abbabis or Hohewater Metamorphic Complex)

2. Coarse grained quartzite *

4. Interpreted extent of coarse grained quartzite (aerial photos)*

6. Coarse grained quartzite as represented on GSN 1:1 000 000 map (Note that positional errors are likely)

Lower marble unit *

Interpreted extent of marble (aerial photos) *

Basement as represented on GSN 1 : 1 000 000 map

Basement gneiss*

Figure 6.5 (Part 2 of 3)

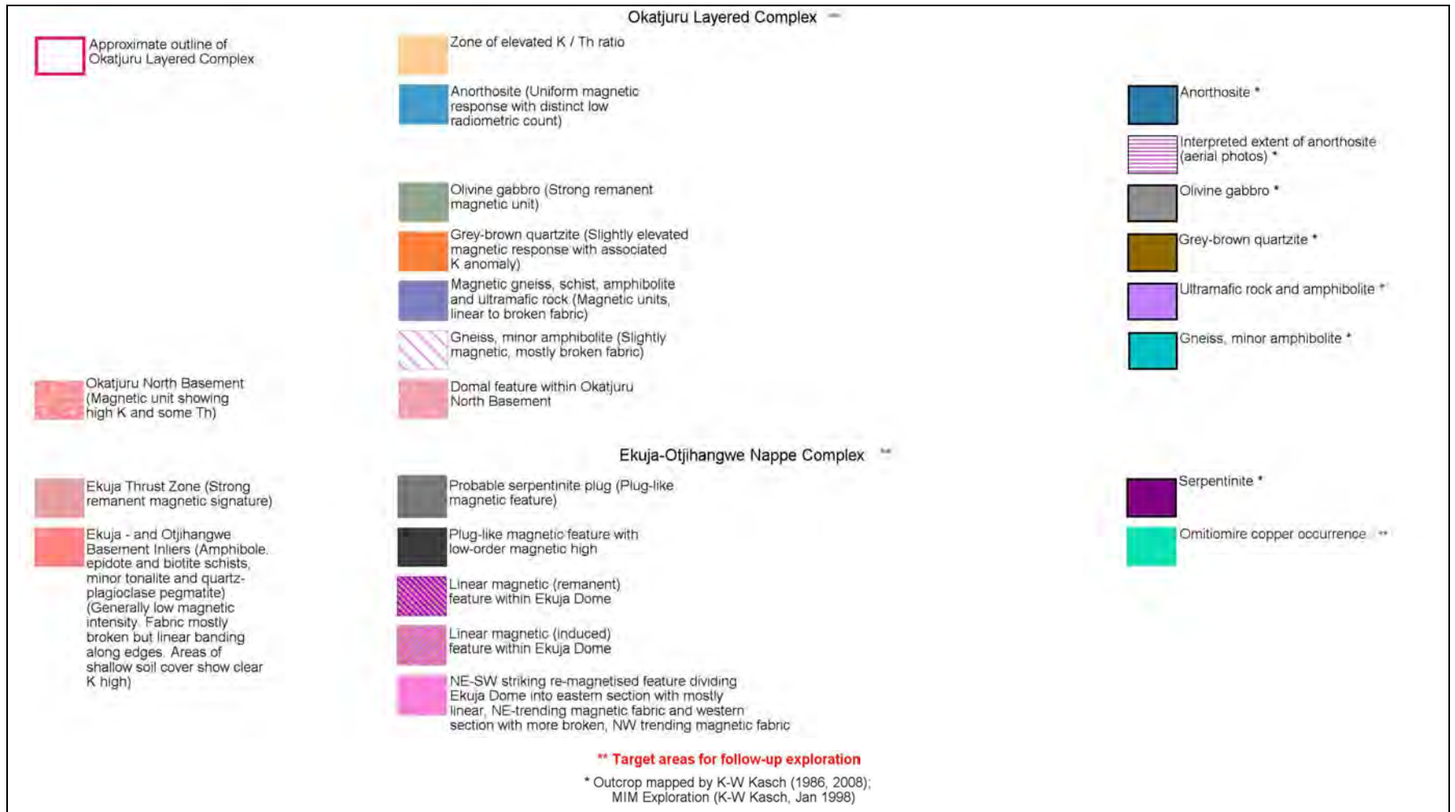

Figure 6.5 (Part 3 of 3)

Figure 6.5: Legend for interpretation map of Steinhausen Project Area.

6.2.1 Features not related to specific stratigraphy

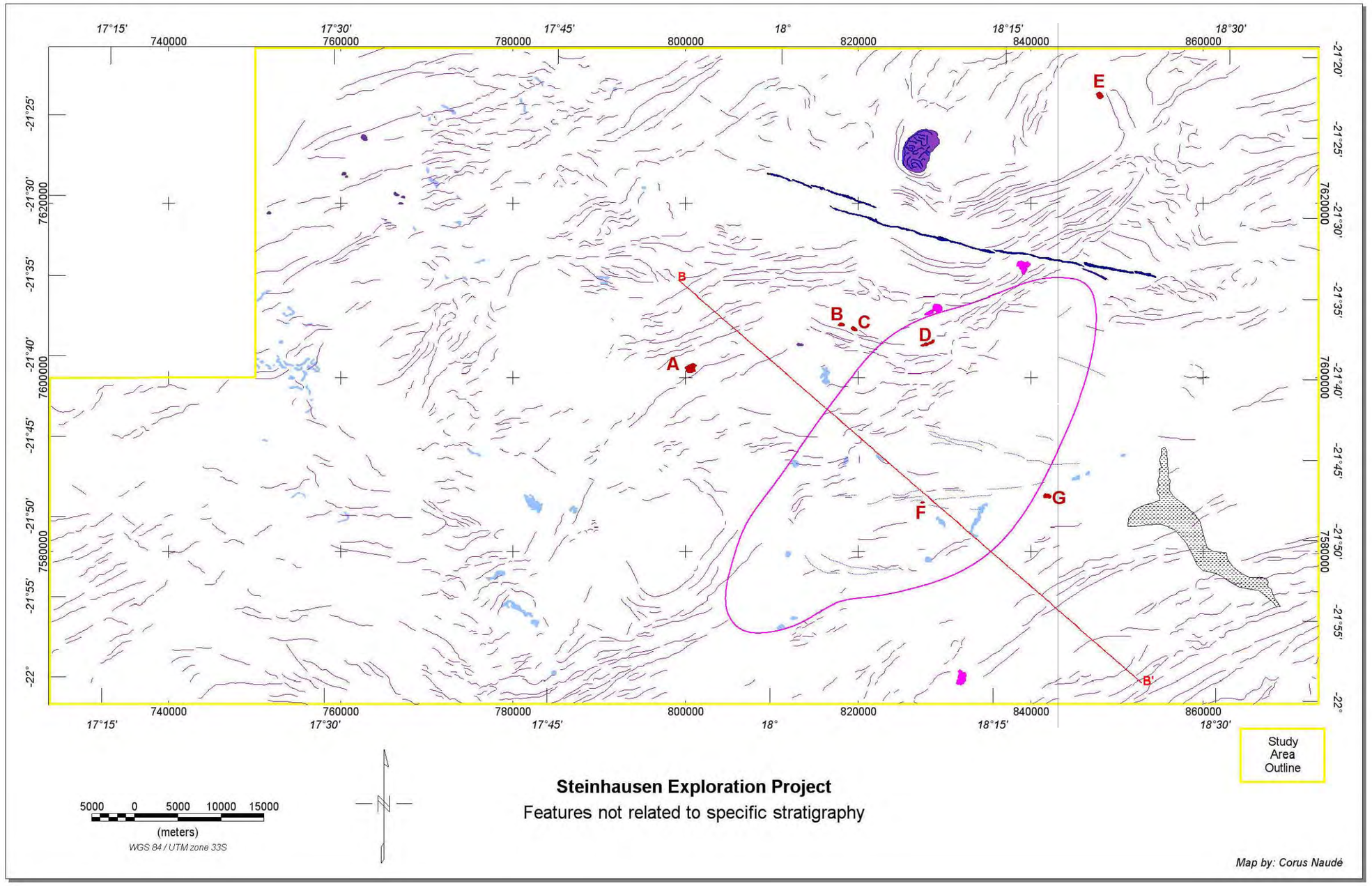

Figure 6.6: Features not related to specific stratigraphy.
For legend refer to Figure 6.7

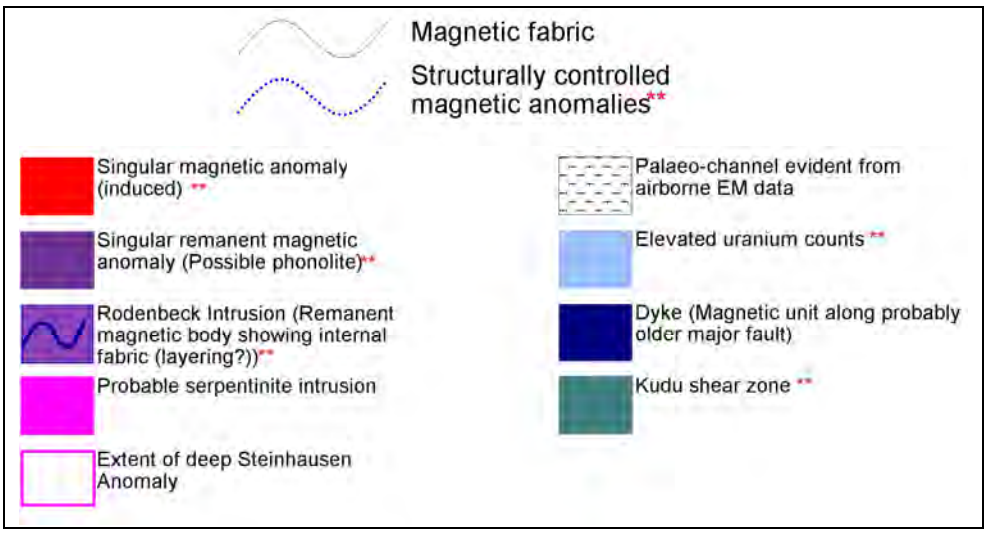

Figure 6.7: Geophysical interpretation legend for Figure 6.6 – features not related to specific stratigraphy.

Interpretation of the geophysical data has identified various features that are younger (late- to post-tectonic, or recent), not obviously correlated to specific stratigraphic units or which cut across known stratigraphy:

- Magnetic fabric lines are mapped within and across all stratigraphic units, aiding the identification, description and separation of lithological units, deformation style, as well as indicating possible strike directions.

- Subtle linear magnetic anomalies occur within a generally magnetically quiet area within what is inferred as Kuiseb Formation Schists. These magnetic anomalies appear to follow or conform to structures within the host rock and are therefore believed to reflect these host rock structures.

- The following singular magnetic anomalies have been identified (refer to Table 6.1 and Figure 6.6):

Table 6.1: Singular magnetic anomalies

Anomaly	Farm Location	Description
A	Ombauejanam-bereke	Large (1 km diameter approx.) circular magnetic anomaly within arenaceous sequence, possibly deep. At intersection of major fault and cross-cutting faults.
B	Mazeppa	Small singular magnetic anomaly on WNW trending fabric at contact of K rich unit.
C	Mazeppa	Same as previous.
D	Natalia	Fault-bound magnetic anomaly on contact of slightly K anomalous stratigraphy.
E	Hinza	Magnetic anomaly on edge of basement inlier and pre-Damara stratigraphy.
F	Okanjesu	Singular magnetic anomaly on E-W trending fault-controlled fabric within the Kuiseb Formation.
G	Otjiwarongo	Singular magnetic anomaly within magnetically quiet Kuiseb Formation.

- A few singular, remanent magnetic anomalies have been identified. One on the farm Okowiruru North which is located in Pre-Damara stratigraphy and is bound by two prominent N and NNW trending faults. Others are situated in the northwest portion of the study area within pre-Damara stratigraphy and inferred to be possible phonolite intrusions.

- A large, remanent magnetic body is interpreted to have intruded pre-Damara stratigraphy on the farms Klein Ombaheme and Rodenbeck (hereafter termed the Rodenbeck Intrusion). The southern lobe of the intrusion is also evident on the radiometric image as low radiometric counts in all channels. Within the body there is clear magnetic fabric visible, indicating some degree of internal structure or differentiation.

- Various magnetic bodies have been mapped with similar responses to known serpentinite bodies. Two of the bodies, one on the border of the farms Tolene and Natalia and the other on the northern border of Bashee, are associated with the Kudu shear zone and were possibly emplaced during the shear event. A third unit was mapped on the farms Vendetta and Talana. To date, none of the known serpentinite bodies within the Damara Orogen have proven to be of economic importance although a larger body south of the survey area has shown traces of Ni mineralisation (Company reports of past EPL holders).

- The Steinhausen Anomaly is a clear magnetic low, east of the EONC, and a singular regional feature in Namibia. It is believed to be as a result of a large, deep area of severe demagnetisation (Corner, 2008) and modelled as such, Figure 6.8.

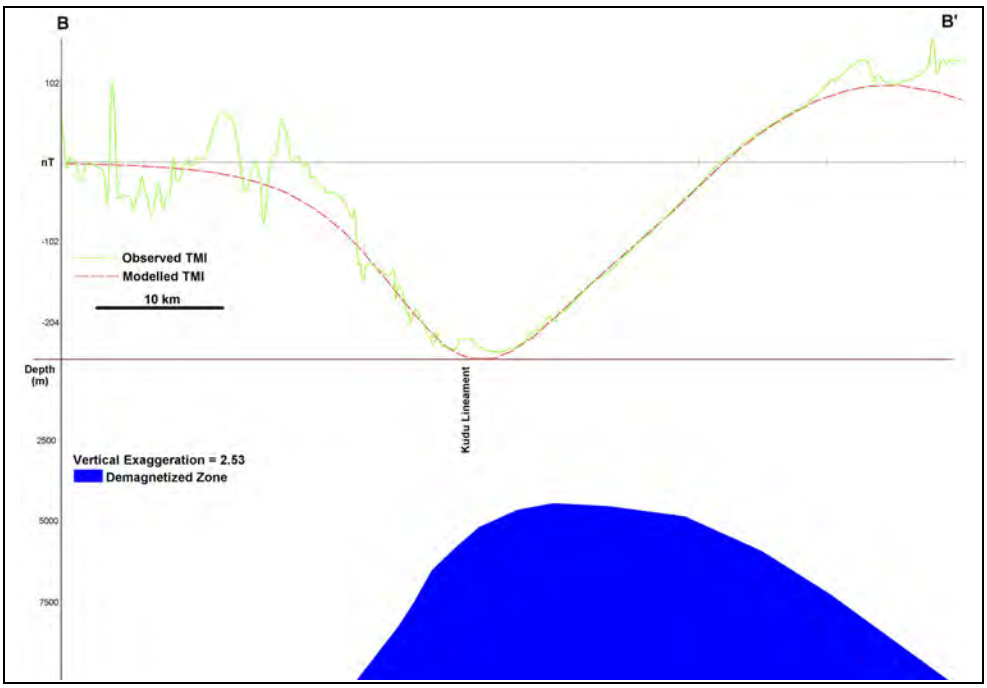

Figure 6.8: Forward model of Steinhausen Anomaly along profile B,B' (Figure 6.6).

- A north-south trending palaeo-channel is evident as a very conductive superficial, pre-Kalahari unit in the GSN airborne electromagnetic data spanning the south-eastern part of the study area.

- Prominent uranium anomalies (Figure 6.9), not apparently related to stratigraphy or structure, are evident, e.g. on the farms Steinhausen and Goedemoed. Although these anomalies roughly coincide with drainages, they are associated with uncharacteristically low K and Th values (Corner, pers. comm., 2009). These are interpreted to be as a result of surficial, relatively recent processes. Other prominent U anomalies are also seen to follow lithological units (e.g. adjacent to K-Th layers within pre-Damara stratigraphy on the farms Eensgezind and Hochberg, as well as the western clusters on the farms Elisenore, Bandolier, Martinsveldt and Elsie which are possibly associated with arenaceous – basement contacts). Other U anomalies include a west-northwest trending anomaly across the Otjihangwe Dome, and some

smaller, plug-like anomalies on the farms Gifpyl, Oehland and Kambingana and in the North western portion of the study area.

- A dyke has intruded along a major (possibly older) fault, cross-cutting pre-Damara stratigraphy and trending west-northwest from the southern portion of the farm Ettric to Omupanda. The dyke is seen as a clear linear magnetic unit.

- A zone of cross-cutting magnetic fabric has been interpreted as a shear zone along the Kudu Lineament northeast of the EONC. This also forms the faulted contact between pre-Damara stratigraphy and the Kuiseb Formation.

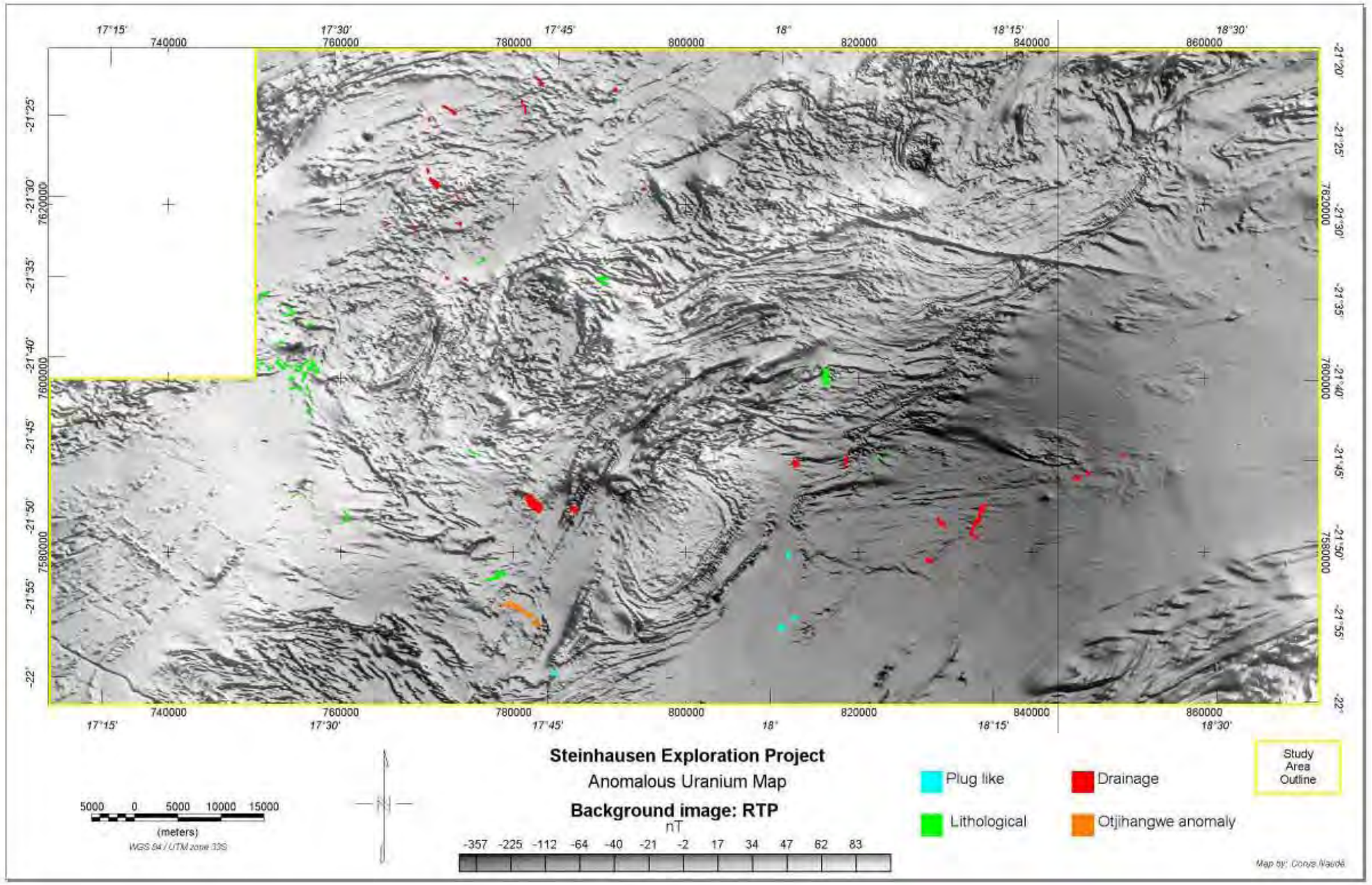

Figure 6.9: Anomalous uranium over Steinhausen Project Area.

Mineralisation potential of features not related to specific stratigraphy

- Various uranium anomalies have been identified from the radiometric data (Figure 6.9). Most of these anomalies are associated with current drainages or possible palaeo-channels. Other anomalies are evidenced as plug-like bodies or strata-bound anomalies.

- The singular, remanent magnetic anomalies that are fault/thrust bound possibly indicate the occurrence of pyrrhotite, a strong remanence carrier, with possible related mineralisation.

- The induced singular magnetic anomalies are either pipe-like or short strike 2D bodies. These occur in different lithological settings, and depending thereon could host deposits associated with hydrothermal copper or gold deposits.

- The Rodenbeck Intrusion is an apparently layered intrusion, possibly ultramafic, that holds potential for Ni - Cu mineralisation.

- The Kudu shear zone is interpreted to consist of a large zone of faulting and fracturing thus providing ample late-, to post-tectonic secondary porosity for fluid movement and related hydrothermal mineral deposits.

- Although not a target in itself due to its deep location and extent, the Steinhausen Anomaly could be indicative of the significant presence of hydrothermal fluids, and therefore be an important control on mineral occurrences in the vicinity.

- Miller (1983b) described the possibility of mineral occurrences associated with fluid movement along faults and thrusts during prograde metamorphism. Taking cognisance of this, various magnetic anomalies along interpreted faults have been identified. These magnetic anomalies fall mostly within the Upper-1 Kuiseb

Formation but some are also evident within the Middle Kuiseb Formation, and are seen as magnetic lows suggesting the occurrence of demagnetisation. (The Upper-1 Kuiseb Formation and Middle Kuiseb Formation are defined in the following section.)

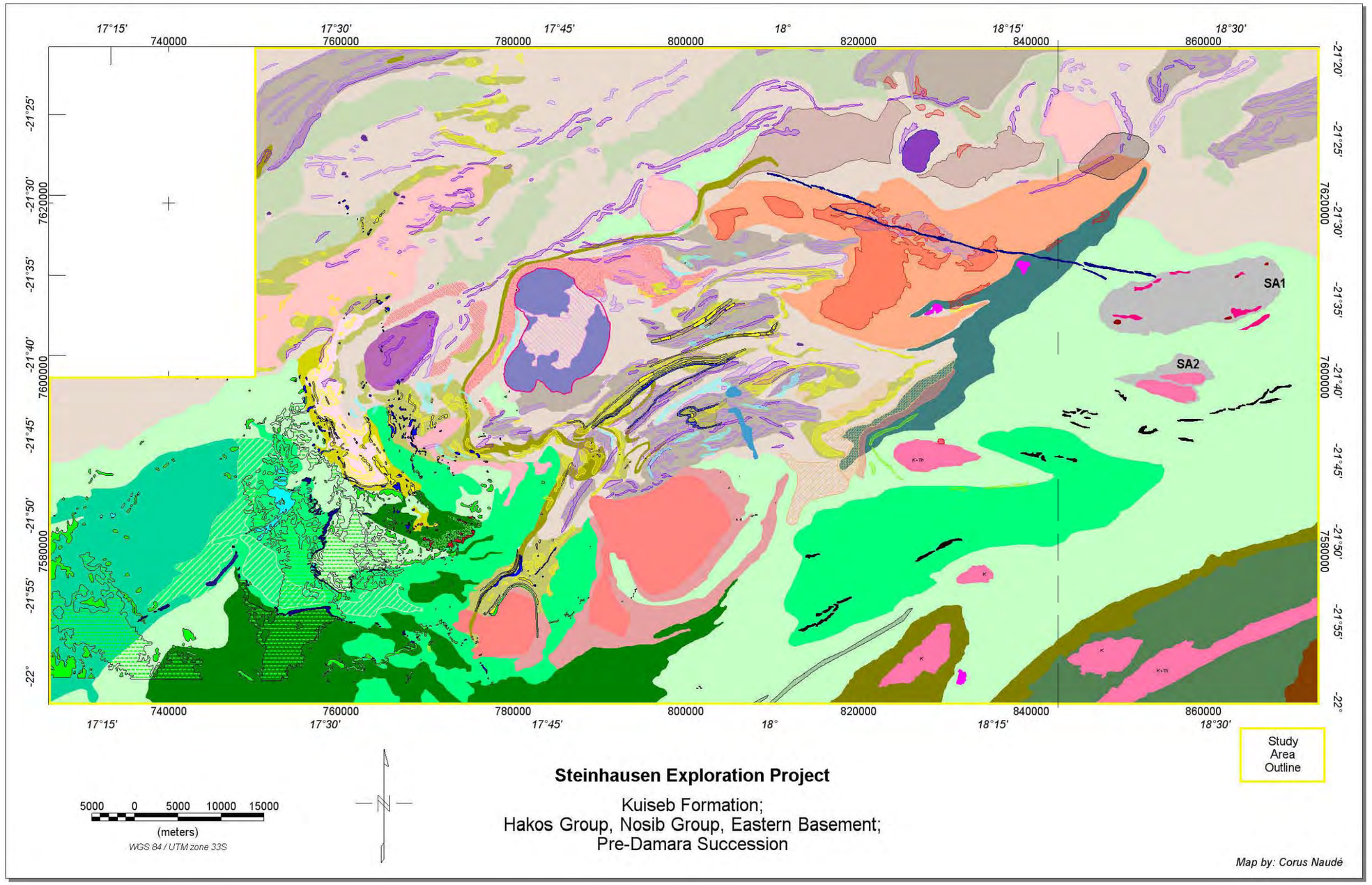

Figure 6.10: Kuiseb Formation; Hakos Group, Nosib Group and Eastern Basement; Pre-Damara Succession.
For legend refer to Figure 6.11 (Kuiseb Formation), Figure 6.13 (Hakos Group, Nosib Group and Eastern Basement), Figure 6.14 (Pre-Damara Succession)

6.2.2 Kuiseb Formation

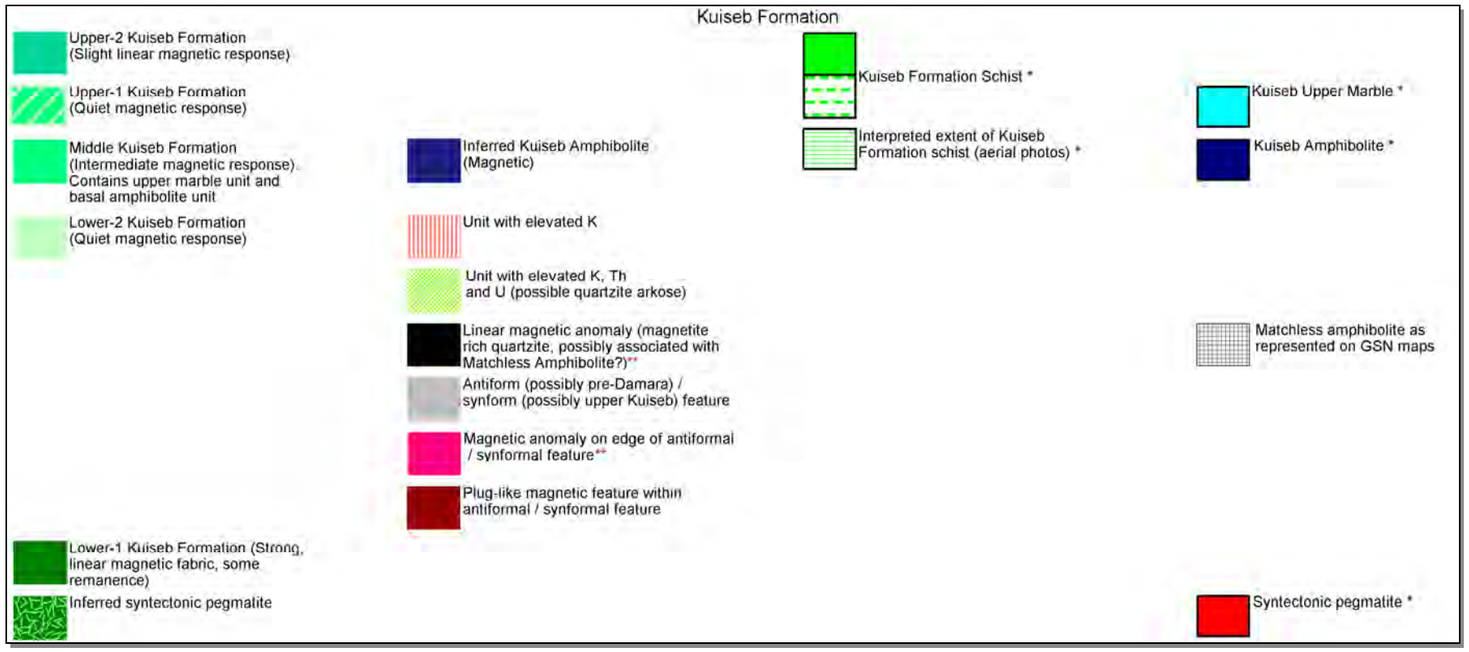

Figure 6.11: Geophysical interpretation legend for Figure 6.10 – Kuiseb Formation.

The Kuiseb Formation is characterised in the western Damara as mostly having a very uniform, smooth magnetic background or minor magnetic fabric. The only variance being slightly magnetic, linear anomalies associated with magnetite quartzites, e.g. in particular those closely associated with the Matchless Amphibolite Belt, as well as some elevated magnetic fabric close to the base of the Kuiseb. However, evident from data at, and west of, the Onganja Mine (southwest of the Steinhausen Area), the Kuiseb Formation is highly magnetic in places. In the Steinhausen Area the Kuiseb Formation has thus been divided into five units (Corner, pers. comm., 2009), based on differences observed in magnetic signature. These, which follow, are in accord with the more recent (2008) detailed mapping of Kasch:

- The Upper-2 Kuiseb Formation displays low-amplitude linear magnetic fabric, also seen in areas west of the study area. The radiometric response is of a low-order in all of K, Th and U.

- The Upper-1 Kuiseb Formation has a generally quiet magnetic signature. The radiometric response is of a low-order in all of K, Th and U.

- The Middle Kuiseb Formation has an intermediate magnetic response and is also characterised by an upper marble unit and basal amphibolite unit (Kasch, 2008). The amphibolite unit shows a strong magnetic response, thus aiding in mapping of the contact with the Lower-2 Kuiseb Formation. The Middle Kuiseb Formation shows a slight increase in radiometric response from the Upper Kuiseb Formations with the increase in Th dominating.

- The Lower-2 Kuiseb Formation displays a very quiet (uniform) magnetic fabric due to the generally non-magnetic properties of the thick schist/greywacke package that makes up this unit. This quiet,

low-magnetic property of the Kuiseb Formation is a common feature of the complete formation southwest of the Steinhausen area. Units of elevated K, U and Th, straddling the granite occurring on the farm Okanjesu, are clear from the radiometric data. These could possibly be correlated to arenaceous metasediments associated with the Lower-2 Kuiseb.

- The Lower-1 Kuiseb Formation is characterised by a very strong linear magnetic fabric, often remanent. This is not a common feature of the Kuiseb Formation, only becoming evident along the eastern extent of the Southern Zone for the first time near the Onganja Mine (southwest of the Steinhausen area). The Lower-1 Kuiseb Formation, which extends into the southern EPL areas, is observed to contain gabbro and highly magnetic epidosite near Onganja. The Lower-1 Kuiseb Formation shows an increase in K with respect to the other Kuiseb lithologies. These strata are interpreted to constitute the deep-level Southern Zone, exposed due to uplift between the OL and KL (Corner, 2008).

Within the Kuiseb Formation, the Landsat data and filters thereof show general increase in clay index and lower Fe index but no clear internal variation could be noted. Sharp boundaries that may suggest contact with bordering lithologies are also not discernable.

Other features identified within the Kuiseb Formation include:

- In the north of the eastern area, interpreted as Lower-2 Kuiseb Formation, there are two structures evident in the magnetic data which are either antiformal (domes) or synformal (both Upper-2 and Lower-1 Kuiseb show similar linear magnetic fabric and it is therefore unclear if the structures are in fact domal or synformal). The northernmost feature (SA1 on Figure 6.10) shows magnetic anomalies associated with its outer rim, while the southernmost structure (SA2

on Figure 6.10) envelopes a unit of uniform magnetic structure possibly indicating basement or a granitic intrusion. Due to superficial cover sediments, these features are not visible on radiometric or Landsat data.

- Some plug-like bodies (round singular magnetic anomalies) have been identified within the northernmost synformal / antiformal feature (SA1, Figure 6.10) described above (farms Manina, Brahmanspan and Indhlunkulu).

- Also within the Lower-2 Kuiseb Formation, two distinct units could be identified based on radiometric response. One shows an elevated K response suggesting a more arkosic clastic and the other shows elevated K and Th counts indicating possible increase in heavy minerals (e.g. monazite, zircon) in a clastic sediment.

- Linear magnetic anomalies within the Lower-2 and Middle Kuiseb Formations possibly indicative of a magnetic quartzite unit.

- A strong magnetic unit within the Middle Kuiseb Formation is inferred to be an amphibolite unit as it correlates with that mapped by Kasch, believed to form the base of the Middle Kuiseb Formation (Corner, pers. comm., 2009). This lower amphibolite shows a marked decrease in radiometric response (dark colours on ternary radiometric image). Also mapped by Kasch within the Middle Kuiseb Formation is a unit referred to as an upper marble unit. The upper marble is characterised by higher K, and lower Th and U than that of the surrounding Kuiseb Formation. A slightly lower clay-index is present on the Landsat imagery. Based on the quiet magnetic response, this unit could not however be distinguished from the rest of the Middle Kuiseb Formation in areas of no outcrop.

- Although the Matchless Amphibolite Belt (MAB) has been indicated on the published 1:1,000,000 geological map, its exact extent is unclear as evidenced from both geophysical data and past exploration programs. Drilling conducted by various exploration companies has indicated the presence of amphibolite in the study area but no clear correlation to the actual Matchless Member could be established, although it has been inferred by some to be so. There is no evidence from the geophysical magnetic or radiometric data to indicate that the MAB extends into the study area as indicated by the GSN maps. In addition, the occurrence of amphibolite, as reported in past EPL reports covering the area, is not uncommon and has been seen in trenches or boreholes at distance from the GSN-mapped MAB which occurs to the south of the study area. Given the more recent (2008) mapping of Kasch, in which an amphibolite unit is mapped in the Middel-Kuiseb unit, it is likely that many of the historically reported amphibolites are of this unit rather than of the MAB. No exploration programs to date have conclusively proven the extension of the MAB east of the Kudu Lineament.

- A few linear magnetic anomalies were identified within the Middle and Lower-2 Kuiseb Formation. Similarities between these anomalies and the magnetic anomaly of the magnetite quartzite marker of the MAB (Figure 6.12) could be indicative of the presence of Matchless-style deposits within the Steinhausen Area.

- The similarity of the magnetic response of the Lower-1 Kuiseb Formation to that of the area surrounding Onganja Mine, suggest the potential for the discovery of Kuiseb Formation hosted hydrothermal copper deposits.

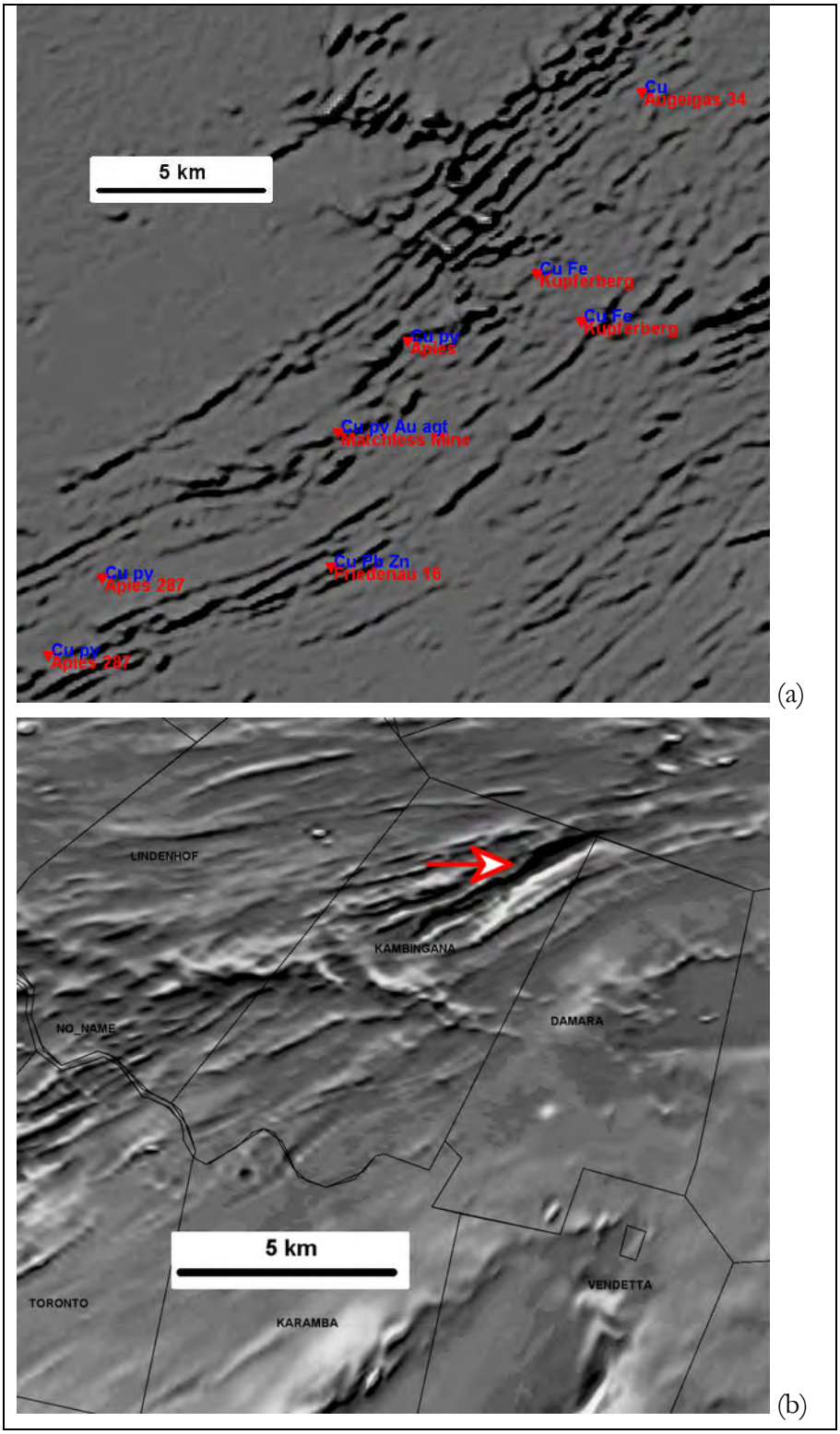

Figure 6.12: Comparison of magnetic data over the Matchless Mine and anomalies within the Kuiseb Formation in the Steinhausen Project Area.

(a) First Vertical Derivative over the Matchless Mine. (b) Similar magnetic anomaly on the farm Kambingana.

6.2.3 Hakos Group, Nosib Group and Eastern Basement

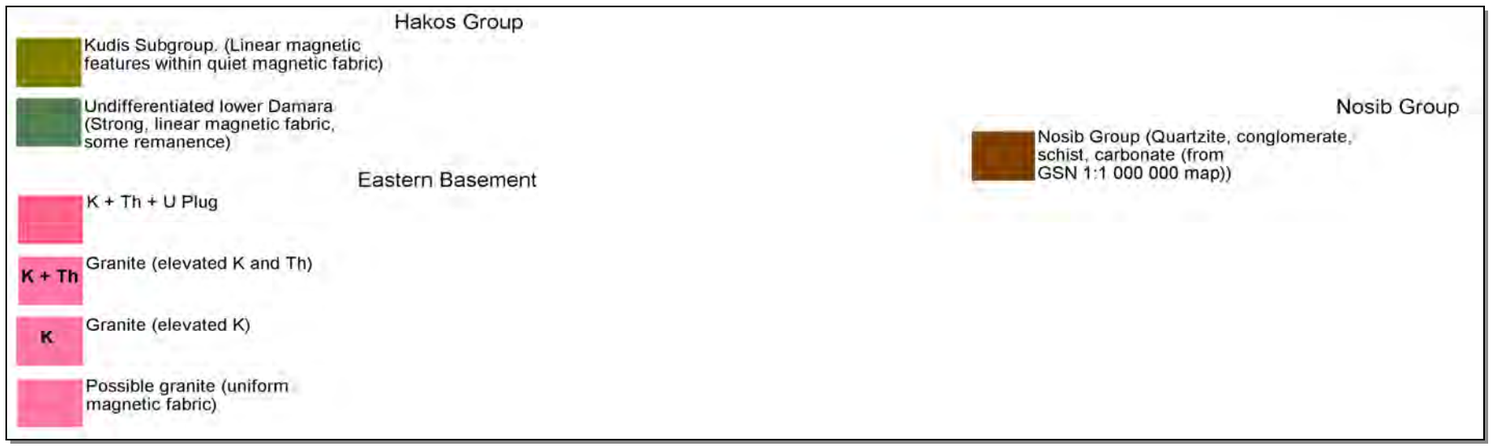

Figure 6.13: Geophysical interpretation legend for Figure 4.10 – Hakos Group, Nosib Group and Eastern Basement.

- The Kudis Subgroup is evident as a unit of linear, intermediate magnetic response.

- Undifferentiated lower Damara units show strong, linear magnetic fabric with some remanence. This magnetic description is similar to that associated with the Otjosondu manganese deposits (magnetic Fe-Mn mineral jacobsite, as well as magnetic quartzites) north-west of the study area. Alternatively, the magnetic response could be attributed to the Chuos Formation or pre-Damara basement.

- The occurrence of Nosib Group quartzite, conglomerate, schist and carbonate in the extreme southeast of the survey area has been mapped on the published GSN maps. Geophysical data over this area shows highly magnetic stratigraphy, suggesting the possible concentration of detrital magnetite within quartzites of the Nosib Group in this area. The radiometric response over the Kudis Subgroup, undifferentiated lower Damara and Nosib group cannot be clearly defined within the study area due to thick cover sediments.

- All basement related features east of the Kudu Lineament were grouped together as Eastern Basement and were sub-divided further into separate groups depending on geophysical signatures, i.e. uniform magnetic fabric, elevated K, elevated K and Th and a plug-like feature with elevated K, U and Th.

Mineralisation potential of the Hakos Group, Nosib Group and Eastern Basement.

- Due to the presence of basement-related mineral occurrences such as Omitiomire, as well as the possibility of REE deposits associated with basement pegmatite, all basement units should be regarded as prospective.

6.2.4 Pre-Damara Succession

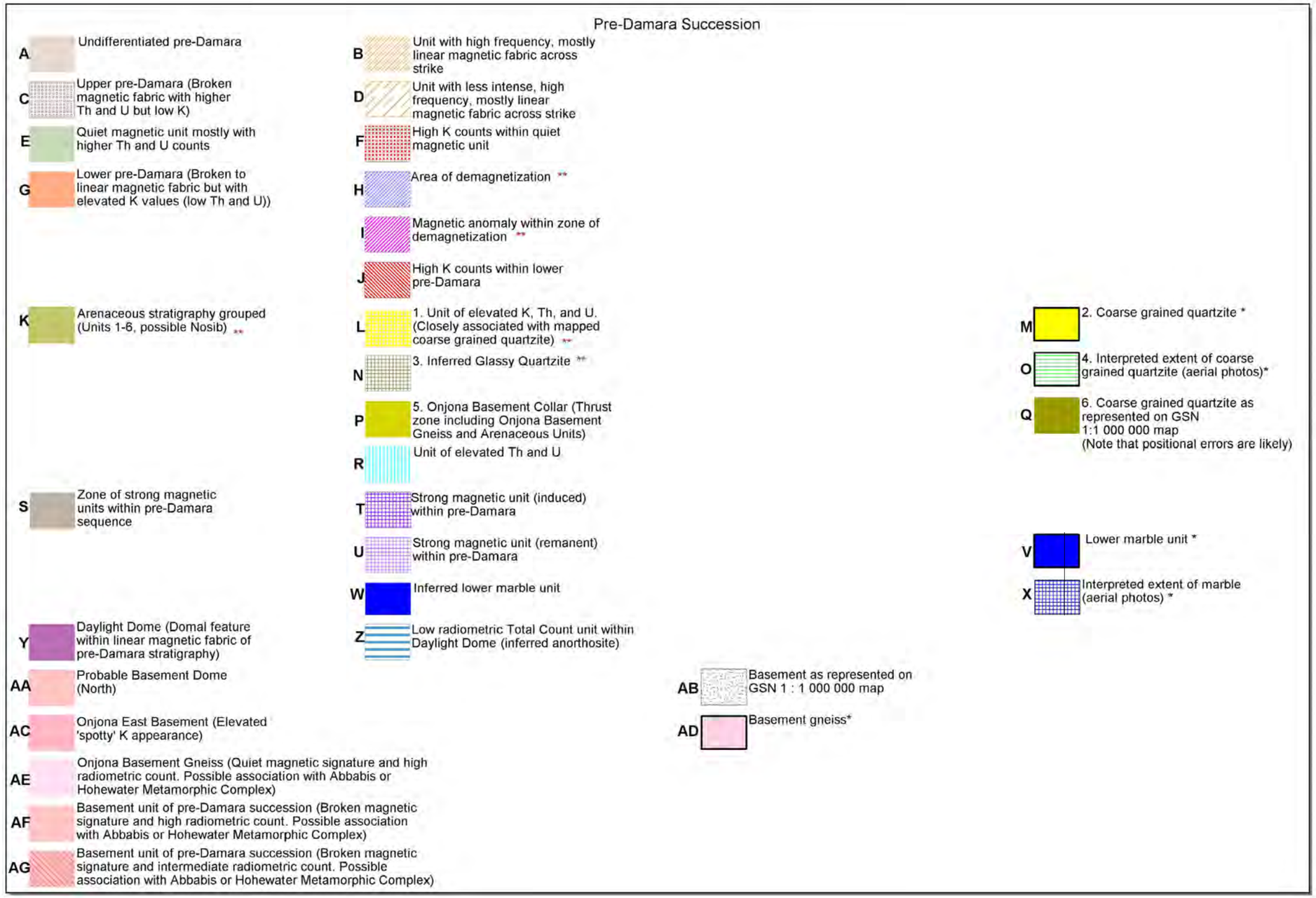

Figure 6.14: Geophysical interpretation legend for Figure 4.10 – Pre-Damara Succession (Upper arenaceous units possibly constituting the Nosib Group).

Kasch (1986) has mapped various outcrops of coarse-grained, white quartzite, white to pale blue marble and grey quartz-muscovite schist which at the time he classified as part of the Onjona-Vrolikheid Fold Complex. The GSN mapping shows a continuous quartzite unit which in part correlates with Kasch's mapping. This was, however, apparently derived by the GSN primarily from interpretation of aerial photographs (Corner, pers. comm., 2009) and positional errors are likely. Later work by Hoffmann (1989a) described an arenaceous stratigraphy associated with the coarse grained quartzite, drawing comparison to the pre-Damara Abbabis Metamorphic Complex below this quartzite unit and the Duruchaus Formation of the Nosib Group overlying it. From the radiometric data it is evident (elevated K, U and Th) that this stratigraphy spans a large area northwest of the Kudu Lineament, north of the EONC. To assist in the following description, units in Figure 6.8 have been labelled A to AG. Ground truthing would be needed to confirm or identify the associated lithologies and / or structures.

- A: Undifferentiated pre-Damara. All of the units B to Z are grouped together with units displaying no clearly identifiable magnetic / radiometric response

- B: Unit within with high frequency, mostly linear magnetic response. Linear magnetic fabric evident within this unit is oblique to strike direction suggested by radiometric data (Intermediate K, Th and U).

- C: Unit with broken magnetic fabric and higher Th and U counts but fairly low K counts. Inferred as an upper pre-Damara unit.

- D: Unit of similar characteristics as B above but with less intense magnetic amplitude.

- E: Unit of quiet magnetic signature and elevated Th and U counts.

- F: Anomalous K counts within unit E.

- G: Unit of broken to linear magnetic fabric but with elevated K values. Low in Th and U counts. Inferred as being a lower unit within the pre-Damara succession.

- H: Associated with a dyke (described in the section "features not related to specific stratigraphy" above) is an area of demagnetisation on the northern section of the farm Wildwasser. This demagnetisation is most probably due to alteration of magnetic minerals from hydrothermal activity associated with the intrusion of the dyke, or in particular with its precursor fault zone. It is therefore considered to be prospective.

- I: Two isolated magnetic anomalies within H (possible relicts of unaltered rock, or targets in their own right).

- J: Within the G unit there are various zones of anomalous K counts. Although it is not clear at this stage as to the cause of these K anomalies they could possibly be associated with potassium-feldspar-rich lithologies, indicative of either late-stage granites or basement. Due to the lack of mapped outcrop the interpretation is equivocal, i.e. basement or late-stage granite.

- K: All of the arenaceous stratigraphy mapped geophysically and geologically are grouped together as a single formational unit, i.e. encompassing units L to Q. This formational package underlies the Middle Kuiseb Formation in the west and may well be the eastern Damaran equivalent of the Nosib Group subjected to high-grade metamorphism. An alternate explanation is that it constitutes the upper part of the pre-Damaran sequence, immediately underlying the Damara. It is noted on the Fe-index created from Landsat data that the inferred arenaceous stratigraphy corresponds to areas of generally lower Fe-index values (lower Fe content) but textural features visible

within these zones suggest narrow (possibly repeating) lithologies of variable Fe-content.

- L: Unit of elevated K, U and Th as evident on radiometric images.
- M: Coarse grained ('glassy') quartzite mapped by Kasch (1998) (Corner, Kasch, pers. comm., 2009)
- N: Inferred occurrences of glassy quartzite unit (Corner, Kasch, pers. comm., 2009).
- O: Interpreted extent of glassy quartzite from aerial photos (Corner, Kasch, pers. comm., 2009)
- P: Onjona Basement Collar, a zone bordering the basement unit on the farm Onjona, which consists of thrust-repeated glassy quartzite and basement (Corner, Kasch, pers. comm., 2009).
- Q: Coarse-grained quartzite as represented on GSN 1:1,000,000 map. Due to possible positional errors as discussed above and the lack of geophysical evidence suggesting the actual continuation of this unit, specifically in the area spanning the farms from Okajura to Geduld, the complete unit was not included under K.
- R: Unit of elevated Th and U counts.
- S: Zone of strong magnetic anomalies encompassing units T and U. North-northwest of the study area similar magnetic signatures are associated with the Otjosondu manganese deposits.
- T: Strong (induced) magnetic unit.
- U: Strong (remanent) magnetic unit.

- V: Marble unit mapped by Kasch during 2008 (Corner, pers. comm., 2009). Referred to as the Lower Marble Unit as opposed to the Upper Marble Unit evident in the Kuiseb Formation.

- W: Lower Marble Unit inferred geophysically. It is believed that this marble unit is closely associated with the glassy quartzite (M) (Corner, pers. comm., 2009).

- X: Continuation of V based on aerial photo interpretation (Corner, Kasch, pers. comm., 2009).

- Y: Distinct domal feature within linear magnetic fabric of pre-Damara stratigraphy, referred to as the Daylight Dome after the farm on which it is evident.

- Z: Inferred anorthosite unit of very low radiometric total count within the Daylight Dome.

- AA: Two inferred basement units, one on the farm Hochfeld characterised by linear magnetic fabric (possibly as a result of faulting) and high K counts, and the other on the farms Cala and Hinza with a more uniform magnetic fabric and no clear radiometric response due to thick surficial sediments in the area.

- AB: Basement units as represented on the GSN 1:1,000,000 map on the farm Hinza. This unit seemingly cuts across various distinct magnetic units and does not correlate with magnetic fabric, or strike direction. It is therefore assumed that positional errors may exist in the GSN mapping or the possibility that the GSN mapping grouped together granitic borehole intersections.

- AC: Onjona East Basement. Unit showing elevated K counts with a spotty appearance.

- AD: Basement gneiss as mapped by Kasch (1998) (Corner, pers. comm., 2009).

- AE to AG: Basement units associated with the Abbabis Metamorphic Complex (Hoffmann, 1989b). Separated on the bases of distinct magnetic fabric and radiometric response.

Mineralisation potential of the Pre-Damara Succession (Upper zone possibly constituting the Nosib Group).

- The arenaceous stratigraphy (K above) hosts various known occurrences of copper mineralisation e.g. on the farms Vrolikheid (Cu in amphibole and quartzo-feldspathic gneiss, biotite schist and kyanite-bearing quartz-biotite schist) and Waaihoek (Cu in calc-silicate rock and plagioclase-amphibole schist) (Schneider and Seeger, 1992). The evaporitic sediments of the Duruchaus Formation are known to contain disseminated Cu as well as tin and possibly gold (Miller, 1983b).

- Units with strong magnetic content (some remanent) are similar to the Otjosondu manganese deposits further to the north-northwest. A siliceous, ferruginous manganese ore horizon has also been identified on the farms Hochfeld and Eahero (Schneider, 1992).

- Basement features within the pre-Damara succession should be investigated for potential Omitiomire-style deposits.

- In particular the dome on the farm Hochfeld (magnetic, K-rich and collared by an arenaceous sequence) has two possible scenarios: 1) If it is basement, then Omitiomire-style occurrences are of interest, or 2) if it is a K-rich granite, the Hochfeld dome has a potentially similar

setting to known mineral occurrences of the Zambian Copperbelt - i.e. granite stocks/domes collared by arenaceous stratigraphy.

- The K-rich units (J), though not clearly interpreted as basement features, have a similar radiometric response to the Hochfeld dome and should therefore also be included for follow-up exploration with possible basement-type (Omitiomire- or Copperbelt style) scenarios as mentioned above.

- The zone of demagnetisation (H) is prospective for occurrences associated with hydrothermal processes. The two isolated magnetic anomalies (I) may be targets in their own right, as mentioned above.

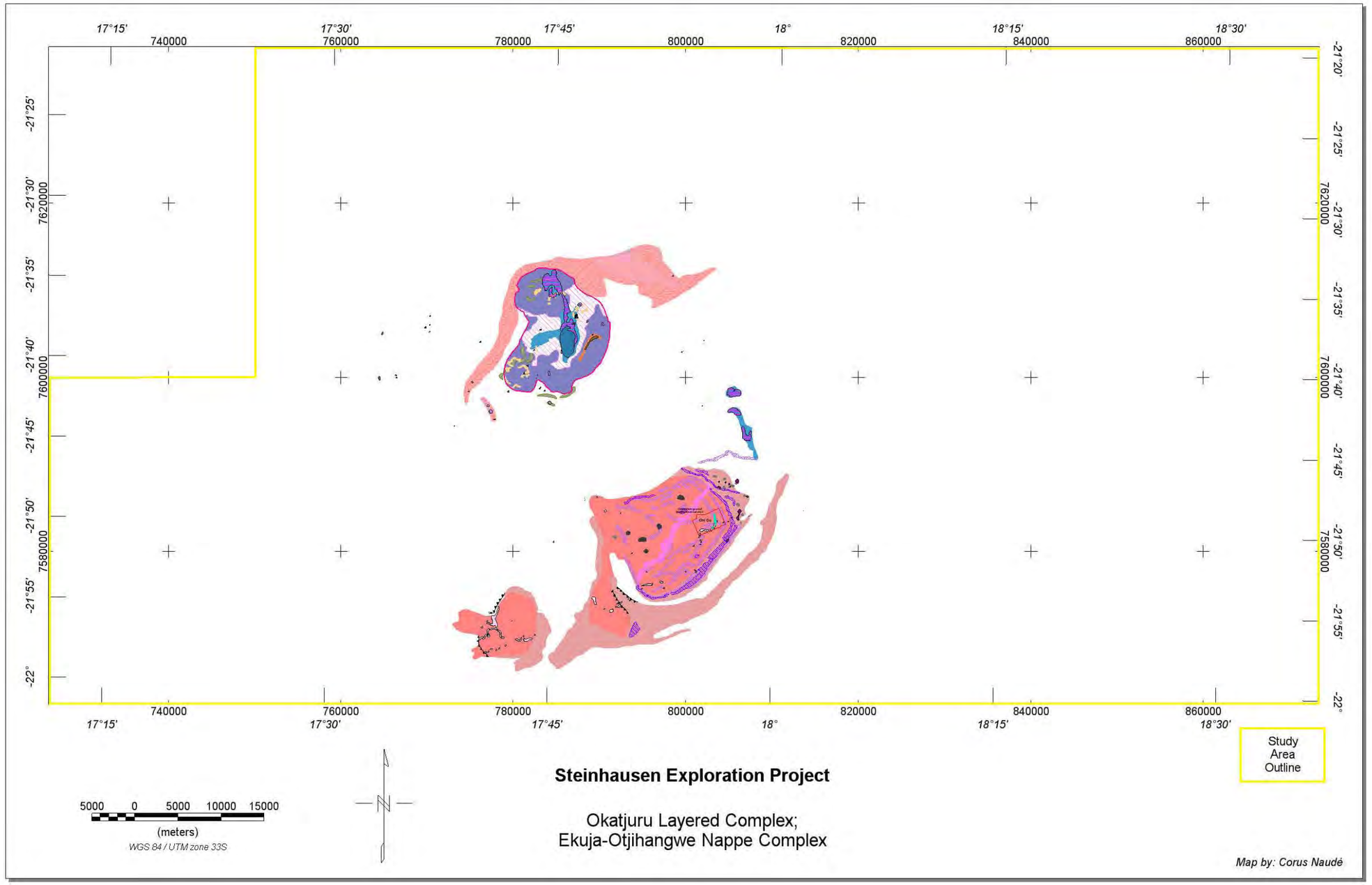

Figure 6.15: Okatjuru Layered Complex; Ekuja-Otjihangwe Nappe Complex.

For legend refer to Figure 6.16 (Okatjuru Layered Complex), Figure 6.17 (Ekuja-Otjihangwe Nappe Complex)

6.2.5 Okatjuru Layered Complex

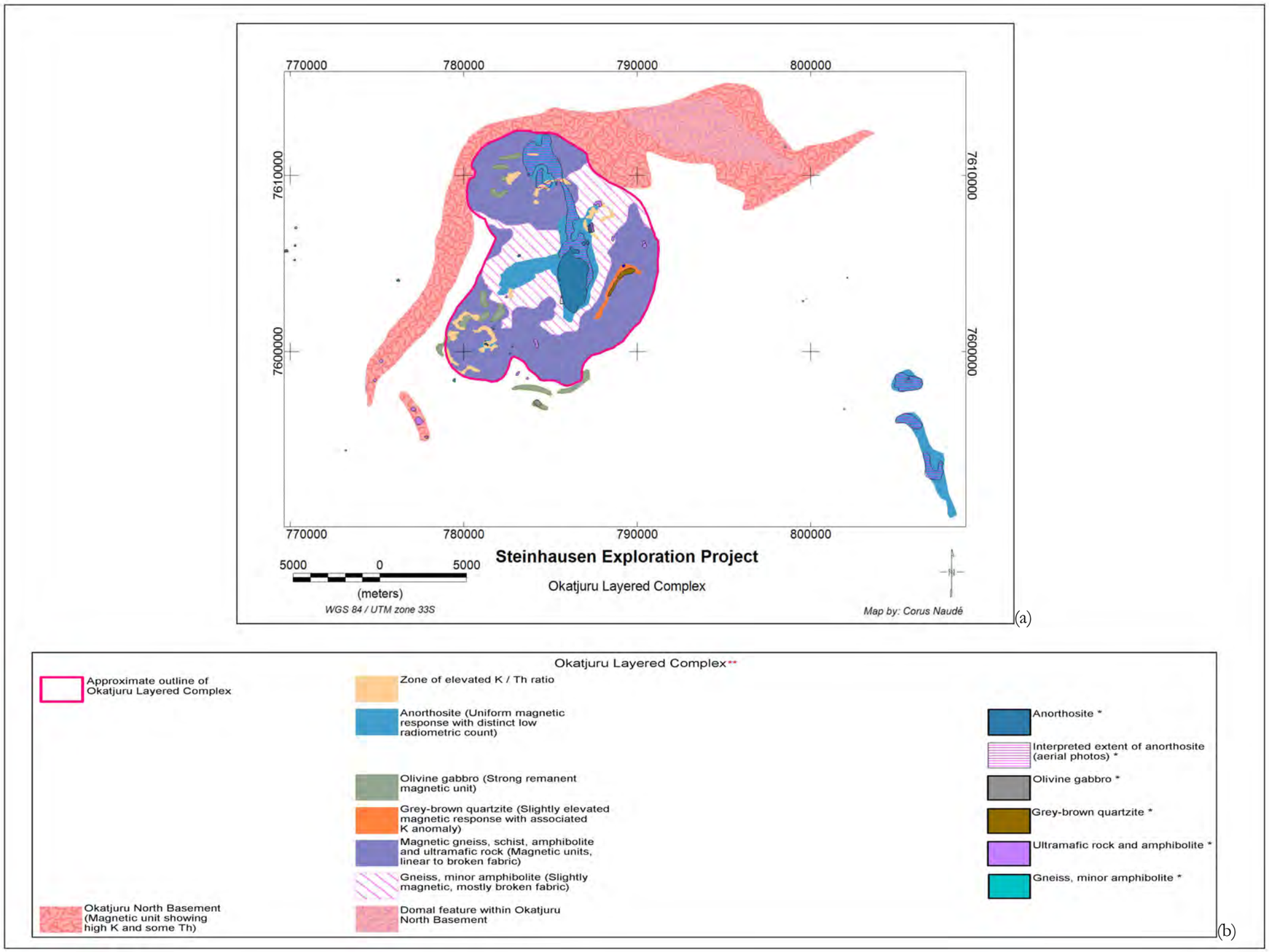

Figure 6.16: Geophysical interpretation (a) and legend (b) – Okatjuru Layered Complex (from Figure 6.15).

The Okatjuru Layered Complex (OLC, Kasch, 1998) is situated in the central-western part of the study area forming a north-northeast-trending anomalous elliptical feature with a major axis of approximately 15 km and a minor axis of 11 km. The OLC is clearly visible on the radiometric images as a lower radiometric count rate than the surrounding stratigraphy.

- The anorthosite has a very uniform magnetic fabric and very low radiometric count rate.

- The olivine gabbro has a strong remanent magnetic signature.

- The grey brown quartzite has a high K signature and is high in Fe content relative to surrounding lithologies as evident from the Fe-index created from Landsat data.

- Magnetic gneiss, schist, amphibole and ultramafic rock which have been intersected by drilling in previous exploration programs, are observed as strong magnetic units with a linear to broken fabric.

- Areas mapped as gneiss with minor amphibolite have a slight magnetic response with broken magnetic fabric.

Mineralisation potential of the Okatjuru Layered Complex.

- Cu occurrences in amphibolite hosted in a succession of magnetic gneiss, schist and ultramafic rocks have been identified on the farms Oorlogsdeel and Ombakatjowinde (Schneider and Seeger, 1992).

- Other mineral occurrences that may be associated with layered ultramafic complexes include chromite, magnetite, ilmenite, nickel and the platinum group elements.

6.2.6 Ekuja-Otjihangwe Nappe Complex

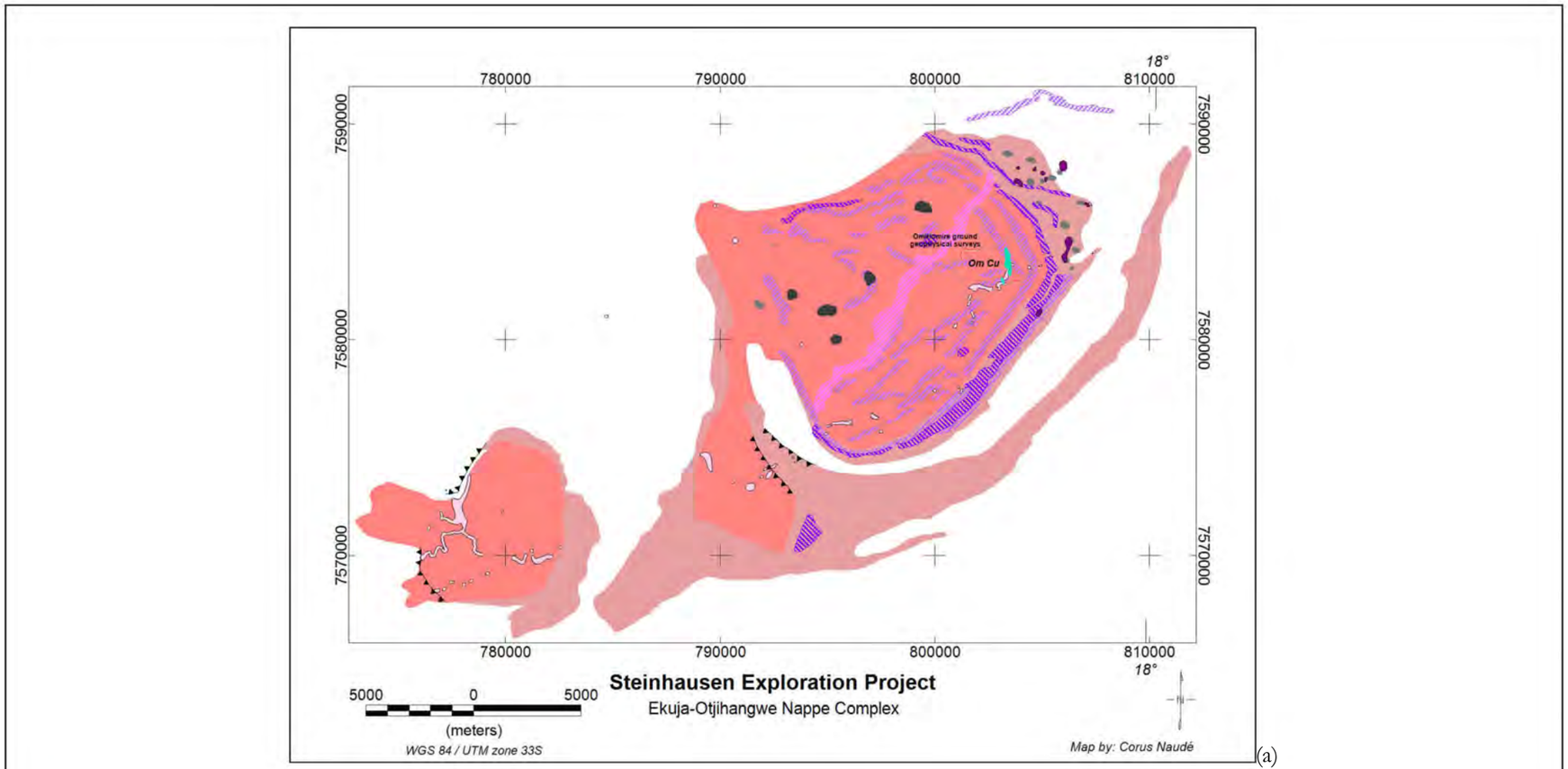

(a)

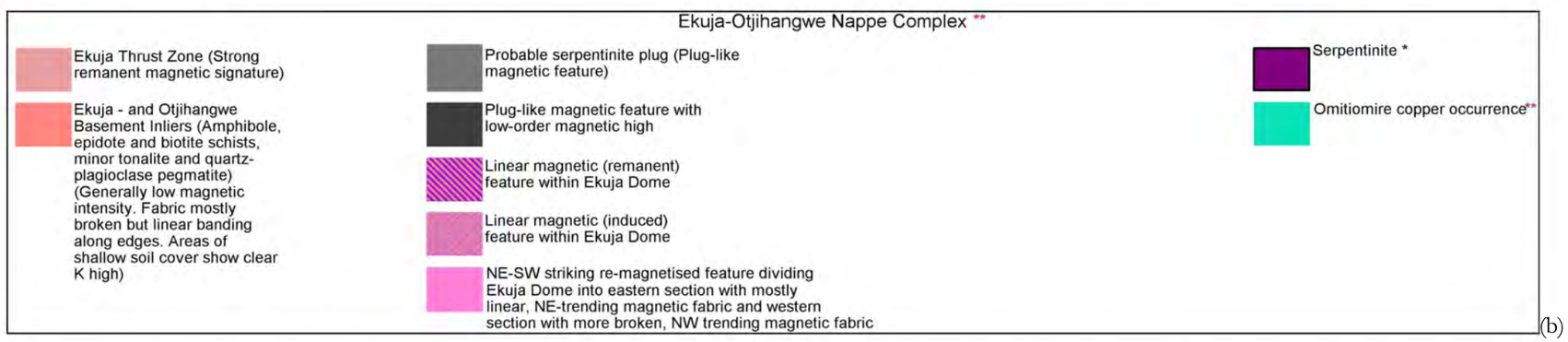

(b)

Figure 6.17: Geophysical interpretation (a) and legend (b) – Ekuja-Otihangwe Nappe Complex (from Figure 6.15).

- The magnetic response of the Ekuja Basement Inlier (Ekuja Dome), as mapped by the GSN and Kasch (1986), has a typically rough, broken fabric that is occasionally concentric closer to the inlier margins. From the radiometric images it is clear that the inlier has elevated K values with respect to the surrounding rocks.

- The Ekuja Thrust Zone, evidenced by Craton in a number of boreholes (Corner, pers. comm., 2009) is a strong remanent magnetic feature flanking the eastern and southern limits of the Ekuja and Otjihangwe basement inliers. The remanent magnetic properties are owed to magnetite concentrations, evident in the boreholes, along thrust boundaries of the basement inliers.

- Within the basement inlier there are a few plug-like magnetic features. These were further sub-divided into possible serpentinite plugs and other low-order magnetic features.

- Within the Ekuja basement inlier, several linear magnetic features have been mapped, as well as a central, north-east trending re-magnetised zone. This re-magnetised zone also divides the basement inlier into a south-eastern zone showing magnetic features generally concentric to the dome margin, and a north-western zone having a more broken magnetic fabric.

- Within the Ekuja Thrust Zone, plug-like features were identified as serpentinite plugs (or phonolites). These correlate well with serpentinite outcrops mapped by Kasch (1986).

Mineralisation potential of the Ekuja-Otihangwe Nappe Complex.

Within the EONC, the copper occurrences at Omitiomire and Barreshagen have been well documented and are the focus of current, ongoing exploration by Craton. Regional geochemical exploration over the EONC by Craton has identified numerous copper in soil anomalies across the entire area (IBML, 2009), suggesting good potential for future discoveries of Omitiomire-style deposits.

6.3 Discussion

Through the synergistic evaluation of GSN-acquired airborne geophysical data, available geological information and satellite imagery some important geological features relating to the lithology and structural context of the soil-covered area around Steinhausen, Namibia, could be brought to light. Figure 6.18 is a summary of the geophysical interpretation, to which the observations below refer.

The Kuiseb Formation within the study area shows uncharacteristically varied magnetic signatures, and can be subdivided into 5 units as follows:

- Upper-2 Kuiseb Formation: low amplitude, linear magnetic fabric.
- Upper-1 Kuiseb Formation: quiet magnetic signature.
- Middle Kuiseb Formation: intermediate magnetic response. Characterised by an upper marble unit and a strongly magnetic basal amphibolite unit.
- Lower-2 Kuiseb Formation: very quiet, uniform magnetic signature.

- Lower-1 Kuiseb Formation: very strong, linear magnetic fabric, often remanent. Contains gabbro and highly magnetic epidosite as observed further west at Onganja Mine.

This subdivision of the Kuiseb Formation will aid future exploration work as Matchless-style massive sulphides are associated with the Middle Kuiseb Formation and Onganja-style copper is associated with the Lower-1 Kuiseb Formation.

The Rodenbeck Intrusion, intruded into pre-Damara basement, is a kidney-shaped, probably mafic or ultramafic body of between 3 and 5 km in diameter, showing internal structure evident of layering or differentiation, and is a likely host to magmatic Ni-Cu deposits.

The Kudu shear zone is characterised by cross-cutting magnetic fabric that also suggests intense brittle deformation thus providing ample late-, or post-tectonic secondary porosity for fluid movement and potential for hydrothermal mineral deposits.

The enigmatic Steinhausen Anomaly, a clear regional magnetic low, is interpreted to be a large, deep area of demagnetisation that may be indicative of abundant hydrothermal fluid and therefore a possible control on mineralisation in the area.

The arenaceous stratigraphy forms an important stratigraphical marker between pre-Damara basement and the Damaran Kuiseb Formation, including a characteristic glassy quartzite.

A structurally complex zone situated between the Okahandja Lineament and the Kudu Lineament east of the Ekuja Dome is inferred as uplifted pre-Damara stratigraphy. Within pre-Damaran stratigraphy areas with elevated potassium counts could be mapped. These areas also fall within a zone of slight linear magnetic fabric suggesting either an antiformal or synformal

structural regime. The high potassium values indicate the possibility that these units may contain high amounts of potassium feldspar and may be granitic in composition.

The Okatjuru Layered Complex could clearly be mapped from radiometric and magnetic data. The extent of this complex is in the order of 15 km by 11 km. Apart from hosting known copper in soil anomalies, the possibility exists for the discovery of other minerals associated with layered ultramafic complexes which include chromite, magnetite, ilmenite, nickel, copper and the platinum group elements

The outline of the Ekuja Dome, host to the Omitiomire copper deposit, is clearly defined by the magnetic data. Cutting across the Ekuja Dome, the E-W Structural Zone (which contains an array of ENE trending structures) is likely to be a controlling factor in copper mineralisation at Omitiomire. Other zones of similar magnetic fabric to the Ekuja Dome are also identified within the same E-W Structural Zone and they are high-priority targets. The domal structural features not in the ENE structural zone are grouped into a single layer, second-priority targets comprising both domes and anticlines.

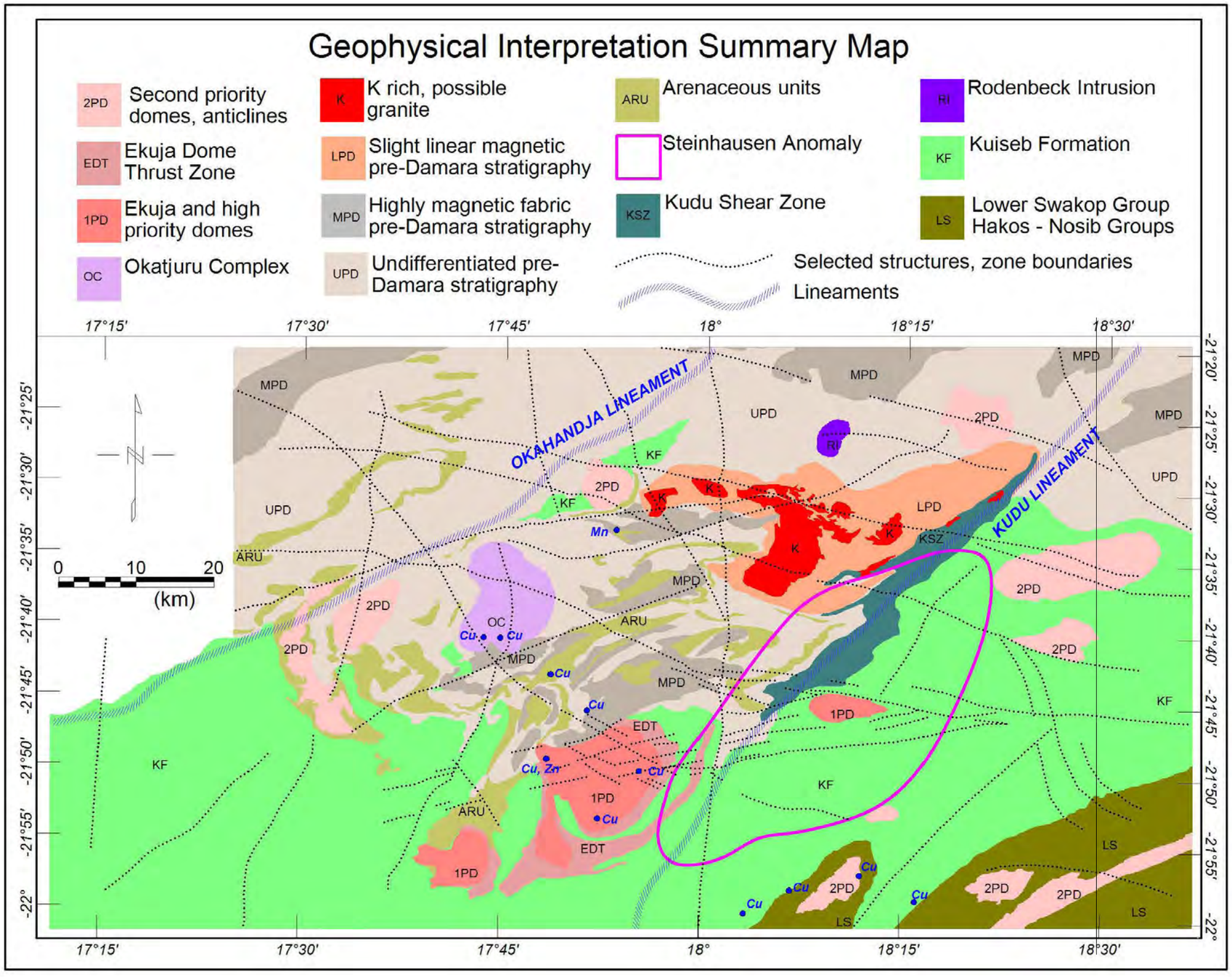

Figure 6.18: Geophysical Interpretation Summary Map

Chapter 7

CONCLUSIONS

Structural features evidenced by this study are as follow:

- Uplifted stratigraphy, possibly pre-Damara, is present between the Okahandja Lineament and the Kudu Lineament.
- The Kudu shear zone, coincident to the KL, is an area of intense brittle deformation likely to host hydrothermal mineral deposits.
- The E-W Structural Zone that cuts across the Ekuja Dome is a possible control to copper mineralisation at Omitiomire.

Important lithological insights are:

- The Kuiseb Formation within the study area is subdivided into 5 units of Lower-1, 2 to Upper-1, 2 parts, showing distinct magnetic features and properties.
- An arenaceous unit, containing a distinct glassy quartzite, underlies the Kuiseb Formation.
- The extent of the Ekuja Dome is evident from the magnetic data.
- The Okatjuru Layered Complex, hosting known copper soil anomalies, has the potential of discovery of other minerals in association with the layered ultramafic complex, such as Cr, magnetite, ilmenite, Ni, Cu and PGEs.

Some direct exploration targets are also identified through this study: They are:

- Singular magnetic anomalies (both induced and remanent) being pipe-like or short strike 2D bodies.
- The Rodenbeck Intrusion.
- Zones of quiet magnetic fabric inferred as demagnetised zones, along which fluids may have passed.
- Linear magnetic units within quiet Kuiseb Formation possibly associated with the Matchless Amphibolite Belt.
- Anomalous uranium associated with drainage systems, plug-like bodies and intra-stratigraphic units.

REFERENCES

Airo, M.L., 2002. *Aeromagnetic and aeroradiometric response to hydrothermal alteration*. Surveys in Geophysics 23, 273-302.

Anglogold Ashanti, 2010. *Mineral resource and ore reserve report 2010*. Accessed from http://www.anglogold.co.za/subwebs/informationforinvestors/reports10/financials/files/AGA-resource-reserves-2010.pdf on 12/10/2011.

Bedell, R.L. and Crósta, A.P., 2009. *Basic image processing*. Reviews in Economic Geology, 16, 237-256.

Bishop, J.R. and Lewis, R.J.G., 1992. *Geophysical signatures of Australian volcanic-hosted massive sulfide deposits*. Economic Geology, 87, 913 - 930.

Breitkopf, J.H., 1988. *Tectonic setting of the Matchless Belt pyritic copper deposits, Namibia*. Economic Geology, 83, 710 - 723.

Bühn, B., Stanistreet, I. G. and Okrusch, M., 1992. *Late Proterozoic outer shelf manganese and iron ore deposits at Otjosondu (Namibia) related to the Damara oceanic opening*. Economic Geology, 87, 1393 – 1411.

Burnett, R.J., 1992. *Gold*. The Mineral Resources of Namibia, 4.1, 1-48.

Charles, P.C.A., 1987. *Gold Fields Prospecting Co (Pty) Ltd. Matchless Amphibolite Belt Project final report on grant M46/3/1313*.

Cooper, G.R.J. and Cowan, D.R., 2005. *Differential reduction to the pole*. Computers and Geosciences, 31, 989-999.

Cooper, G.R.J. and Cowan, D.R., 2006. *Enhancing potential field data using filters based on the local phase*. Computers and Geosciences, 32, 1585-1591.

Cooper, G.R.J. and Cowan, D.R., 2008. Edge e*nhancement of potential field data using normalised statistics*. Geophysics, 73 (3), H1-H4.

Corner, B., 1983. *An interpretation of the aeromagnetic data covering the western portion of the Damara Orogenic Belt in S.W.A./Namibia*. Spec. Publ. Geol. Soc. S.A., 11, 339-354.

Corner, B., 2000. *Crustal framework of Namibia derived from magnetic and gravity data*. Communs. Geol. Surv. Namibia, 12, 13-19 (Henno Martin Special Volume).

Corner, B., 2006. *Cheetah Minerals Exploration (PTY) Ltd. Exclusive prospecting license 74, Steinhausen, final report*.

Corner, B., 2008 (in press). *Crustal framework of Namibia derived from an integrated interpretation of geophysical and geological data.* In: Miller, R. McG. (Ed.) The Geology of Namibia, 1, 2-1 – 2-19. Geol. Surv. Namibia.

Corner, B., Sinclair, H. and Verran, D., 2009. *A radon emanometry case study of the Rössing South deposit, Namibia.* 11th Biennial Technical Meeting and Exhibition, Swaziland, 16-18 September, 471-474.

Crósta, A.P. and De Souza Filho, C.R., 2009. *Mineral exploration with Landsat Thematic Mapper (TM) / Enhanced Thematic Mapper Plus (ETM+): A review of fundamentals, characteristics, data processing, and case studies.* Reviews in Economic Geology, 16, 59-82.

Eckstrand, O. R. and Hulbert, L. J., 2007. *Magmatic nickel-copper-platinum group element deposits.* Mineral deposits of Canada: a synthesis of major deposit-types, district metallogeny, the evolution of geological provinces, and exploration methods; Goodfellow, W D (ed.); Geological Association of Canada, Mineral Deposits Division, Special Publication no. 5, 205-222.

Fairhead, J.D. and Williams, S.E., 2006. *Evaluating normalised magnetic derivatives for structural mapping.* SEG2006 New Orleans Extended Abstract.

Farr, T. G., Rosen, P. A., Caro, E., Crippen, R., Duren, R., Hensley, S., Kobrick, M., Paller, M., Rodriguez, E., Roth, L., Seal, D., Shaffer, S., Shimada, J. and Umland, J., 2007. *The Shuttle Radar Topography Mission.* Rev. Geophys., 45, RG2004, doi:10.1029/2005RG000183. Accessed from http://www2.jpl.nasa.gov/srtm/SRTM_paper.pdf on 06/07/2010.

Ford, K., Keating, P. and Thomas, M. D., 2007. *Overview of geophysical signatures associated with Canadian ore deposits.* Mineral deposits of Canada: a synthesis of major deposit-types, district metallogeny, the evolution of geological provinces, and exploration methods; Goodfellow, W D (ed.); Geological Association of Canada, Mineral Deposits Division, Special Publication no. 5, 939-970.

GETEC, 2010. *Advanced processing and interpretation of gravity and magnetic data.* Accessed from http://www.getech.com/services/advanced_processing_and_interpretation.pdf on 18/11/2010.

Gunn, P. J. and Dentith, M. C., 1997. *Magnetic responses associated with mineral deposits.* ASGO Journal of Australian Geology & Geophysics, 17(2), 145-158.

Hoffmann, K. H., 1989a. *New aspects of lithostratigraphic subdivision and correlation of late Proterozoic to early Cambrian rocks of the southern Damara Belt and their correlation with the central and northern Damara Belt and the Gariep Belt.* Communs Geol. Surv. Namibia, 5, 59-67.

Hoffmann, K. H., 1989b. *Aspects of relative age, stratigraphic correlation and origin of metaquartzites and associated Fe-Mn deposits of the Otjozondu Mine in the Eastern Okahandja District.* Unpublished Geological Survey of Namibia Internal Report.

IBML, 2008. *Geological factsheet on the Omitiomire Project.* Accessed from http://www.interbasemetals.com/docs/PDFs/Fact_Sheets_/2008/Omitiomire%20is%20IBML.pdf. on 10/12/2009.

IBML, 2009. *International Base Metals Limited Annual Report 2009*; Accessed from http://www.interbasemetals.com/docs/PDFs/2009/Final%20Annual%20Report%202009WEB.pdf on 10/12/2009.

Kasch, K. W., 1986. *Tectonic subdivision, lithostratigraphy and structural geology of the Upper Black Nossob River Area.* Communs Geol. Surv. S.W. Africa/Namibia, 2, 117-129.

Kasch, K. W., 1998. *Hochfeld – EPL 2252 Interpreted Geology, Scale 1:100,000.* Mount Isa Mines Namibia (Pty.) Ltd., Drawing No. 0420.

Klemd, R., Maiden, K. J., Okrusch, M. and Richter, P., 1989. *Geochemistry of the Matchless metamorphosed massive sulfide deposit, South West Africa / Namibia: Wall-rock alteration during submarine ore-forming processes.* Economic Geology, 84, 603-617.

Li, X., 2006. *Understanding 3-D analytic signal amplitude.* Geophysics, 71 (2), L13–L16.

Lightfoot, P.C., 2007. *Advances in Ni-Cu-PGE sulphide deposit models and implications for exploration technologies.* Proceedings of Exploration 07: Fifth Decennial International Conference on Mineral Exploration, Milkereit, B. (ed), 629-646.

MacLeod, I. N., Jones, K. and Dai, T. F., 1993. *3-D analytic signal in the interpretation of total magnetic field data at low magnetic latitudes.* Exploration Geophysics, 24, 679–687.

Miller, R. McG., 1983a. *The Pan-African Damara Orogen of South West Africa/Namibia.* Spec. Publ. Geol. Soc. S. Afr., 11, 431-515.

Miller, R. McG., 1983b. *Economic implications of plate tectonic models of the Damara Orogen*. Spec. Publ. Geol. Soc. S. Afr., 11, 385-395.

Miller, R. McG., 1983c. *Tectonic implications of the contrasting geochemistry of Damaran mafic volcanic rocks, South West Africa/Namibia*. Spec. Publ. Geol. Soc. S. Afr., 11, 115-138.

Miller, R. McG., 1992a. *Mineral exploration targets in Namibia*. The Mineral Resources of Namibia, 1.1, 1-8.

Miller, R. McG., 1992b. *Stratigraphy*. The Mineral Resources of Namibia, 1.2, 1-22.

Miller, R. McG, Barnes, S. and Balkwill, G., 1983. *Possible active margin deposits within the southern Damara Orogen: The Kuiseb Formation between Okahandja and Windhoek*. Spec. Publ. Geol. Soc. S. Afr., 11, 73-88.

Mindat.org, 2011. *Navachab Gold Mine, Karibib District, Erongo Region, Namibia*. Accessed from http://www.mindat.org/loc-126645.html on 12/10/2011.

Moore, J. M., 2010. *Comparative study of the Onganja Copper Mine, Namibia: a link between Neoproterozoic Mesothermal Cu (-Au) mineralization in Namibia and Zambia*. South African Journal of Geology, 113 (4), 445-460.

Naldrett, A. J., 2010. *From the mantle to the bank: The life of a Ni-Cu-(PGE) sulphide deposit*. South African Journal of Geology, 113, 1-32.

Nash, J. T. and Granger, H. C., 1981. *Geology and concepts of genisis of important types of uranium deposits*. Economic Geology 75th Anniversary Volume, 63 – 116.

Nicolet, J. P. and Erdi-Krausz, G., 2003. *Guidelines for radiometric mapping using gamma ray spectrometry data*. International Atomic Energy Agency Technical Document 1363. ISBN 92-0-108303-3. ISSN 1011-4289.

Pirajno, F. and Jacob, R. E., 1991. *Gold mineralisation in the intracontinental branch of the Damara Orogen, Namibia: a preliminary survey*. Journal of African Earth Science, 13 (3/4), 305-311.

Porada, H., 1985. *Stratigraphy and facies in the upper Proterozoic Damara Orogen, Namibia, based on a geodynamic model*. Precambrian Research, 29, 235-264.

Richards, J. R., 2000. *Lineaments revisited*. SEG Newsletter, 42.

Roesener, H. and Schreuder, C.P., 1992. *Cobalt and Nickel*. The Mineral Resources of Namibia, 2.2, 1-7.

Roesener, H. and Schreuder, C.P., 1992b. *Uranium.* The Mineral Resources of Namibia, 7.1, 1-62.

Robb, L.J., 2005. *Introduction to ore-forming processes.* Blackwell Publishing. 373p.

Schneider, G.I.C., 1992. *Manganese.* The Mineral Resources of Namibia, 2.6, 1-11.

Schneider, G.I.C. and Seeger, K.G., 1992. *Copper.* The Mineral Resources of Namibia, 2.3, 1-172.

Steven, N., Armstrong, R., Smalley, T. and Moore, J., 2000. *First geological description of a late Proterozoic (Kibaran) metabasaltic andesite-hosted chalcosite deposit at Omitiomire, Namibia.* Geology and Ore Deposits 2000: the Great Basin and Beyond Proceedings Volume II, 711-734.

Verduzco, B., Fairhead, j. D. and MacKenzie, C., 2004. *New insights into magnetic derivatives for structural mapping.* The Leading Edge, 116 -119.

APENDIX A

Metadata Files for Landsat Images:

Landsat Image - Path 177 Row 75 - Metadata File	Landsat Image - Path 178 Ro 75 – Metadata File
GROUP = METADATA_FILE PRODUCT_CREATION_TIME = 2004-02-12T15:04:28Z PRODUCT_FILE_SIZE = 647.4 STATION_ID = "EDC" GROUND_STATION = "EDC" GROUP = ORTHO_PRODUCT_METADATA SPACECRAFT_ID = "Landsat7" SENSOR_ID = "ETM+" ACQUISITION_DATE = 2000-04-24 WRS_PATH = 177 WRS_ROW = 075 SCENE_CENTER_LAT = -21.6698707 SCENE_CENTER_LON = +18.7076477 SCENE_UL_CORNER_LAT = -20.7311284 SCENE_UL_CORNER_LON = +18.0214026 SCENE_UR_CORNER_LAT = -20.9858478 SCENE_UR_CORNER_LON = +19.7755296 SCENE_LL_CORNER_LAT = -22.3458954 SCENE_LL_CORNER_LON = +17.6304863 SCENE_LR_CORNER_LAT = -22.6065494 SCENE_LR_CORNER_LON = +19.4020961 SCENE_UL_CORNER_MAPX = 189781.500 SCENE_UL_CORNER_MAPY = -2295247.500 SCENE_UR_CORNER_MAPX = 372723.000 SCENE_UR_CORNER_MAPY = -2321068.500 SCENE_LL_CORNER_MAPX = 152902.500 SCENE_LL_CORNER_MAPY = -2474997.000 SCENE_LR_CORNER_MAPX = 335758.500 SCENE_LR_CORNER_MAPY = -2500846.500 BAND1_FILE_NAME = "p177r075_7t20000424_z34_nn10.tif" BAND2_FILE_NAME = "p177r075_7t20000424_z34_nn20.tif" BAND3_FILE_NAME = "p177r075_7t20000424_z34_nn30.tif" BAND4_FILE_NAME = "p177r075_7t20000424_z34_nn40.tif" BAND5_FILE_NAME = "p177r075_7t20000424_z34_nn50.tif" BAND61_FILE_NAME = "p177r075_7k20000424_z34_nn61.tif" BAND62_FILE_NAME =	GROUP = METADATA_FILE PRODUCT_CREATION_TIME = 2004-02-12T15:09:57Z PRODUCT_FILE_SIZE = 669.4 STATION_ID = "EDC" GROUND_STATION = "EDC" GROUP = ORTHO_PRODUCT_METADATA SPACECRAFT_ID = "Landsat7" SENSOR_ID = "ETM+" ACQUISITION_DATE = 2000-05-17 WRS_PATH = 178 WRS_ROW = 075 SCENE_CENTER_LAT = -21.6686995 SCENE_CENTER_LON = +17.1639746 SCENE_UL_CORNER_LAT = -20.7289496 SCENE_UL_CORNER_LON = +16.4786312 SCENE_UR_CORNER_LAT = -20.9848161 SCENE_UR_CORNER_LON = +18.2307334 SCENE_LL_CORNER_LAT = -22.3466967 SCENE_LL_CORNER_LON = +16.0863728 SCENE_LR_CORNER_LAT = -22.6044742 SCENE_LR_CORNER_LON = +17.8589668 SCENE_UL_CORNER_MAPX = 653961.000 SCENE_UL_CORNER_MAPY = -2292853.500 SCENE_UR_CORNER_MAPX = 835933.500 SCENE_UR_CORNER_MAPY = -2323861.500 SCENE_LL_CORNER_MAPX = 611866.500 SCENE_LL_CORNER_MAPY = -2471605.500 SCENE_LR_CORNER_MAPX = 793924.500 SCENE_LR_CORNER_MAPY = -2502556.500 BAND1_FILE_NAME = "p178r075_7t20000517_z33_nn10.tif" BAND2_FILE_NAME = "p178r075_7t20000517_z33_nn20.tif" BAND3_FILE_NAME = "p178r075_7t20000517_z33_nn30.tif" BAND4_FILE_NAME = "p178r075_7t20000517_z33_nn40.tif" BAND5_FILE_NAME = "p178r075_7t20000517_z33_nn50.tif" BAND61_FILE_NAME = "p178r075_7k20000517_z33_nn61.tif" BAND62_FILE_NAME =

```
"p177r075_7k20000424_z34_nn62.tif"
        BAND7_FILE_NAME                 =
"p177r075_7t20000424_z34_nn70.tif"
        BAND8_FILE_NAME                 =
"p177r075_7p20000424_z34_nn80.tif"
        GROUP = PROJECTION_PARAMETERS
            REFERENCE_DATUM = "WGS84"
            REFERENCE_ELLIPSOID = "WGS84"
            GRID_CELL_ORIGIN = "Center"
            UL_GRID_LINE_NUMBER = 1
            UL_GRID_SAMPLE_NUMBER = 1
            GRID_INCREMENT_UNIT = "Meters"
            GRID_CELL_SIZE_PAN = 14.250
            GRID_CELL_SIZE_THM = 57.000
            GRID_CELL_SIZE_REF = 28.500
            FALSE_NORTHING = 0
            ORIENTATION = "NUP"
            RESAMPLING_OPTION = "NN"
            MAP_PROJECTION = "UTM"
        END_GROUP                       =
PROJECTION_PARAMETERS
        GROUP = UTM_PARAMETERS
            ZONE_NUMBER = +34
        END_GROUP = UTM_PARAMETERS
        SUN_AZIMUTH = 44.7612373
        SUN_ELEVATION = 43.4426438
        QA_PERCENT_MISSING_DATA = 0
        CLOUD_COVER = 0
        PRODUCT_SAMPLES_PAN = 17132
        PRODUCT_LINES_PAN = 15082
        PRODUCT_SAMPLES_REF = 8566
        PRODUCT_LINES_REF = 7541
        PRODUCT_SAMPLES_THM = 4283
        PRODUCT_LINES_THM = 3771
        OUTPUT_FORMAT = "GEOTIFF"
    END_GROUP                           =
ORTHO_PRODUCT_METADATA
    GROUP = L1G_PRODUCT_METADATA
        BAND_COMBINATION = "123456678"
        CPF_FILE_NAME                   =
"L7CPF20000401_20000630_09"
        GROUP = MIN_MAX_RADIANCE
            LMAX_BAND1 = 191.600
            LMIN_BAND1 = -6.200
            LMAX_BAND2 = 196.500
            LMIN_BAND2 = -6.400
            LMAX_BAND3 = 152.900
            LMIN_BAND3 = -5.000
            LMAX_BAND4 = 157.400
            LMIN_BAND4 = -5.100
            LMAX_BAND5 = 31.060
            LMIN_BAND5 = -1.000
            LMAX_BAND61 = 17.040
            LMIN_BAND61 = 0.000
            LMAX_BAND62 = 12.650
```

```
"p178r075_7k20000517_z33_nn62.tif"
        BAND7_FILE_NAME                 =
"p178r075_7t20000517_z33_nn70.tif"
        BAND8_FILE_NAME                 =
"p178r075_7p20000517_z33_nn80.tif"
        GROUP = PROJECTION_PARAMETERS
            REFERENCE_DATUM = "WGS84"
            REFERENCE_ELLIPSOID = "WGS84"
            GRID_CELL_ORIGIN = "Center"
            UL_GRID_LINE_NUMBER = 1
            UL_GRID_SAMPLE_NUMBER = 1
            GRID_INCREMENT_UNIT = "Meters"
            GRID_CELL_SIZE_PAN = 14.250
            GRID_CELL_SIZE_THM = 57.000
            GRID_CELL_SIZE_REF = 28.500
            FALSE_NORTHING = 0
            ORIENTATION = "NUP"
            RESAMPLING_OPTION = "NN"
            MAP_PROJECTION = "UTM"
        END_GROUP                       =
PROJECTION_PARAMETERS
        GROUP = UTM_PARAMETERS
            ZONE_NUMBER = +33
        END_GROUP = UTM_PARAMETERS
        SUN_AZIMUTH = 38.8979999
        SUN_ELEVATION = 38.7676211
        QA_PERCENT_MISSING_DATA = 0
        CLOUD_COVER = 0
        PRODUCT_SAMPLES_PAN = 17400
        PRODUCT_LINES_PAN = 15356
        PRODUCT_SAMPLES_REF = 8700
        PRODUCT_LINES_REF = 7678
        PRODUCT_SAMPLES_THM = 4350
        PRODUCT_LINES_THM = 3839
        OUTPUT_FORMAT = "GEOTIFF"
    END_GROUP                           =
ORTHO_PRODUCT_METADATA
    GROUP = L1G_PRODUCT_METADATA
        BAND_COMBINATION = "123456678"
        CPF_FILE_NAME                   =
"L7CPF20000401_20000630_09"
        GROUP = MIN_MAX_RADIANCE
            LMAX_BAND1 = 191.600
            LMIN_BAND1 = -6.200
            LMAX_BAND2 = 196.500
            LMIN_BAND2 = -6.400
            LMAX_BAND3 = 152.900
            LMIN_BAND3 = -5.000
            LMAX_BAND4 = 157.400
            LMIN_BAND4 = -5.100
            LMAX_BAND5 = 31.060
            LMIN_BAND5 = -1.000
            LMAX_BAND61 = 17.040
            LMIN_BAND61 = 0.000
            LMAX_BAND62 = 12.650
```

LMIN_BAND62 = 3.200	LMIN_BAND62 = 3.200
LMAX_BAND7 = 10.800	LMAX_BAND7 = 10.800
LMIN_BAND7 = -0.350	LMIN_BAND7 = -0.350
LMAX_BAND8 = 243.100	LMAX_BAND8 = 243.100
LMIN_BAND8 = -4.700	LMIN_BAND8 = -4.700
END_GROUP = MIN_MAX_RADIANCE	END_GROUP = MIN_MAX_RADIANCE
GROUP = MIN_MAX_PIXEL_VALUE	GROUP = MIN_MAX_PIXEL_VALUE
QCALMAX_BAND1 = 255.0	QCALMAX_BAND1 = 255.0
QCALMIN_BAND1 = 1.0	QCALMIN_BAND1 = 1.0
QCALMAX_BAND2 = 255.0	QCALMAX_BAND2 = 255.0
QCALMIN_BAND2 = 1.0	QCALMIN_BAND2 = 1.0
QCALMAX_BAND3 = 255.0	QCALMAX_BAND3 = 255.0
QCALMIN_BAND3 = 1.0	QCALMIN_BAND3 = 1.0
QCALMAX_BAND4 = 255.0	QCALMAX_BAND4 = 255.0
QCALMIN_BAND4 = 1.0	QCALMIN_BAND4 = 1.0
QCALMAX_BAND5 = 255.0	QCALMAX_BAND5 = 255.0
QCALMIN_BAND5 = 1.0	QCALMIN_BAND5 = 1.0
QCALMAX_BAND61 = 255.0	QCALMAX_BAND61 = 255.0
QCALMIN_BAND61 = 1.0	QCALMIN_BAND61 = 1.0
QCALMAX_BAND62 = 255.0	QCALMAX_BAND62 = 255.0
QCALMIN_BAND62 = 1.0	QCALMIN_BAND62 = 1.0
QCALMAX_BAND7 = 255.0	QCALMAX_BAND7 = 255.0
QCALMIN_BAND7 = 1.0	QCALMIN_BAND7 = 1.0
QCALMAX_BAND8 = 255.0	QCALMAX_BAND8 = 255.0
QCALMIN_BAND8 = 1.0	QCALMIN_BAND8 = 1.0
END_GROUP = MIN_MAX_PIXEL_VALUE	END_GROUP = MIN_MAX_PIXEL_VALUE
GROUP = PRODUCT_PARAMETERS	GROUP = PRODUCT_PARAMETERS
CORRECTION_METHOD_GAIN_BAND1 = "CPF"	CORRECTION_METHOD_GAIN_BAND1 = "CPF"
CORRECTION_METHOD_GAIN_BAND2 = "CPF"	CORRECTION_METHOD_GAIN_BAND2 = "CPF"
CORRECTION_METHOD_GAIN_BAND3 = "CPF"	CORRECTION_METHOD_GAIN_BAND3 = "CPF"
CORRECTION_METHOD_GAIN_BAND4 = "CPF"	CORRECTION_METHOD_GAIN_BAND4 = "CPF"
CORRECTION_METHOD_GAIN_BAND5 = "CPF"	CORRECTION_METHOD_GAIN_BAND5 = "CPF"
CORRECTION_METHOD_GAIN_BAND61 = "CPF"	CORRECTION_METHOD_GAIN_BAND61 = "CPF"
CORRECTION_METHOD_GAIN_BAND62 = "CPF"	CORRECTION_METHOD_GAIN_BAND62 = "CPF"
CORRECTION_METHOD_GAIN_BAND7 = "CPF"	CORRECTION_METHOD_GAIN_BAND7 = "CPF"
CORRECTION_METHOD_GAIN_BAND8 = "CPF"	CORRECTION_METHOD_GAIN_BAND8 = "CPF"

```
        CORRECTION_METHOD_BIAS = "IC"
        BAND1_GAIN = "H"
        BAND2_GAIN = "H"
        BAND3_GAIN = "H"
        BAND4_GAIN = "H"
        BAND5_GAIN = "H"
        BAND6_GAIN1 = "L"
        BAND6_GAIN2 = "H"
        BAND7_GAIN = "H"
        BAND8_GAIN = "L"
        BAND1_GAIN_CHANGE = "0"
        BAND2_GAIN_CHANGE = "0"
        BAND3_GAIN_CHANGE = "0"
        BAND4_GAIN_CHANGE = "0"
        BAND5_GAIN_CHANGE = "0"
        BAND6_GAIN_CHANGE1 = "0"
        BAND6_GAIN_CHANGE2 = "0"
        BAND7_GAIN_CHANGE = "0"
        BAND8_GAIN_CHANGE = "0"
        BAND1_SL_GAIN_CHANGE = "0"
        BAND2_SL_GAIN_CHANGE = "0"
        BAND3_SL_GAIN_CHANGE = "0"
        BAND4_SL_GAIN_CHANGE = "0"
        BAND5_SL_GAIN_CHANGE = "0"
        BAND6_SL_GAIN_CHANGE1 = "0"
        BAND6_SL_GAIN_CHANGE2 = "0"
        BAND7_SL_GAIN_CHANGE = "0"
        BAND8_SL_GAIN_CHANGE = "0"
    END_GROUP                                   =
PRODUCT_PARAMETERS
    GROUP = CORRECTIONS_APPLIED
        STRIPING_BAND1 = "NONE"
        STRIPING_BAND2 = "NONE"
        STRIPING_BAND3 = "NONE"
        STRIPING_BAND4 = "NONE"
        STRIPING_BAND5 = "NONE"
        STRIPING_BAND61 = "NONE"
        STRIPING_BAND62 = "NONE"
        STRIPING_BAND7 = "NONE"
        STRIPING_BAND8 = "NONE"
        BANDING = "N"
        COHERENT_NOISE = "N"
        MEMORY_EFFECT = "N"
        SCAN_CORRELATED_SHIFT = "N"
        INOPERABLE_DETECTORS = "N"
        DROPPED_LINES = N
    END_GROUP                                   =
CORRECTIONS_APPLIED
  END_GROUP                                     =
L1G_PRODUCT_METADATA
END_GROUP = METADATA_FILE
END
```

```
        CORRECTION_METHOD_BIAS = "IC"
        BAND1_GAIN = "H"
        BAND2_GAIN = "H"
        BAND3_GAIN = "H"
        BAND4_GAIN = "H"
        BAND5_GAIN = "H"
        BAND6_GAIN1 = "L"
        BAND6_GAIN2 = "H"
        BAND7_GAIN = "H"
        BAND8_GAIN = "L"
        BAND1_GAIN_CHANGE = "0"
        BAND2_GAIN_CHANGE = "0"
        BAND3_GAIN_CHANGE = "0"
        BAND4_GAIN_CHANGE = "0"
        BAND5_GAIN_CHANGE = "0"
        BAND6_GAIN_CHANGE1 = "0"
        BAND6_GAIN_CHANGE2 = "0"
        BAND7_GAIN_CHANGE = "0"
        BAND8_GAIN_CHANGE = "0"
        BAND1_SL_GAIN_CHANGE = "0"
        BAND2_SL_GAIN_CHANGE = "0"
        BAND3_SL_GAIN_CHANGE = "0"
        BAND4_SL_GAIN_CHANGE = "0"
        BAND5_SL_GAIN_CHANGE = "0"
        BAND6_SL_GAIN_CHANGE1 = "0"
        BAND6_SL_GAIN_CHANGE2 = "0"
        BAND7_SL_GAIN_CHANGE = "0"
        BAND8_SL_GAIN_CHANGE = "0"
    END_GROUP                                   =
PRODUCT_PARAMETERS
    GROUP = CORRECTIONS_APPLIED
        STRIPING_BAND1 = "NONE"
        STRIPING_BAND2 = "NONE"
        STRIPING_BAND3 = "NONE"
        STRIPING_BAND4 = "NONE"
        STRIPING_BAND5 = "NONE"
        STRIPING_BAND61 = "NONE"
        STRIPING_BAND62 = "NONE"
        STRIPING_BAND7 = "NONE"
        STRIPING_BAND8 = "NONE"
        BANDING = "N"
        COHERENT_NOISE = "N"
        MEMORY_EFFECT = "N"
        SCAN_CORRELATED_SHIFT = "N"
        INOPERABLE_DETECTORS = "N"
        DROPPED_LINES = N
    END_GROUP                                   =
CORRECTIONS_APPLIED
  END_GROUP                                     =
L1G_PRODUCT_METADATA
END_GROUP = METADATA_FILE
END
```

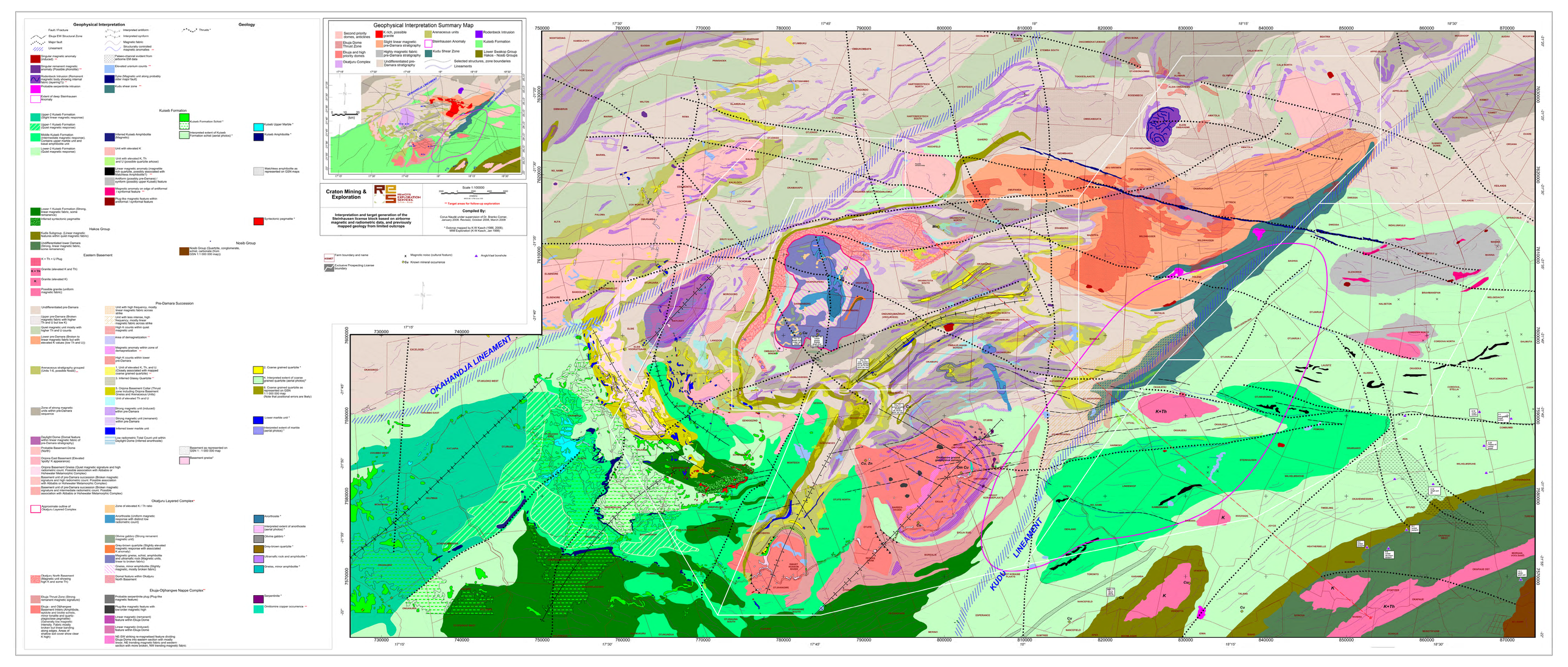
Geophysical Interpretation
Fault / Fracture
Ekuja EW Structural Zone
Major fault
Lineament
Singular magnetic anomaly (induced) **
Singular remanent magnetic anomaly (Possible phonolite) **
Diabase/basalt intrusion (Remanent magnetic body showing internal fabric (layering?)) **
Probable serpentinite intrusion
Extent of deep Steinhausen Anomaly
Interpreted antiform
Interpreted synform
Magnetic fabric
Structurally controlled magnetic anomalies **
Paleo-channel evident from airborne EM data
Elevated uranium counts **
N-Ve (Magnetic unit along probably major fault)
Kudu shear zone **
Thrusts *
Geology
Kuiseb Formation
Upper-2 Kuiseb Formation (Slight linear magnetic response)
Upper-1 Kuiseb Formation (Quiet magnetic response)
Middle Kuiseb Formation (Intermediate magnetic response), comprising mainly mica unit and basal amphibolite unit
Lower-2 Kuiseb Formation (Quiet magnetic response)
Kuiseb Formation Schist *
Interpreted extent of Kuiseb Formation schist (aerial photos) *
Kuiseb Upper Marble *
Kuiseb Amphibolite *
Inferred Kuiseb Amphibolite (Magnetic)
Unit with elevated K
Unit with elevated K, Th, and U (possible quartzite arkose)
Linear magnetic anomaly (magnetite rich quartzite, possibly associated with Kuiseb Amphibolite)
Antiform (possibly pre-Damara) / synform (possibly upper Kuiseb) feature
Magnetic anomaly on edge of antiformal / synformal feature **
Plug-like magnetic feature within antiformal / synformal feature
Matchless amphibolite as represented on GSN maps
Lower-1 Kuiseb Formation (Strong, linear magnetic fabric, some remanence)
Inferred syntectonic pegmatite
Syntectonic pegmatite *
Hakos Group
Kuibis Subgroup. (Linear magnetic features within quiet magnetic fabric)
Undifferentiated lower Damara (Strong, linear magnetic fabric, some remanence)
Nosib Group
Nosib Group (Quartzite, conglomerate, arkose, undifferentiated GSN 1:1 000 000 map))
Eastern Basement
K + Th + U Plug
K+Th
Granite (elevated K and Th)
K
Granite (elevated K)
Possible granite (uniform magnetic fabric)
Pre-Damara Succession
Undifferentiated pre-Damara
Upper pre-Damara (Broken to linear magnetic fabric, higher Th and U but low K)
Quiet magnetic unit mostly with higher Th and U counts
Lower pre-Damara (Broken to linear magnetic fabric but with elevated K values (low Th and U))
Arenaceous stratigraphy grouped (Units 1-6, possible fossil)
Zone of strong magnetic units within pre-Damara sequence
Daylight Dome (Donal feature within linear magnetic fabric of pre-Damara stratigraphy)
Okahandja Basement Dome (North)
Orijona East Basement (Elevated 'spotty' K appearance)
Orijona Basement Gneiss (Quiet magnetic signature and high radiometric count. Possible association with Abbabis or Hohewater Metamorphic Complex)
Basement unit of pre-Damara succession (Broken magnetic signature and intermediate radiometric count. Possible association with Abbabis or Hohewater Metamorphic Complex)
Basement unit of pre-Damara succession (Broken magnetic signature and intermediate radiometric count. Possible association with Abbabis or Hohewater Metamorphic Complex)
Unit with high frequency, mostly broken magnetic fabric across strike
Unit with less intense, high frequency, mostly broken magnetic fabric across strike
High K counts within quiet magnetic unit
Area of demagnetization **
Magnetic anomaly within zone of demagnetization **
High K counts within lower pre-Damara
1. Unit of elevated K, Th, and U. Interpreted extent of mapped coarse grained quartzite **
3. Inferred Glassy Quartzite **
5. Orijona Basement Collar (Thrust zone including Orijona Basement Gneiss and Arenaceous Units)
Strong magnetic unit (induced) within pre-Damara
Strong magnetic unit (remanent) within pre-Damara
Inferred lower marble unit
Low radiometric Total Count unit within Daylight Dome (inferred anorthosite)
Basement as represented on GSN 1 : 1 000 000 map
Basement gneiss*
2. Coarse grained quartzite *
4. Interpreted extent of coarse grained quartzite (aerial photos)*
6. Coarse grained quartzite as represented on GSN 1:1 000 000 map (Note that positional errors are likely)
Lower marble unit *
Interpreted extent of marble (aerial photos) *
Okatjuru Layered Complex**
Approximate outline of Okatjuru Layered Complex
Zone of elevated K / Th ratio
Anorthosite (Uniform magnetic response with distinct low radiometric count)
Olivine gabbro (Strong remanent magnetic unit)
Grey-brown quartzite (Slightly elevated magnetic response with associated K anomaly)
Magnetic gneiss, schist, amphibolite (Slightly elevated magnetic units, loose to broken fabric)
Gneiss, minor amphibolite (Slightly magnetic, mostly broken fabric)
Domal feature within Okatjuru North Basement
Okatjuru North Basement (Magnetic unit showing high K and some Th)
Anorthosite *
Interpreted extent of anorthosite (aerial photos) *
Olivine gabbro *
Grey-brown quartzite *
Ultramafic rock and amphibolite *
Gneiss, minor amphibolite *
Ekuja-Otjihangwe Nappe Complex**
Ekuja Thrust Zone (Strong remanent magnetic signature)
Ekuja - and Otjihangwe Metamorphic Complex: amphibolite, epidote and biotite schists, minor tonalite and quartz-diorite gneiss. Generally low-magnetic intensity. Fabric mostly broken but linear banding along edges. Areas of alluvial soil cover show clear K highs
Probable serpentinite plug (Plug-like magnetic feature)
Plug-like magnetic feature with low-order magnetic high
Linear magnetic (remanent) feature within Ekuja Dome
Linear magnetic (induced) feature within Ekuja Dome
NE-SW striking re-magnetised feature dividing Ekuja Dome into eastern section with mostly broken magnetic fabric and western segment section with more broken, NW trending magnetic fabric
Serpentinite *
Omitiomire copper occurrence **
Geophysical Interpretation Summary Map
Second priority domes, anticlines
Ekuja Dome Thrust Zone
Ekuja and high priority domes
Okatjuru Complex
K-rich, possible granite
Slight linear magnetic pre-Damara stratigraphy
Highly magnetic fabric pre-Damara stratigraphy
Undifferentiated pre-Damara stratigraphy
Arenaceous units
Steinhausen Anomaly
Kudu Shear Zone
Selected structures, zone boundaries
Lineaments
Rodenbeck Intrusion
Kuiseb Formation
Lower Swakop Group Hakos - Nosib Groups
OKAHANDJA LINEAMENT
KUDU LINEAMENT
Craton Mining & Exploration
REMOTE EXPLORATION SERVICES
Scale 1:100000
** Target areas for follow-up exploration
Interpretation and target generation of the Steinhausen license block based on airborne magnetic and radiometric data, and previously mapped geology from limited outcrops
Compiled By:
Corus Naudé under supervision of Dr. Branko Corner, January 2009. Revised, October 2008, March 2009
* Okatonqi mapped by K-W Kasch (1986, 2008); MM Exploration (K-W Kasch, Jan 1998)
Farm boundary and name
KISMET
Exclusive Prospecting License boundary
Magnetic noise (cultural feature)
Known mineral occurrence
Airgh/Vaal borehole
17°30'
760000
770000
780000
17°45'
790000
800000
810000
18°
820000
830000
840000
18°15'
850000
860000
18°30'
870000
7530000
7540000
7550000
7560000
7570000
7580000
7590000
7600000
7610000
7620000
7630000
7640000
7650000
-21°45'
-21°30'
-21°15'
-21°
-20°45'
-20°30'
-20°15'
-20°
730000
740000
17°15'